Addis Ababa University

Addis Ababa Institute of Technology

School of Electrical and Computer Engineering

DEVELOPMENT OF VOLTAGE SECURITY ASSESSMENT AND REACTIVE POWER MANAGEMENT SCHEMES FOR ONLINE APPLICATION

PhD dissertation submitted to the School of Electrical and Computer Engineering, Addis Ababa Institute of Technology Graduate Studies, Addis Ababa University in partial fulfilment of the requirements for the degree of Doctor of Philosophy in Electrical Engineering (Electrical Power Engineering)

BY

Ahadu Hilawie

Supervisor: Dr. Ing. Fekadu Shewarega (Asso. Professor)

September, 2024

Addis Ababa

SCHOOL OF ELECTRICAL AND COMPUTER ENGINEERING

ADDIS ABABA INSTITUTE OF TECHNOLOGY

ADDIS ABABA UNIVERSITY

I, hereby, declare that this PhD dissertation contains no material that has been submitted previously, in whole or in part, for the award of any other academic degree, except where otherwise indicated. This PhD dissertation is my own original work.

Ahadu Hilawie		24/09/2024
PhD Candidate	Signature	Date

As this dissertation supervisor, I, hereby, notify that I have read and evaluated this PhD dissertation work prepared by Ahadu Hilawie, under my guidance, under the title **"Development of voltage security assessment and reactive power management schemes for online application".** I recommend that it be accepted as fulfilling the PhD dissertation requirement.

Dr. Ing. Fekadu Shewarega		24/09/2024
Supervisor	Signature	Date

As members of the examining board of the PhD dissertation presentation, we certify that we have read and evaluated the dissertation prepared by Ahadu Hilawie, and recommend that it be accepted as fulfilling the PhD dissertation requirement.

Chairman	Signature	Date
Getachew Biru (Ph.D.		03.10.2024
Internal examiner	Signature	Date
Belachew Bantyirga (PhD)		03.10.2024
External examiner	Signature	Date

ABSTRACT

Voltage security issues continue to be the concerns of power systems as the stress on power systems increases due to increasing energy demand. To manage this stress and prevent voltage security problems, online voltage security assessment (VSA) and reactive power management (RPM) strategies are coming to play crucial role. However, selecting suitable approach and developing one's own method requires rigorous assessment of the gaps in existing approaches and devising a strategy to fill the gaps. In this regard, this dissertation work aims at developing VSA and RPM schemes for online application to help the efforts made to mitigate the increasing voltage security problems.

The dissertation has two major components, voltage security assessment (VSA) scheme development and reactive power management (RPM) scheme development, as separate entities and as complementary entities. The work focuses on designing the components of the schemes by devising new and improved contents of each scheme.

The developed VSA scheme performs three major tasks; estimating the network Thevenin equivalent impedances, determining the voltage stability indices and interpreting the results of voltage stability indices. Computational efficiency improving strategies, which are necessary for online application, are adopted at different levels of the VSA scheme. This begins from selecting the method of voltage security assessment, i.e. Thevenin equivalent based approach. Then, to address the limitation of previous Thevenin equivalent determination techniques this work comes up with a new Thevenin impedance determination technique. The developed Thevenin impedance determination technique requires two power flow computations in offline analysis case and only one power flow analysis in the case of online estimation. For the voltage stability assessment task of the VSA scheme two types of voltage stability indices are formulated, which measure proximity to voltage instability, one directly using the power margin and the other indirectly as a simple closeness indicator. The third capability of the VSA scheme is PV and QV curve plotting capability for interpreting the process of development of voltage security problems. The Thevenin equivalent determination capability, greatly, simplifies the maximum power transfer capacity estimation and PV or QV curve determination, which was previously a computationally intensive task.

The capabilities of the VSA scheme are tested using simple four bus test system, IEEE 14 bus and IEEE 30 bus test systems. The tests produced results meeting the objectives of producing high accuracy Thevenin parameters, tracking system loading changes, identifying weakest buses, showing the impact of reactive power compensation and showing impact of load increments. Then the scheme is applied to existing Ethiopian Electric Power (EEP) system to examine the performance on large power systems. The application of VSA scheme to EEP system revealed a number of important features of the EEP system pertinent to voltage security, including weakest areas, weakest buses and voltage instability contributing lines.

The other scheme, the reactive power management scheme, depends on the results of VSA process. In this case, two approaches are devised for reactive power management purpose. The first is fast reactive power management (FRPM) approach and the second is continuous reactive power management (CRPM) approach.

FRPM is proposed considering contingent operating conditions. In this approach the voltage stability indices are used as an indicator of voltage security improvement, while reactive power provisions are made. Reactive power provisions cease when the weakest load buses get far enough from voltage instability.

On the CRPM side the objective is to adress the optimization needs of reactive power provisions. In this approach, an improved multi objective particle swarm optimization (IMOPSO) algorithm is proposed. Together with voltage deviation objective function, the algorithm uses the indices developed on the VSA scheme for the multi objective function formulation. In this algorithm, the common multi objective particle swarm optimization (MOPSO) is improved by introducing an adapted binary crossover (ABX) to the new positions obtained by the basic PSO algorithm. Additionally, diversity maintenance strategy is added to the algorithm by employing crowding distance (CD) computation. The developed algorithm is, then, tested and compared with standard MOPSO and NSGA II algorithms. The comparison is made based on the degree of closeness to the true pareto front, as measured by the inverted generational distance (IGD), and based on diversity, as measured by the CDs. The test is made using ZDT1, ZDT2, and ZDT3 common test functions. The IMOPSO showed improved performance over MOPSO and NSGA II algorithms in terms of

convergence to the true pareto front and in terms of the speed of convergence as well as in maintaining diversity. The algorithm is then implemented to reactive power optimization of IEEE 14 bus test system and the EEP system. This implementation has resulted diverse options of optimal settings of reactive power controlling parameters. The optimal settings proved to produce an improved voltage security as measured in terms of voltage deviation and voltage stability.

AKNOWLEDGEMENT

First, I want to thank the All-Mighty God for granting me courage, motivation, and endurance to pass through the ups and downs during this research project.

My deepest gratitude goes to Dr. Ing. Fekadu Shewarega my supervisor. The support, encouragement and guidance you put unceasingly from the inception to the completion of the work was immense. This research work couldn't get realized otherwise.

The power engineering professors Prof. N.P. Singh, Dr. Ing. Getachew Biru, Dr. Getachew Bekele your continuous evaluation of the research progress through the seminars and your encouragements realized a more refined work. My thanks is extended to you too.

The SECE and power engineering chairs, management bodies your readiness to address our academic requests is worth of thanks.

I want to thank the EEP officials at different levels, who showed curiosity on the work, as their work, and were so open to provide the necessary data for the consumption of the work.

I want also to thank my home university, Woldia University, officials who gave me the opportunity to join this PhD program, and were ready to provide the necessary support my study was demanding.

My companions Mr. Teshome Lindi and Dr. Shewit Tsegay, the time we spend together, the help we exchanged throughout our study was precious. I want to say thank you.

My Last, but not the least thanks goes to my family, my spouse Mekdes Adibaruu, daughter Aleph Ahadu and son Beaman Ahadu. Without your understanding, patience and encouragement, this work would not get realized.

Thank you all!

TABLE OF CONTENTS

LIST OF FIGURES

LIST OF TABLES

ACRONYMS

ABX	Adapted Binary Crossover
CD	Crowding Distance
CRPM	Continuous Reactive Power Management
EEP	Ethiopian Electric Power
EMS	Energy Management System
FACTS	Flexible AC Transmission Systems
FRPM	Fast Reactive Power Management
IEC	International Electronic Committee
IEEE	International Electronics and Electrical Engineering Association
IGD	Inverted Generational Distance
MOPSO	Multi Objective Particle Swarm Optimization
NSGA	Non dominated Sorting Genetic Algorithm
NISI	New Impedance Stability Index
PF	Pareto Front
PMU	Phasor Measurement Unit
PPMI	Active Power Margin Index
PSO	Particle Swarm Optimization
RPM	Reactive Power Management
RPO	Reactive Power Optimization
SCADA	Supervisory Control and Data Acquisition System
SPMI	Apparent Power Margin Index
VSA	Voltage Security Assessment

CHAPTER 1

INTRODUCTION

1.1. Background

Global population is, ever, growing at high rates. Over the past ten years, the population increased by 1.5 billion reaching today over 7.9 billion [1, 2]. This population growth caused the energy demand to increase high, despite the universal effort of promoting and implementing economical energy usage [3, 4].

This high demand increment, in turn, has brought overloading of power systems. The overloading is further exacerbated by the transmission system operators' tendency of keeping existing network size, rather than having new infrastructure expansions, due to growing economic, public interest and environmental concerns [5-7].

Power system operators are seen operating their systems near to the loadability limit. This closeness to the loadability limit has increased risk of system collapse when exposed to system contingencies, such as faults, generator losses, transmission line losses, and even load increments in amounts which would have been tolerable, otherwise.

On the customer side, customers demand reliable and quality power supply. Reliable and quality power supply can be maintained by building a secured system regardless of the level of complexity and size it has. By secured system it is meant a system with high degree ability of surviving eminent disturbances and with the ability of maintaining system standards at all times [8].

Closeness to system loadability limit and the associated system collapse risk, prominently, related to the issue of voltage security. Voltage security has two components [9-11]. The first component is the state of a system operating within predefined standard voltage magnitude limits. Whilst, the second component is the distance of the system from voltage instability during steady state operating state or post contingency operating states.

Voltage stability is the ability of the system to maintain steady state voltage levels at all system buses following any credible contingency [8]. Voltage instability comes with high system stress level [12]. The more loaded the system is, the closer the system gets to

voltage instability, and hence, deteriorating voltage security. The stress not only comes from system load increment, but poor reactive power management and the impact of contingencies also constitute significant portion of the cause [13].

In response to this system stress, a number of system stress relieving mechanisms are adopted by power system operators. The common strategies include transmission infrastructure expansions [14], active power rescheduling techniques [15] , load shedding schemes [16, 17], and reactive power provisions [18]. Each of these approaches differ in the way they relieve the stress of the system.

Among these options, network infrastructure expansion is economically expensive. Additionally, active power rescheduling and load shedding schemes reduce the active power transfer, which affects reliability of a power system. On the other hand, reactive power compensation maximizes active power transfer and the means are more economical when compared with transmission expansion.

Due to this fact, power system operators choose utilizing existing network infrastructure equipped with real-time voltage security assessment mechanisms and effective reactive power management schemes to maintain system voltage security. This approach allows them to use the network capacity efficiently with a calculated confidence.

In this regard, this dissertation work comes up with voltage security assessment (VSA) and reactive power management (RPM) schemes to be used for online application.

On the voltage security assessment scheme development, to comply with requirement of fast computational capability for online security assessments, efficiency-improving strategies are implemented at different levels of the VSA scheme.

Regarding to the reactive power management scheme two approaches, named as fast reactive power management (FRPM) and continuous reactive power management (CRPM) approaches, are devised by this work.

The FRPM approach is intended to be used during contingencies which demand fast actions. In this option, the stability indices developed for VSA are used as indicator while switching system reactive resources so as to keep the system far away from point of

collapse. No optimizations are made here. This is due to optimization techniques' requirement of considerable processing time to respond timely to contingencies.

The CRPM bases on the idea that an optimized system is secured against security threats. For this part an improved multi objective particle swarm optimization (IMOPSO) algorithm is devised. The algorithm developed has achieved better performance when compared with commonly utilized MOPSO and non-dominated sorting genetic algorithm (NSGA II).

In the way of realizing this dissertation project the following contributions are made.

- New Thevenin impedance determination technique, suitable for online application, is devised.
- Two voltage stability indices are developed. The first index measures nearness to voltage instability indirectly, meaning without the power related terms, and the other shows directly the active power transfer margin before the inception of voltage instability.
- The way the voltage instability indices are used for FRPM is investigated.
- An improved multi objective particle swarm optimization (IMOPSO) algorithm is devised for CRPM.
- The tests for the verification of the schemes are made on standard IEEE 14 bus and IEEE 30 bus test systems.
- VSA scheme is applied to the Ethiopian power system under different scenarios, and important characteristics of the EEP system is explored.
- IMOPSO algorithm is applied to the Ethiopian power system, and the improvements are shown.

1.2. Problem Statement

Voltage security continued to be power system security concern as power systems get more loaded and more complex than ever. The voltage security problems are capable of causing fatal system collapses, if not identified and corrective mechanisms are not adopted timely.

In this regard, online voltage security problem identifying and correcting schemes play a crucial role, for the normal functioning of power systems. In line with this fact, this work comes with the voltage security assessment and reactive power management schemes.

The schemes are realized through designing the components of the schemes and putting together the components so as to give the schemes different capabilities. In doing so problems at different levels of the scheme development are addressed.

Online methods are required to be computationally efficient so as to make timely decisions. Hence, bringing computational efficiency is targeted at different levels of the VSA scheme. This begins from the selection of the method of assessment, i.e. Thevenin impedance-based voltage security assessment scheme. Thevenin impedance-based voltage security assessment methods are accompanied with simple expressions. These simple expressions bring computational efficiency for the assessment.

However, the process of determining the Thevenin equivalents of power systems is still a difficult task due to the large size of power systems. This presents the other problem dimension.

For determining Thevenin equivalent of a power system, some works proposed approximate estimations which introduced error of approximation. Other works solely depended on system measurements. These latter approaches require a minimum of two differing measurement sets. This class of approaches is experiencing the following problems, which need further consideration. The problems are;

- If system topology changes between consecutive measurements, erroneous Thevenin equivalent values will result. This puts a question on the practical implementation of the class.
- The methods in this class require perturbation of values between set of measurements. During steady state operation, however, the measurement sets taken are identical. This creates vacant times when Thevenin equivalents cannot be determined.
- The requirement of two or more measurements widens the time window of processing. This increases the processing time which is demanded to be short.
- These methods do not put a way for the computation of the Thevenin voltage, which is mandatory for the computation of the maximum active power transfer and the critical voltage. Without the Thevenin voltage, power-based indices cannot be

formulated. This forces the methods to relay on only impedance-based indices, which falls short on giving information on the power reserve to go before collapse point.

The method of Thevenin equivalent determination, developed in this dissertation work, is a mixed approach, which uses both measurement and system network model. Solving the problems noted above in measurement-based approaches, the new method relies on a single shot measurement. Hence, system configuration change, time window width, number of measurement vs accuracy issues are not the concerns anymore.

The method, also, has solved the problem of approximation that come with model and measurement based mixed approaches. Additionally, the method put the way to determine the Thevenin voltage, which is necessary for maximum power transfer capacity estimation.

The determination of system Thevenin equivalent, this way, simplifies the voltage security assessment. This makes the realization of the following important capabilities and components of the VSA scheme easy. The capabilities are;

- Two types of voltage stability assessment indices are devised. The first index New Impedance Stability Index (NISI) serves as an indirect measurement of proximity to voltage instability. Whilst, the second index Active Power Margin Index (PPMI) directly quantifies the active power margin to go before the point of voltage collapse. The first letter 'P' in the acronym PPMI comes from the representation of active power in power flow analysis studies.
- The maximum active power loading limit which is important for the index development is calculated in a simplistic way. Previously, the computation of the maximum active power loading requires either repetitive power flow computation or continuous power flow approach, which are both iterative methods and hence computationally intensive. The method of Thevenin equivalent computation in this work makes the calculation of the maximum active power transfer non-iterative and computationally efficient.
- In this scheme QV and PV curves are determined easily in a non-iterative way. These curves help to visualize the progress of voltage instability, graphically. Previous computation of the PV and QV curves require a number of power flow calculations at different loading levels. Power flow computation itself, being an iterative process,

consumes a considerable computational effort. The same time, increasing the number of power flows multiplies the computation time.

On the reactive power management scheme side two approaches are proposed considering contingency and optimization requirements separately. The first approach is identified as fast reactive power management (FRPM) and the second as continuous reactive power management (CRPM).

Contingencies within power systems require fast reactive power provisions so as to limit cascading voltage security failures. Optimization needs this time are luxury quests since they require considerable processing time. To go in line with this fact, this work proposed FRPM approach. FRPM uses the voltage stability indices, developed in VSA scheme, to identify weak areas and observe the changes that come on these weak buses with reactive power provisions. This approach uses the voltage stability indices as an indicator to switch on reactive power resources. Reactive power provision ceases when the stability indices are seen to be far enough from point of collapse.

On the other hand, CRPM approach is proposed to address the optimization need of the system operator. For CRPM approach an improved multi objective particle swarm optimization (IMOPSO) algorithm is devised. The IMOPSO algorithm improved the performance of the standard MOPSO algorithm in terms of quality of the optimal solutions, diversity of the solutions and speed of convergence. Additionally, in the application of IMOPSO for reactive power optimization the problems on the objective function formulation are also fixed.

1.3. Objectives

1.3.1. General objective

The general objective of this dissertation is developing voltage security assessment and reactive power management schemes for online application. To realize this general objective the following specific objectives are set.

1.3.2. Specific objectives

- Identify suitable approach for online voltage security assessment scheme development.

- Assess the gaps in existing voltage security assessment approaches and develop a strategy to fill the gaps in existing approaches.
- Develop the VSA scheme components and realize the scheme.
- Test the resulting VSA scheme and ensure the identified gaps are filled and the scheme performs the desired tasks.
- Identify the requirements needed from reactive power management by power systems pertinent to voltage security.
- Design a strategy to achieve those needs and realize reactive power management scheme.
- Test the developed RPM scheme if it meets the demand required.

1.4. Scope of the Study

The scope of this work is devising the voltage security assessment and reactive power management schemes. The work focuses on choosing suitable method, assessing the gaps in existing works, providing the way the gaps get filled and testing the resulting components.

The data accessing mechanisms are not the focus of this work. The work considers the data necessary for the schemes, whether from PMU, SCADA or simulations; are available as a complete processed input. Hence, the tests are made using the data generated using simulations.

1.5. Significance of the Study

The first significance of the study is that it provides a complete scheme on which a user interactive software tool can easily get realized. This is important from the view point of developing an own analysis tool for power systems like the Ethiopian power system. EEP relays on power analysis software tools developed by companies of developed countries. This brings unnecessary, continuous costs related to the installation, maintenance and upgrading of the tools. Moreover, this limits technology transfer and self-reliant technological developments, which are crucial for the sustainable development of a country.

On the other hand, the new contributions of the research, i.e. Thevenin impedance determination, stability indices and the IMOPSO, will further facilitate upcoming researches in the area of power system stability and power system optimization studies.

1.6. List of Publications

The following published journal papers are the result of this dissertation work;

1. A. Hilawie and F. Shewarega, "Developing New Thevenin Impedance Determination Technique and Voltage Stability Assessment Index for Online Application," IEEE PES/IAS Power Africa, 2021, pp. 1-5, doi:10.1109/PowerAfrica52236.2021.9543381.
2. A. Hilawie and F. Shewarega, "Static Voltage Stability Assessment of Ethiopian power System Using Normalized Active Power Margin Index," *EAI Endorsed Transactions on Energy Web,* vol. 9, no. 40, 2022, doi: 10.4108/ew.v9i40.141.
3. A. Hilawie and F. Shewarega, " Improved multi objective particle swarm optimization based reactive power optimization for ensuring voltage security of power systems," *Engineering Express, IOP publishing,* 2023 Vol. 5 Issue 4 Pages 045062, DOI 10.1088/2631-8695/ad0afc.

1.7. Dissertation Content

Chapter two contains the review of basic concept of voltage security; introduces the VSA methods developed, so far, by literature and industry for online voltage security assessment; selects an approach for this work and explores the problems associated with this class. It also introduces reactive power management scheme devised for the objective of ensuring voltage security.

Chapter three analyzes the basic components of Thevenin equivalent determination technique selected for this work, which is the foundation of the work. It assesses the gap in the previous Thevenin equivalent determination techniques and devises the new Thevenin equivalent determination technique. It, procedurally, develops the capabilities of the VSA scheme. It shows the procedures for the development of an IMOPSO algorithm for the reactive power management.

Chapter four is devoted for presenting the test results of foundational capabilities of VSA and RPM schemes, i.e. the Thevenin equivalent determination technique, voltage stability assessment indices and the IMOPSO. For this purpose, simple four bus test system and standard IEEE 14 bus and IEEE 30 bus test systems are employed. The results are compared with relevant benchmarks and the improvements are communicated.

Chapter five is devoted to investigate the application of the VSA and RPM schemes on the Ethiopian electric power system. The EEP system voltage security is assessed for different scenarios and the reactive power management optimization is performed.

Chapter six contains the conclusions drawn from the whole sum of the work. It makes recommendations and shows future expansion direction of the work.

CHAPTER 2 LETERATURE REVIEW

This chapter introduces the basic concept of voltage security; shows the voltage security assessment techniques introduced so far; selects the voltage security assessment approach for this project; assesses the gaps in this approach. It also reviews the current status, achievements and gaps of voltage security enhancing reactive power optimization.

2.1. Voltage Security of Power Systems

Power system security is the ability of a power system to operate steadily and within the various security limits imposed on the system. These limits are pre-defined thermal limit, voltage limit, frequency limit, active power limit, reactive power limit, and stability limits.

Power system security is commonly classified based on level of security [19, 20] and type of security [21-24]. Level of security deals with the level of severity of the security problems. On the other hand, type-based classification considers the cause of security problems. The type-based power system security classification is shown in Figure 2.1 below.

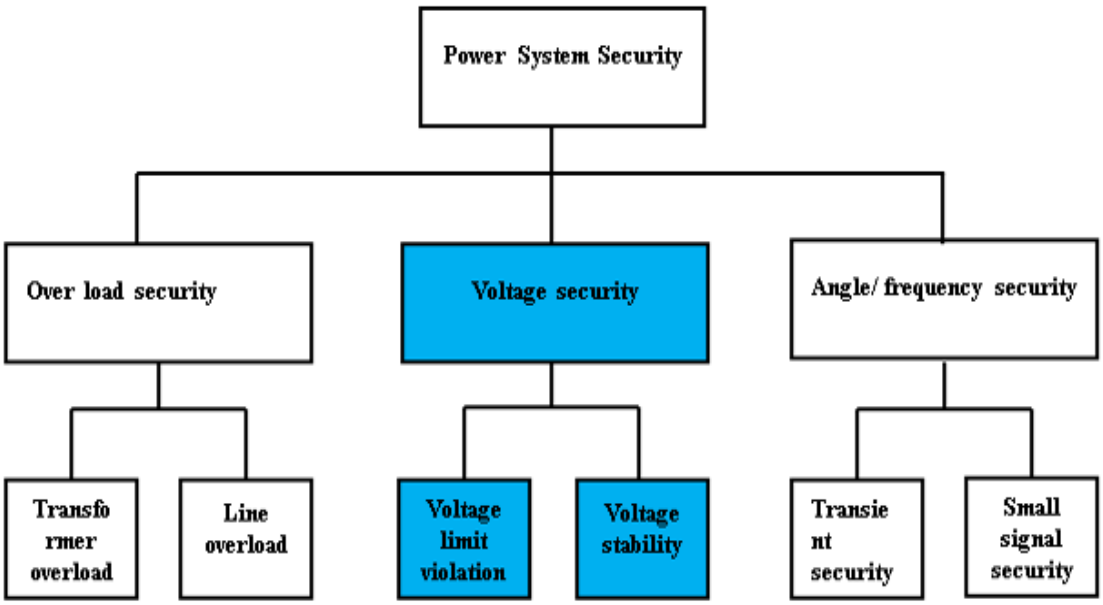

Figure 2.1: Power system security type classification [22, 24]

Based on this classification voltage security is one component of the broader power system security spectrum.

There are times, inconsistency occurs among the literature, in defining the voltage security issue. There are works who consider individual of these two aspects. In works [25-28], only voltage limit violation is taken as a voltage security issue. However, this treatment of the subject is problematic. Because systems well operating within the voltage limits may be under voltage instability. Other works took voltage stability issue as a voltage security question [10, 29].

By compiling the views of the literature voltage security problems can be considered as having two aspects; voltage limit violation and voltage instability.

2.1.1. Voltage limit violation

Voltage profile limits are imposed on the system with the aim of ensuring equipment safety, providing quality power to the customer, and preventing the inception of the other voltage security problem, i.e. voltage instability.

Based on The international standard, i.e. IEC 60038, allowed load bus voltages to vary $\pm 5\ \%$ (0.5 pu value) from the nominal voltage setting [30]. If this limit is passed, voltage limit violation is considered taking place and the system is identified as voltage insecure.

When the system goes above the upper voltage limit, the system is identified as experiencing overvoltage. Overvoltages are destructive to the system safety and cause equipment damages at various transmission levels. Voltage higher limit violations occur with load rejection. The load rejection can come, primarily, with faults and the associated protective actions which isolate significant load centres from grid connection. Additionally, power systems where industrial loads are highly reduced from the initial system plan are seen experiencing overvoltages [31].

On the other hand, the lower voltage limit violation, i.e. under voltage, comes from high system loading. Undervoltage is a detrimental security problem, and the impact is critical for industrial load areas [13, 32, 33]. Industrial load areas significantly constitute induction machine loads. Induction machines, when experience undervoltage, draw large amount of current from the system, which further cause a more voltage drop within the

transmission system. This voltage drop is, further, accompanied by a more current demand of these machines. This cycle of events leads to the other component of voltage security issue, i.e. voltage instability.

2.1.2. Voltage instability

Voltage instability is the second component of voltage security problems. Voltage instability is a load dependent power system instability problem, and is characterized by uncontrolled voltage decline in one or more load buses, regardless of the amount of reactive power compensation [34]. The IEEE/ CIGRIE joint task force defined voltage stability as; “the ability of a power system to maintain steady voltages at all buses in the system after being subjected to a disturbance.” [8].

Voltage instability occurs due to system stress. When the system gets more loaded, it will be pushed to its power transfer limit and culminate in system collapse [12, 35]. In real power systems, where the system load is dominantly inductive, when active power loading increases the load bus voltage declines, as dictated by PV relation curve as shown in Figure 2.2.

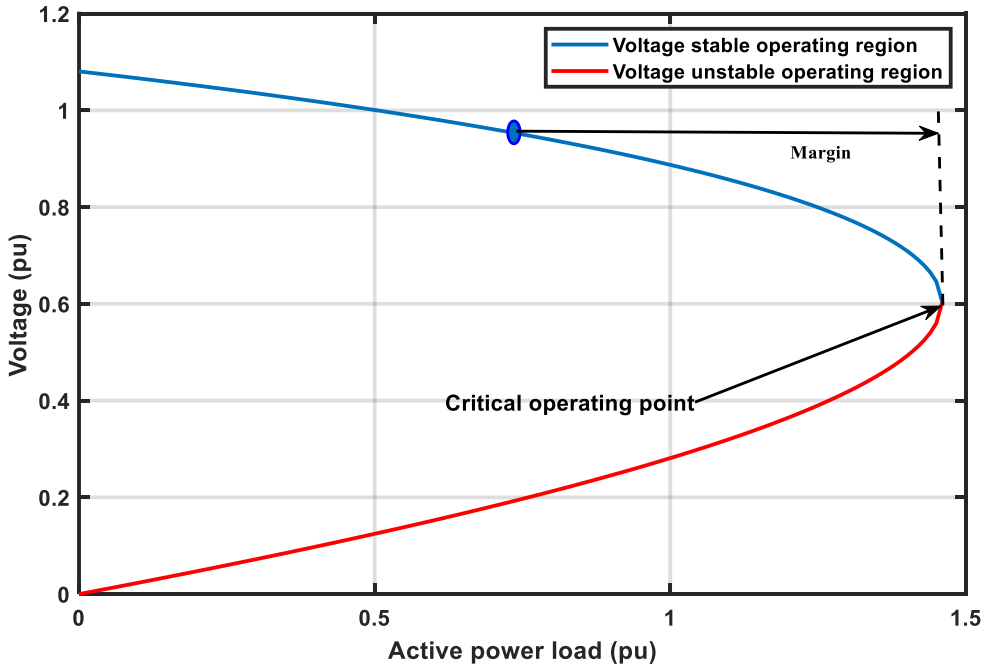

Figure 2.2: PV characteristic curve of a load bus

In the voltage stable state of the load bus, the decline of the voltage profile is controllable by switching appropriate amount of reactive power compensation. Controllability continues until the active power loading reaches the critical loading point. The active power transfer at the critical point is the possible maximum transferable active power from the system to the load.

Further increasing the active power loading, beyond the critical point, makes the load bus to experience reduced active power transfer to the load, with a lower voltage profile. This is the voltage instability condition. In this state, the load bus voltage gets no more controllable, despite any amount of reactive power compensation [36].

There are various causes of voltage instability in power systems [13]. The causes of voltage instability can fall into two classes. The first class is characterized by the inability of the generation-transmission system to meet the active power demand of the loads. The second class is occurrence of reactive power deficiency to meet both the reactive demand and the reactive losses.

The inability of a transmission system to provide the power demand requested by the load occurs when the load end of a transmission system reaches its maximum power transfer limit. Further demand increment will no longer get responded by the system. Instead, it results in reduced voltage at the load end, which mean a high current demand to maintain the power demand. The increased current in the transmission system further causes a more voltage drop and more active power loss in the transmission system. This aggravates the voltage instability problem in a cyclic trap.

This condition further worsens by the action of tap changers of the power transformers. A tap changer, when sensing low voltage at the load end, tries to adjust this low voltage by increasing its secondary current through number of turns adjustment. This current increment is problematic causing a more active power loss and a more voltage drop in the transmission system.

Poor reactive power management in the system, on the other hand, results in increased reactive voltage drops on the transmission system, aggravating both voltage limit violation and voltage instability [35]. Poor reactive power management has a double impact on system voltage security. The first it reduces the voltage profiles of load buses. The other effect is; it reduces the active power transfer limit of the load buses. Hence,

poor reactive power provision and its poor management endangers system voltage security.

Contingencies also can cause voltage instability by forcing transmission lines to carry power beyond their limits due to power flow rerouting in the network.

The voltage instability at a single bus gets reflected to the whole system, and may lead to cascading events which culminate in total system collapse [12]. Hence, voltage instability entails a high security concern that system operators need to ensure that the operating point is secure in terms of maintaining system voltage stability, following contingencies or system operating point change.

2.2. Power System Voltage Security Assessment

Maintaining power system voltage security is a crucial task of power system operators. By maintaining the voltage security, one can readily mitigate power interruptions which would, otherwise, have a detrimental penalty on economy.

The task of maintaining a safe distance from voltage collapse requires continuous voltage security checkups. The voltage limit violation component of voltage security requires a trivial identification that can be defined as within the limit or out of the limit by observing the bus voltage profiles. But the voltage stability component needs rigorous computational analysis. Due to this fact, the majority of the discussion, in this work, is devoted to voltage stability, while, voltage limit violation issue will be raised upon demand. In this work, one needs to understand speaking about voltage stability is speaking about voltage security.

Since our interest is to evaluate the nearness of the system to voltage insecurity, this work focuses on static voltage stability. Static voltage security assessment evaluates how far current operating point is from voltage insecurity [37].

So far, a number of methods and associated indices have been proposed by literature for assessing static system voltage security/ stability [38]. These indices focus on either load buses [39] or transmission lines [40] for detecting voltage instability.

2.3. Online Voltage Security Assessment Practices

The real time voltage security assessment mechanisms can be classified into two broad classes. The first class is one which use power flow analysis integrated with the energy management system (EMS) [41]. However, these methods are resented for being computationally intensive. This burden comes from the dependency of the techniques on repetitive power flow analysis until the point of loadability limit [13, 34, 42]. This situation contradicts with the primary requirement needed from the online assessment tools which is; fast computational capability to deploy instability prevention strategies before system fatality takes place.

Other class of techniques base their data source on fast real time measurements using systems such as SCADA and phasor measurement units (PMUs). This class enabled fast, model free computations to be carried out for the assessments, solving the problems posed by the class mentioned earlier [43]. The problem that arises in this class is the inevitable inaccuracy of the measurements. Some approaches in this class require considerable amount of measurement sets to be taken for the computation [44-46] which increases the time window of computation. This creates tradeoff between accuracy and processing time.

Here below some techniques devised for online voltage security/stability assessment are discussed.

2.3.1. Modal analysis technique

Voltage stability analysis using modal analysis of a reduced Jacobian matrix is first devised by [39] as a model-based approach. A number of literatures have dealt about the technique afterwards. The technique is still important both in industry and literature [47].

Voltage modal analysis technique's unique feature is, it sees system voltage and reactive power changes as a composition of modal entities. Voltage stability, in VQ-modal analysis technique, is studied based on modal voltage variations and modal reactive power variations, while other methods focus on actual bus voltage and reactive power variations. This method enables a capability of decoupling among modal quantities. By decoupling it is meant one modal voltage variation is only affected by reactive power variation of the same mode only. This avoids computational burdens that might have come due to

combined effects. This method also provides means of measuring the relative contribution of buses, transmission lines and generators to voltage instability.

There are some industrial real-time software tools that claim of using modal analysis as the core processor of voltage security analysis [48].

The issues raised on this approach include:

- It doesn't show the operational margin of the current operating state to the point of collapse [49].
- Each operating point needs modal analysis to be performed to assess voltage stability. This means large amount of computation is required until the point of collapse.
- The other problem is convergence issue near the point of collapse. The basics on modal analysis is an inversion of the sensitivity matrix. This inversion would go to infinite near the point of collapse.

2.3.2. Quasi steady state simulation

Quasi steady-state simulation is claimed to be fast time domain method for the analysis of long-term dynamic voltage stability phenomena [34]. The approximation relies on time-scale decomposition. The basics of this method is that faster phenomena can be represented by their equilibrium conditions instead of their full dynamics. This greatly reduces the complexity of the resulting model and hence provides the computational efficiency required to meet the constraints of an online application. There are global projects that claim use of this method for online voltage security assessment [35].

However, this approach being time domain analysis, each operating point along the operating time needs to be analysed using other methods for nearness to voltage instability. They are only used to see the trend of voltage reductions or boosts. This way they do not quantify nearness to voltage instability.

2.3.3. Extended-time local identification of voltage emergency situations

This measurement-based method is proposed by [50]. The method suited for online long-term voltage stability identification. This method uses locally available voltage measurements, which are easily accessible. The approach depends on taking measured

voltage data from the controlled, distribution side of the power transformers. Then a linear regression model is developed from the data taken using recursive least square method. A decreasing slop indicate the presence of long-term voltage instability, while a constant or positive slop being a normal state.

Coming to the critics, the first critic is based on the fact that not all voltage reductions are voltage instability conditions. Hence, normal reductions would wrongly be interpreted for voltage instability. Additionally, the method doesn't show the distance from instability. Only it identifies the presence of stability or instability.

2.3.4. Lyapunov exponent method

The Lyapunov exponent, a measurement-based method, is an idea taken from dynamical system analysis. The maximum Lyapunov exponent is the measure of the rate of separation between two trajectories in the system and used to investigate the presence of instability. If the maximum Lyapunov exponent is negative then the trajectories converge to a stable point of equilibrium. If the maximum Lyapunov exponent is positive then the trajectories are diverging, showing instability. For the voltage stability application, the exponent is computed as [51, 52]:

$$\lambda_i(k\Delta t) = \frac{1}{Nk\Delta t}\sum_{m=1}^{N} log\frac{||V_i\big((k+m)\Delta t\big) - V_i\big((k+m-1)\Delta t\big)||}{||V_i\big((m)\Delta t\big) - V_i\big((m-1)\Delta t\big)||} \qquad (2.1)$$

$V_i\big((m)\Delta t\big)$ – is the m[th] sample of voltage measurement at the i[th] bus. $\lambda_i(k\Delta t)$-the Lyapunov exponent at the i[th] bus at time $k\Delta t$, Δt-the sampling period, k-the count of the sampling period, N- the number of initial conditions.

This method is used to identify weakest buses in the system, as well. The bus with the largest Lyapunov exponent is the main contributor of the instability. The instability prevention approaches implemented at this bus has large stabilizing effect within the system. The method is further adapted for short-term voltage instability by making the comparison between measured voltage and reference voltage, produced with off-line studies to have fast detection [51].

This method shares the same critics with the method in section 2.3.3.

2.3.5. Spectrum estimation based stability indicator (SESI) [53]

This method begins from the representation of power flow equation using the Jacobian matrix. The difference values of voltages, currents and powers are computed from the measurement data. The index is based on the largest singular value of the Jacobian matrix. This index is computed using statistical methods from the set of measurements.

This method is dependent on the fast measurement so that it ensures there exists no alteration of the system setup between the measurements. However, alterations of the system setup are inevitable. This presents the first challenge. The other challenge this method faces is the presence of repetitive matrix multiplication through the algorithm process. This brings computational burden for the online application of the method. The third challenge is the computational burden that come with the inversion of the Jacobian matrix.

2.3.6. Voltage stability assessment algorithm (VSAA) [54]

This method bases on determining the maximum active power transfer based on the last three consecutive measurements. Whenever, a new measurement is recorded the P_{max} is recomputed. To avoid the oscillatory nature of the P_{max} the average value of the last P_{max} computations are taken. The method also considers the occurrence of large disturbances by omitting the pre-disturbance measurements and by utilizing new measurements.

The first question on this method is the method purely dependent on the load connected on the load bus not on the external supplying environment. It is well established that PV relations are pretty dependent on the external network setup. This setup includes the external system loading. Hence, assuming the external network to be unaltered contradicts with the huge variability of the external network.

2.3.7. Artificial neural network (ANN) based methods

There are papers that are proposing utilizing artificial neural techniques for application of online voltage security assessment [55-58]. In ANN approach there are two processes: the learning algorithm and the processing algorithm. The learning algorithm adapts the

weights based on all the input training vectors. The processing algorithm determines the output vector for any input vector.

The methods in this class have the problems of:

- The memory requirement and the processing time is significantly large for the large power system.
- Power system operation possess infinite set of operation points. Hence, training of the artificial neural network could not include all sets of operating points. Hence, the application comes across states where the voltage security could not be determined.

2.3.8. Voltage stability assessment index (VSAI)

This method is developed in [59], which is used to fill the gap that comes from the computational burden imposed by model-based approaches and limited availability of phasor measurement units within the system. Hence this method is a hybrid of model-based approaches and measurement-based approaches. This index computes the distance from voltage collapse using non iterative way. The method is a variant of Thevenin equivalent.

The implementation is, first, linearized Jacobian matrix is found from the network topological data and other system parameters. Using the Jacobian matrix system characteristics (i.e. current and voltage) of all buses are specified. Finally, the Thevenin equivalent is formulated from the measured data. The index for bus 'i' has the form:

$$VSAI_i = \frac{\left| Average\left\{\left(\frac{V_i - V_{i(+ve)}}{I_{i(+ve)} - I_i}\right), \left(\frac{V_{i(-ve)} - V_i}{I_i - I_{i(-ve)}}\right)\right\}\right|}{\left|\frac{V_i}{I_i}\right|} \tag{2.2}$$

The numerator of the index is the Thevenin equivalent, averagely computed from the measured data, while the denominator $\left|\frac{V_i}{I_i}\right|$, which is actual load impedance obtained from actual system parameters. V is the measured voltage and I is the measured current. The value of the index ranges between 0 and 1. The value close to one mean bus i is close to voltage instability, while values close to 0 indicate a more stable bus.

The challenges this approach faces are two, which are common in measurement-based approaches. The first is the alteration of system topology between measurements in this

approach alters the voltage and current relations which are required to be constant. Secondly, this method requires a minimum of four measurement sets which widens the time window of processing.

Generally, for online voltage stability application, a given method is required to be computationally efficient, so that the computation has to be performed with a minimum time. For this purpose, in this work, Thevenin Equivalent based class is selected for the development of an index. Thevenin equivalent based voltage stability assessment methods provide an advantage of low computational effort [12]. The expressions, used to represent Thevenin relations, are simple and computations can be performed with a minimum time [60].

2.4. Thevenin Equivalent Theory and Application to Power Systems

The Thevenin equivalent theory is widely known in basic circuit analysis and other application areas such as communication systems and power systems. The Theory says from a load point a given linear circuit can be represented by equivalent single voltage source and equivalent impedance. The equivalent voltage is designated as Thevenin equivalent voltage and the equivalent impedance is named as Thevenin equivalent impedance [61]. In this work, mostly, terminologies Thevenin voltage and Thevenin impedance, respectively, are used in short.

The Thevenin theorem visualizes the whole system, from the load, as a single power source and equivalent impedance as shown in Figure 2.3.

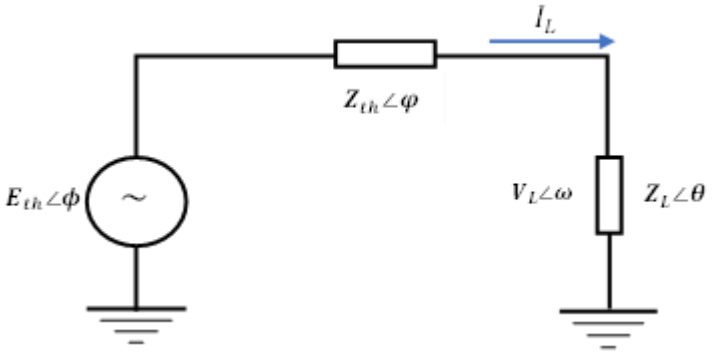

Figure 2.3: Thevenin equivalent representation of a power system from a load point

Thevenin equivalent theory is applicable for linear electric circuits. A given electrical circuit is linear when [62]:

1. The output of the sum of two signals is the same as the sum of the output of individual signals.
2. Scaling the input signal by some factor scales up the output by the same factor.

These two characteristics holds true for power system steady state analysis including power flow analysis. It is evident that steady state power flow analysis relays on common circuit analysis techniques that are devised for linear circuits. These techniques include super position principle and nodal analysis techniques. The Thevenin equivalent principle is no different.

However, nonlinearity consideration is emerging in modern power systems with the introduction of FACTs devices and renewable energy sources [63]. This will give a new future research direction whether the existing power system steady state analysis techniques still getting importance or other analysis approaches being followed [64].

Coming to Thevenin equivalent representation, power system circuit reduction techniques trace back from earlier works of [65]. Still network reduction techniques are given a wider acceptance in existing power system studies [66]. Thevenin equivalent based network reduction is still widely accepted in existing power systems, even in the presence of FACTS and renewable energy generations [60, 67]. Despite the importance of studying the impact of emerging nonlinearity, utilizing Thevenin equivalent method for power system study together with other power analysis approaches is still important. The continuing importance can be envisioned in the cited works at the next section.

2.5. Thevenin Equivalent Based VSA Methods

The application of Thevenin equivalent theory for voltage instability investigation has traces from the works by [68].

In Thevenin equivalent based voltage instability assessment approaches, there are two basic tasks. The first one is estimating the system equivalent Thevenin impedance and the second one is locating the critical point where the system enters to voltage instability (index formulation). The process of Thevenin impedance-based voltage stability assessment is shown in Figure 2.4

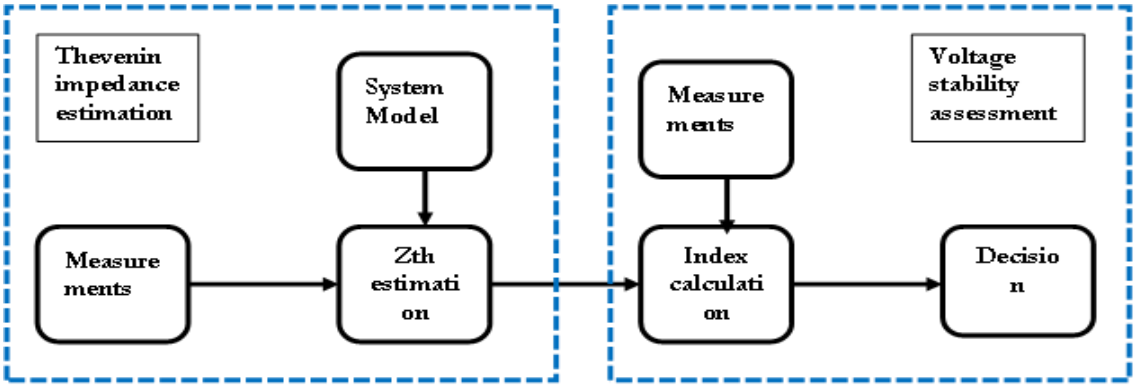

Figure 2.4: Thevenin equivalent based voltage stability assessment process

2.5.1. Thevenin Equivalent determination of a power system

This step of Thevenin equivalent based approaches is usually the easily bypassed component by most papers, but the difficult task. The difficulty arises from the large size of power systems, which makes Thevenin equivalent computations rigorous and time consuming.

The Thevenin equivalent impedance determination techniques, known so far, are either measurement based or model-based, or a mix of the two techniques.

The measurement-based approaches relay on the voltage and current measured at the load point. These techniques, without the consideration of the make-up of the system, uses the currents and voltages measured at the load point to calculate the Thevenin parameters [69, 70] [70-72]. These approaches promote the current and voltage measurements at a load point contain information about the Thevenin equivalent of the rest system.

In this class, however, four problems need to be taken into account.

Issue of large time window requirement is the first problem in this class. This class needs a minimum of two sets of measurements to compute the Thevenin impedance [70]. Some works, to increase the accuracy of estimation process, take large number of measurement sets for the calculation [73, 74]. This significantly increases the processing time, which is undesirable for online applications.

The other problem, this class comes across, is the issue of system topology change. Power systems may undergo system topology change between consecutive measurements. This presents wrong estimation of the Thevenin values. The works on this class assume the

system setup to be unaltered between two measurement sets [75, 76]. This assumption makes them to be unrealistic.

The third problem is; this class requires perturbation of values at the load point [70]. The perturbation gives two consecutive measurements with different values. However, at steady state times the consecutive measurements will have the same values. Hence, it becomes difficult to estimate the Thevenin equivalent at these times, creating vacancies.

One more issue with this class is; the measurement-based computations do not provide information on the Thevenin equivalent voltage, which is mandatory for computing the maximum active power transfer capability. This limitation hinders the works from developing power-based voltage stability indices, and got them limited to formulate their indices based on impedance, which show only the relative closeness to the critical point.

On the other class, model-based techniques make use of the system network model parameters to formulate the Thevenin equivalent parameters. These methods do not track the inherent system variability. They are only suitable for offline planning studies and applicable only for smaller size systems. Despite the size limitation, they can come up with accurate Thevenin equivalent estimations. This way of calculation is common in circuit systems analysis [61].

On the third class, the mixed approaches use suitable features from both classes aforementioned [77, 78]. This third approach splits the Thevenin impedance to variable and fixed components and determines fixed components using the network model and addresses varying components using measurements.

Fixed components, once calculated, will be saved and utilized whenever needed, until the next system topology change occurs. This once calculated values bring maximization of computational efficiency. Whilst, the variable components are continuously read from system measurements.

However, the mixed approaches, which are proposed to-date, has limitations due to approximations [79, 80]. Popular work in this regard is [81]. In this work, a detailed procedure under a concept named as coupled single port technique is proposed to determine the Thevenin impedance. The Thevenin impedance from this approach is, however, an approximated one.

Expanding the concept of coupled network technique, two approaches are proposed in [82] to get best approximation for the Thevenin impedance. However, the approximations, still, brought errors for different system states, for different bus locations and for different system load types [77].

The approximation arises from the inability to split a coupling term, which appears in the process of determining the Thevenin equivalent impedance.

In this regard, this dissertation work has solved the coupling problem by first finding the Thevenin equivalent voltage and subtracting it from the relation containing the coupling term. The Thevenin voltage is obtained from load flow analysis at the terminal where the load is removed. This is discussed latter in chapter 3.

This enabled to come across a new Thevenin equivalent impedance determination technique and development of a new voltage stability indices, which are suitable for online application. As a result, the work managed to readily remove the errors that arise from approximations.

Additionally, our method, differing from the measurement-based approaches which use a minimum of two measurement sets, uses a single measurement shot. This avoids:

- the problem that come from system topology change during the time window at which consecutive measurements are taken.
- the time required for recording two or more measurement sets. This capability comes without compromising the accuracy.
- limitation on computing the maximum active power transfer by providing the way to compute the Thevenin voltage.

2.5.2. Voltage stability index development

The second task of Thevenin based voltage stability assessment is locating the critical point where voltage instability occurs. This process is performed by developing an index that makes use of the results of the Thevenin equivalent determination process.

As explained in the basic concepts, voltage instability occurs when a system reaches at its maximum power delivery capacity. When a load bus requests power beyond this maximum capacity the system enters to voltage instability.

This concept is directly related with maximum power transfer theorem. Maximum power transfer theorem states; “The possible, maximum power that can be transferred to a load occurs when the load impedance matches with the apparent impedance of the supplying system under constant power factor” [61, 83].

$$|Z_{th}| = |Z_l| \tag{2.3}$$

The two impedances of (2.3) are utilized in two ways for the index development, in the literature. The first class of the indices is known by the name Impedance matching techniques.

In impedance matching techniques, the discrepancy between the load impedance and the Thevenin impedance is the basis for the index development. The closer the load impedance gets to the Thevenin impedance, the closer the system gets to voltage instability.

Under normal system condition, the load impedance is much larger than the Thevenin impedance seen by the load. When the load increases the load impedance decreases approaching to the Thevenin impedance. More power demand by the load, decreases the load impedance to the point where the two impedances meet. This point is where the maximum possible power will be transferred.

Increasing the demand beyond this point gets accompanied by decreased power transfer from the system. After this point, the more loaded the system gets, the less would be the power transferred to the load. This situation shows the entrance of the system to voltage instability [36] [84]. This concept is used for the development of a variety of indices in the literature [70].

The other class of indices uses the two Thevenin equivalent parameters, Thevenin impedance and Thevenin voltage, and calculates the maximum possible power transfer. These indices are power based indices. The concept, behind these indices, is the direct application of the maximum power transfer theorem. The difference between current power loading and the maximum possible power transfer is taken as indicator of closeness to voltage instability.

A method known as power matching is proposed by [85]. This work aimed at using a more characteristic expression of power margin than voltage margin or impedance margin. The rest of the approach is a variation of impedance matching technique. The maximum loadability is calculated by using the Thevenin impedance in [80] and apparent power-based index is developed. A method to formulate the Thevenin equivalent parameters and an index named as S-ZI index is developed by this work. This index depends on the derivatives of the load power to load impedance.

In this dissertation, using the result of the Thevenin impedance determination, two indices from both classes are formulated. The first is based on the impedance matching technique. However, the impedance matching based index only measure the relative closeness of the operating point to voltage instability. It does not show the necessary power margins to the point of collapse. Hence, to address the demand to know the power margins, additional index based on the active power margin is, also, introduced under the name active power margin index (PPMI). Additionally, other capabilities of the VSA scheme are realized using the results of the Thevenin impedance determination step. These capabilities include maximum power determination, PV and QV curve determination and reactive power margin determination.

2.6. Reactive Power Management in Power Systems

Reactive power provision improves the voltage stability of a power system by improving the maximum active power transfer capability of a transmission network [86]. Additionally, reactive power compensation minimizes the transmission reactive voltage drop, as a result giving improved voltage profile at the load points [28, 87]. Hence, both the voltage security demands, i.e voltage limit maintenance and voltage stability, can be ensured by managing the reactive power resources within the system.

The reactive power management scheme is proposed incorporating two components which are identified as fast reactive power management (FRPM) component and continuous reactive power management (CRPM) component.

2.6.1. Fast reactive power management (FRPM)

The reason for the need of this approach is fast action demand of contingent operating conditions. During contingency, optimization processes are too slow to be considered.

They require considerable processing time. Hence, the tools employing optimization couldn't respond timely for an urgency related to contingency. Hence, to address the urgency, using the developed VSA indices for identifying weakest buses and adjusting the reactive power supply is proposed as voltage security improving mechanism. Additionally, PV and QV curves are employed to visualize the nearness to voltage collapse point.

This way of reactive power management enables a fast reactive power allocation capability, which is critically needed during contingencies. The method is employed by most papers who focused on weakest bus identification and reactive power allocation [88] [89].

FRPM can be viewed as voltage stability index computation, while making reactive power compensation. Hence, it is important to note here that FRPM goes in tandem with VSA index calculation.

2.6.2. Continuous reactive power management (CRPM)

This component of reactive power management bases on reactive power optimization. The reason behind CRPM is from the idea; an optimized system is secured against an anticipated insecurity. The voltage security ensuring approach in CRPM is a preventive strategy. Reactive power management will be done ahead of contingencies.

The need to make the optimizations continuous, lays from the fact of occurrence of continuous system makeup change. The system makeup change can be due to topology changes or system loading changes. For CRPM purpose this work proposed an Improved Multi Objective Particle Swarm Optimization (IMOPSO).

Unlike FRPM which considers weakest buses, this class focuses on total voltage security improvement by taking the sum voltage security status of all system buses.

2.6.3. Reactive power optimization

Most times, reactive power optimization (RPO) is formulated as a single objective optimization problem, with such single objectives as loss minimization, operating cost minimization, voltage deviation minimization, etc [90-93]. However, the presence of

many objectives that need simultaneous RPO forced the treatment of the subject to employ multi objective optimization.

The two components of voltage security, i.e. ensuring voltage stability and voltage profile improvement, through reactive power management poses a two objective optimization problem.

Some researches that focus on RPO, thought to treat voltage stability from the objective function which is based on voltage profile deviation [94]. However, voltage profile deviation cannot always be indicator of voltage instability, for voltage unstable systems can have voltage profiles within the set limit [95]. This situation demands the inclusion of an objective function based on voltage stability indices. In this regard, the most utilized indices include static voltage stability margin [96, 97], fast voltage stability index [98], line loading index [99] and line stability index [100].

The other problem, that is observed in the inclusion of voltage stability to the objective function set, is a double inclusion of voltage stability issue to the set of objective functions, in the form of both transmission losses and stability indices [96, 100]. However, studies well established that transmission active power loss can be used as an indicator of voltage instability [13, 101].

In this regard, this dissertation begins the formulation of the voltage security objective function from the basic components of voltage security, i.e. voltage stability and voltage limit maintenance. These components are sufficient for identifying the voltage security level of the system.

Multi objective (MO) reactive power optimization problems, as a component of the general MO optimization problem, are solved using two ways. The first approach is converting a multi objective problem to a composite single objective problem. The single objective is expressed as a weighted sum of the individual objectives [97, 98]. This approach brings the issue of weight assignment for each objective, i.e. as to what amount of weight to assign for each objective.

The second way of solving multi objective optimization problems is based on the pareto optimality principle, which comes up with a number of solutions with equal chance to be chosen. The set of the optimal solutions is identified as pareto optimal solution or pareto

front (PF). According to pareto optimality principle, in the PF no solution is superior than the other [94, 100]. The selection of the PF member is done based on the principle of dominance.

A number of evolutionary optimization algorithms are employed to solve multi objective reactive power optimization problems. Particle swarm optimization [102], genetic algorithm family techniques [103] , differential evolution [100], multi objective immune system [96] are some to mention.

Despite applying the multi objective evolutionary algorithms to handle reactive power optimization problems, investigations to improve the performance of these algorithms, as applied to reactive power optimization are rare. As a general study of multi objective optimization algorithms, there are studies made to improve their performance [104, 105].

In this work, multi objective particle swarm optimization (MOPSO) algorithm is chosen for handling our problem. Particle swarm optimization is a meta-heuristic nature inspired optimization algorithm, whose application is important in a number of fields [12]. The inspiration of PSO comes from the cooperation behaviour displayed by bird flocks and fish schooling in food search. The heuristic nature comes from the dependence of the search on self-experience and the group best experience. Particle swarm optimization is known for fast convergence, robust adaptability and relative simplicity for implementation [94] [106, 107].

The problem with PSO is convergence to the false optimal positions. In the case of MOPSO, this problem is seen affecting the quality of the pareto front [108, 109]. To address this problem, introducing a disturbance to bypass false traps is proposed as a solution by literature [110, 111]. This improves the quality of the pareto front.

As a means of improving the quality of the pareto front and improving the convergence speed, this dissertation introduced a disturbance based on adapted binary crossover (ABX), which is adapted from [112, 113]. Previously, as a means of avoiding premature convergence, different crossover techniques are introduced to PSO in works [114-116]. However, these works focused on a single objective optimization. This creates a need to study the performance of applying crossover to multi objective PSO. In this regard, this part of the dissertation work differs from them in applying the crossover to MOPSO and in uniquely applying adapted binary crossover (ABX) to MOPSO.

In our algorithm, i.e. Improved MOPSO (IMOPSO), positions are, initially, created using normal PSO position estimation technique. Then, ABX technique is applied to these positions to create more potential solution set. The newly searched positions are, then, mixed with the original positions and best positions are selected from this merged group based on dominance and crowding distance. The introduction of crowding distance to MOPSO is used as a diversity maintenance strategy.

The performance of IMOPSO is evaluated using ZDT1, ZDT2 and ZDT3 test functions [117]. The method used for performance evaluation is inverted generational distance (IGD) and crowding distance. The IGD shows the quality of the pareto front in terms of closeness to the true pareto front [118-120], and the CD measures the diversity of the PF. The result is compared with popular algorithms of standard MOPSO and NSGA II algorithms. The comparison shows an improved performance of IMOPSO over MOPSO and NSGA II algorithms. The algorithm is, then, applied to IEEE 14 bus test system and EEP system reactive power optimization with the objective of improving the voltage deviation and voltage stability. The method effectively identified the optimum value of the control variables. With these optimum settings voltage deviation and voltage stability are seen improved.

The unique contributions of this part of the dissertation are;

- an improved algorithm (IMOPSO) that shows improved performance over standard MOPSO and NSGA II algorithms.
- application of the developed algorithm to reactive power optimization of IEEE 14 bus and EEP power system for improving voltage security.
- an improved formulation of the voltage security based objective functions, in a way avoiding the discrepancies seen in the formulation by previous works.

CHAPTER 3 DEVELOPMENT OF VOLTAGE SECURITY ASSESSMENT AND REACTIVE POWER MANAGEMENT SCHEMES

The construction of VSA and RPM schemes begins from the development of Thevenin impedance determination technique. In this work, the Thevenin impedance determination technique development begins from analysis of gaps of the previous approaches. This helps to understand the improvements that come with the new Thevenin impedance determination method. The Thevenin impedance determination results are then used for the development of the voltage security assessment indices and the associated PV and QV graphs. In the case of RPM scheme, the formulation of IMOPSO algorithm is discussed in this chapter.

3.1. Coupled Single Port Circuit Based Thevenin Equivalent Determination

According to [78] a power system which is, evidently, a multi-port network can be represented by single port Thevenin equivalent at a load bus. In this work, the impact of other loads on the voltage profile of a given bus is represented by a coupling term. This approach is named as coupled single port approach for this reason.

Coupled single port circuit approach is the direction of research in this dissertation for the method being a more progressed and organized one in the thematic area of Thevenin impedance determination. However, the approach comes across a fundamental issue, which needs further consideration. The issue is the inability to decompose the coupling term that arise through the process of Thevenin impedance determination.

The inability to decompose this coupling term hinders the previous works from coming with accurate Thevenin representation of a system and makes them relay on approximate Thevenin equivalent proposals. This part of the dissertation, hence, focuses on decomposing the coupling term and coming with more accurate Thevenin equivalent parameters.

The following sections introduce coupled single port circuit approach and show the gaps that come with approximate Thevenin equivalent representations of the approach. For ease of discussion, the expression “coupled single port circuit” is shortened as ‘coupled

circuit', here after. For Thevenin equivalent representation is known to be single port circuit, omitting the term 'single port' doesn't create a discrepancy.

3.1.1. Coupled circuit based Thevenin impedance determination

Coupled circuit based Thevenin impedance determination starts from classifying system busses as generator buses (G), load buses (L) and tie buses (T). A tie bus is a bus where there is no current absorption or injection. Using nodal circuit representation and grouping the equations to the three bus groups, (3.1) is set up.

$$\begin{bmatrix} -I_L \\ 0 \\ I_G \end{bmatrix} = \begin{bmatrix} Y_{LL} & Y_{LT} & Y_{LG} \\ Y_{TL} & Y_{TT} & Y_{TG} \\ Y_{GL} & Y_{GT} & Y_{GG} \end{bmatrix} \begin{bmatrix} V_L \\ V_T \\ V_G \end{bmatrix} \tag{3.1}$$

Where I_L is the load current vector, I_G generator current vector, V_L-load bus voltage vector, V_T- tie bus voltage vector, V_G- generator bus voltage vector, Y_{LL}admittance matrix among load buses, Y_{TT} admittance matrix among tie buses, Y_{GG} admittance matrix among generator buses, Y_{LT}, Y_{TL}, Y_{LG}, Y_{GL}, Y_{GT}, Y_{TG} admittance matrices among the respective entities.

The regrouping of load buses in this equation produces a more convenient arrangement of the admittance matrix for latter utilization.

Expanding (3.1) and eliminating the tie bus voltage from the equations, give the relation between generator bus voltages and load bus voltages, transferred by a transmission network representing parameter.

From the first equation of (3.1) it can be drawn:

$$V_L = -Y_{LL}^{-1}(Y_{LT}V_T + Y_{LG}V_G) - Y_{LL}^{-1}I_L \tag{3.2}$$

From the second equation of (3.1) V_T is expressed as;

$$V_T = -Y_{TT}^{-1}(Y_{TL}V_L + Y_{TG}V_G) \tag{3.3}$$

Substituting (3.3) to (3.2) and rearranging, results the following;

$$V_L = (Y_{LL} - Y_{LT}Y_{TT}^{-1}Y_{TL})^{-1}(Y_{LT}Y_{TT}^{-1}Y_{TG} - Y_{LG})V_G - I_L(Y_{LL} - Y_{LT}Y_{TT}^{-1}Y_{TL})^{-1} \quad (3.4)$$

Concisely expressing this equation gives the form;

$$V_L = E_{open} - Z_{LL}I_L \quad (3.5)$$

Where:

$$Z_{LL} = (Y_{LL} - Y_{LT}Y_{TT}^{-1}Y_{TL})^{-1}$$

$$E_{open} = Z_{LL}(Y_{LT}Y_{TT}^{-1}Y_{TG} - Y_{LG})V_G = KV_G$$

E_{open} is the generator voltage as seen by the load buses. For this reason, this work alternatively uses the term 'transferred generated voltage'. *K* is a transfer function, which is, solely, determined from the transmission parameters.

Expanding the expression (3.5) for a single bus i gives;

$$V_{Li} = E_{open,i} - Z_{LLii}I_{Li} - \sum_{j=1, j\neq i}^{nl} Z_{LLji}I_{Lj} \quad (3.6)$$

nl- is the number of load buses.

The term $\sum_{j=1,j\neq i}^{nl} Z_{LLij}I_{Lj}$ is a coupling voltage drop term and the focus point of this research. The coupling term shows the influence of loads at other buses on the Thevenin parameters at the bus of concern. This coupling term should be carefully examined for finding accurate E_{th} and Z_{th} representation.

Letting the coupling term;

$$E_{couple,i} = \sum_{j=1, j\neq i}^{nl} Z_{LLji}I_{Lj} \quad (3.7)$$

Taking this and (3.6) gives;

$$V_{Li} = E_{open,i} - E_{couple,i} - Z_{LLii}I_{Li} \quad (3.8)$$

From the Thevenin circuit of Figure 2.3 the load voltage can be formulated as;

$$V_{Li} = E_{thi} - Z_{thi} I_{Li} \tag{3.9}$$

Substituting this to (3.8) will give;

$$E_{thi} - Z_{thi} I_{Li} = E_{open,i} - E_{couple,i} - Z_{LLii} I_{Li} \tag{3.10}$$

In this equation, even if the two sides are equivalent, setting equivalence between individual terms is difficult, due to the coupling term that exists on the right side of (3.10).

[78] [82] tried to solve the coupling issue through approximate method. Next, approximate models developed by these works are shown.

Accordingly, using (3.10) the results of the first approximate model are;

$$E_{thi} \approx E_{open,i} - E_{couple,i} \tag{3.11}$$

$$Z_{thi} \approx Z_{LLii}$$

This method lumps the coupling term with the Thevenin voltage and constructs the Thevenin impedance purely from the transmission impedances.

Coming to the second approximate model, using (3.5);

$$V_{Li} = \sum_{j=1}^{ng} K_{LGij} V_{Gj} - \sum_{j=1}^{nl} Z_{LLij} I_{Lj} \tag{3.12}$$

ng- is the number of generator buses.

Some manipulations give;

$$V_{Li} = \sum_{j=1}^{ng} K_{LGij} V_{Gj} - \left(\sum_{j=1}^{nl} \frac{Z_{LLij} I_{Lj}}{I_{Li}} \right) I_{Li}$$

$$V_{Li} = \sum_{j=1}^{ng} K_{LGij} V_{Gj} - \left(\sum_{j=1}^{nl} Z_{LLij} \frac{S_{Lj}^*}{S_{Li}^*} \frac{V_{Li}^*}{V_{Lj}^*} \right) I_{Li} \tag{3.13}$$

Setting equivalence between (3.13) and (3.9), the second approximate model gives;

$$Z_{thi} = \sum_{j=1}^{nl} Z_{LLij} \frac{S_{Lj}^*}{S_{Li}^*} \frac{V_{Li}^*}{V_{Lj}^*} \tag{3.14}$$

The Thevenin voltage is, also, approximated by;

$$E_{thi} = \sum_{j=1}^{ng} K_{LGij} V_{Gj} \tag{3.15}$$

Equations (3.14) and (3.15) give the second model to represent approximate Thevenin equivalent parameters. This second model, differing from the first model, lumps the coupling term to the Thevenin impedance term. Seeing (3.14), Thevenin impedance determination this way, can be hence a mix of model-based approach and measurement-based approaches. Z_{LLij} and K_{LGij} are topological terms that can be computed from the system model while V_{Li}, I_{Li} are quantities that can be found either from system measurements or from power flow computations.

3.1.2. Characteristics of the coupled circuit parameters

Before solving the problem of coupling investigating the coupled circuit terms that appear in the previous derivations helps to understand the nature of coupling. For this purpose, IEEE 14 bus test system is chosen. Here, below, the investigations are made for different parameters under different system loading conditions.

i) Short circuit impedance drop, Esc

The short circuit impedance drop is the term $Z_{LLii} I_{Li}$ of (3.8). Z_{LLii} is the diagonal element of the impedance matrix Z_{LL} and is similar to the impedance seen by bus i when all loads are short circuited. That is why it is named as short circuit impedance drop. This drop is dependent on the amount of the load on the target bus and Z_{LLii}.

The short circuit impedance drop is plotted for IEEE 14 bus load buses below in Figure 3.1. Based on this figure, the E_{sc} drop for all the buses shows increment with increasing self-load. If the loading of the target bus is not changing E_{sc} keeps constant, i.e. not affected by loading of other buses. Bus 9 and bus 14 has almost a similar E_{sc}. The loading on these buses is different. However, multiplication between the impedance Z_{LLii} and the load current produced a balancing effect. The highest short circuit drop is of these two buses. The lowest drop is for bus five, due to minimum values of both the load current and Z_{LLii}. This totally indicates the short circuit drop depends on the load of the target bus and the specific location of the load bus, which is expressed in terms of the network parameter Z_{LLii}.

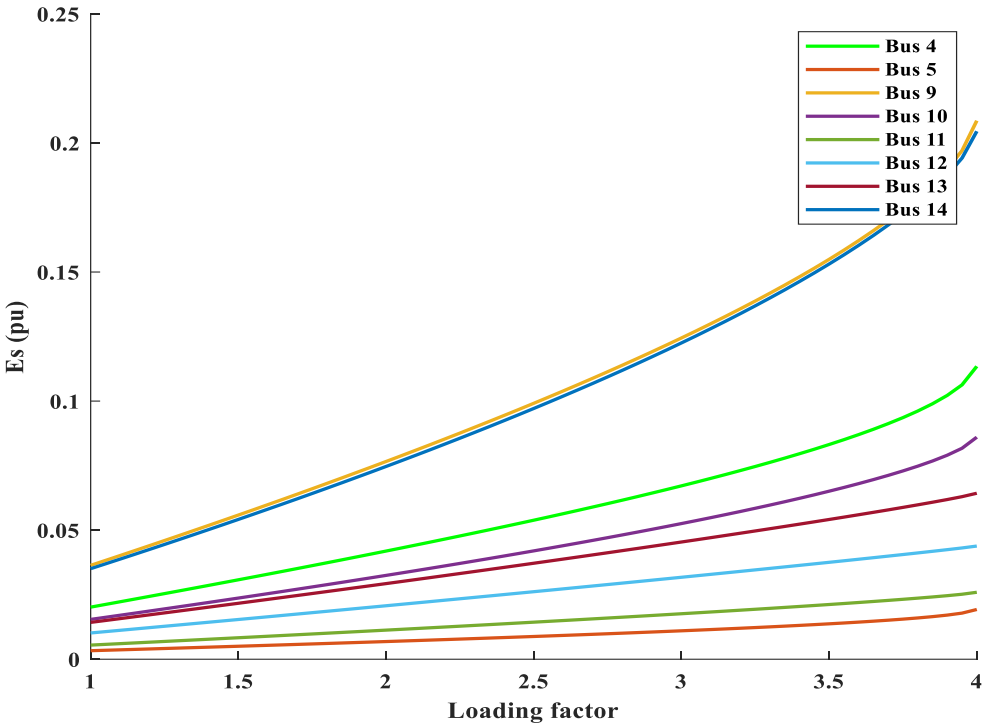

Figure 3.1: Short circuit impedance drop of the load buses

ii) Transferred generated voltage (E_{open})

The transferred generated voltage is represented by $\sum_{j=1}^{ng} K_{LGij} V_{Gj}$ from (3.5). This entity is the generator voltages as seen by the load buses. This voltage is dependent on the network model dependent parameter, K_{LGij}.

K_{LGij} values for the IEEE 14 bus system are shown in Table 3.1. Individual K_{LGij}, values are far much less than 1pu. These values are dependent on the network model. Different load buses have different values of voltage transfer constant, according to their unique positions in the network.

An important finding this parameter showing is that as load points get far from the generator, the voltage transfer constant gets small. This means the voltage has to pass a more voltage drop path before reaching the bus of concern.

Having seen the characteristics of the voltage transfer constant, the transferred generated voltages for the 14-bus test system are shown in Figure 3.2, below. The lowest transferred voltages attribute to buses 4 and 5.

Table 3.1: Voltage transfer constant for different load buses

Gen. bus / Load bus	1	2	3	6	8
4	0.1148+0.0026i	0.3736+0.0283i	0.2317+0.0266i	0.1689 - 0.0221i	0.1043 - 0.0348i
5	0.1888+0.0017i	0.3771+0.0354i	0.1416+0.0226i	0.2161 - 0.0391i	0.0651 - 0.0186i
9	0.0498- 0.0059i	0.1634- 0.0107i	0.1019- 0.0027i	0.3934 + 0.0762i	0.3197 - 0.0606i
10	0.0411- 0.0053i	0.1350- 0.0103i	0.0842- 0.0032i	0.4994 + 0.0686i	0.2637 - 0.0531i
11	0.0211- 0.0032i	0.0692- 0.0067i	0.0432- 0.0025i	0.7437 + 0.0405i	0.1348 - 0.0300i
12	0.0036+0.0001i	0.0118+0.0010i	0.0073+0.0009i	0.9559 - 0.0011i	0.0235 - 0.0009i
13	0.0072- 0.0012i	0.0236- 0.0027i	0.0148- 0.0011i	0.9125 + 0.0153i	0.0460 - 0.0110i
14	0.0313- 0.0040i	0.1026- 0.0078i	0.0640- 0.0024i	0.6196 + 0.0519i	0.2004 - 0.0402i

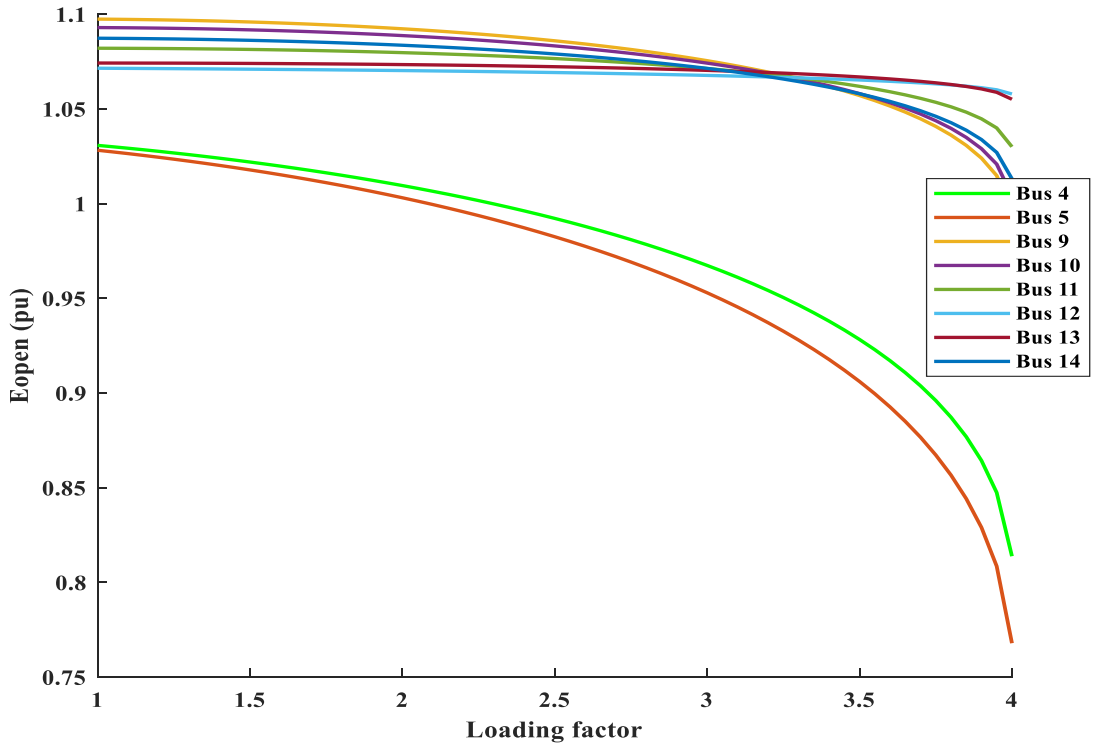

Figure 3.2: Transferred generated voltages of the load buses

The impact of each generator on $\boldsymbol{E_{open}}$ of a given load bus depends on the voltage transfer constant and the voltage outputs of generators. The amount of the load within the system or the load on the target bus has no impact on the Transferred generated voltage.

iii) Coupling voltage drop term ($\boldsymbol{E_{coupling}}$)

The coupling voltage drop term is noted in previous sections to be the term $\sum_{j=1,j\neq i}^{nl} Z_{LLji} I_{Lj}$. This term shows the impact of other loads and the apparent impedance between the bus of concern and other buses, represented by Z_{LLji}, on the voltage profile of the target bus i. $\boldsymbol{E_{coupling}}$ entails the meaning; loading of each bus affects system voltage in the form of a distributed voltage drop by the factor of Z_{LLji}. Having high load at other load buses results in voltage reduction at the target bus. In other words, voltage drop due to any load increment in the system is shared among other load buses. This is shown by (3.8).

The characteristic of $\boldsymbol{E_{coupling}}$ under different system loading is shown in Figure 3.3, below, for the IEEE 14 bus system.

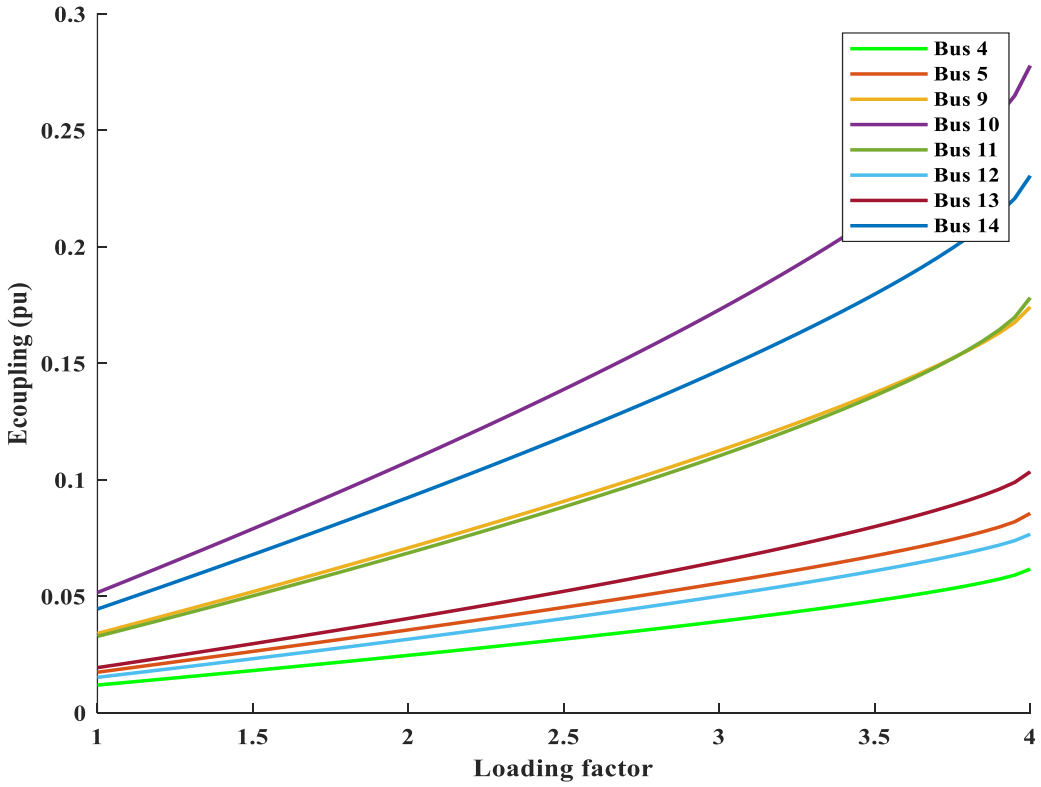

Figure 3.3: Coupling voltage drop characteristic of the load buses

Accordingly, $\boldsymbol{E_{coupling}}$ increases as system loading increases. The effect of coupling is high on buses 10 and 14. The effect of coupling on bus 11 and bus 9 is the same for this particular case. Additionally, the lowest coupling impact is on bus 4 and bus 12, respectively.

In this work, the contribution of the other loads on the coupling term of a given target bus is quantified by a coefficient named as Impact of Coupling (IC). According to this coefficient, the impact of bus j load on bus i voltage profile is measured as;

$$IC_{i,j} = \frac{|Z_{LLij} I_{Lj}|}{\sum_{\substack{k=1 \\ k \neq i}}^{n} |Z_{LLik} I_{Lk}|} \tag{3.16}$$

For IEEE 14 bus system, the impact of coupling, calculated at the nominal load, is shown on Table 3.2 following. For depiction purpose this data is shown by the following bar graphs of Figure 3.4.

A load bus cannot influence itself. The zeros along the diagonal of Table 3.2. show this fact. The highest coupling impact is on bus 5 by bus 4 and the lowest coupling impact is on bus 5, too, by bus 12. The extreme coupling impacts occurs at bus 5.

The other important point that can be seen from this result is; for the majority buses, the highest coupling impact comes from the neighbouring loads.

Table 3.2: Impact of coupling on the voltage profile of target bus

Impacting bus j / Target bus i.	**4**	**5**	**9**	**10**	**11**	**12**	**13**	**14**
4	0	0.1655	0.4949	0.1300	0.0244	0.0067	0.0314	0.1472
5	0.6660	0	0.1981	0.0520	0.0098	0.0027	0.0126	0.0589
9	0.2546	0.0253	0	0.2756	0.0517	0.0141	0.0665	0.3120
10	0.1397	0.0139	0.5756	0	0.0555	0.0077	0.0365	0.1711
11	0.1126	0.0112	0.4642	0.2383	0	0.0062	0.0294	0.1380
12	0.0417	0.0041	0.1719	0.0452	0.0085	0	0.4645	0.2641
13	0.0658	0.0065	0.2711	0.0712	0.0134	0.1556	0	0.4164
14	0.1228	0.0122	0.5062	0.1329	0.0250	0.0352	0.1657	0

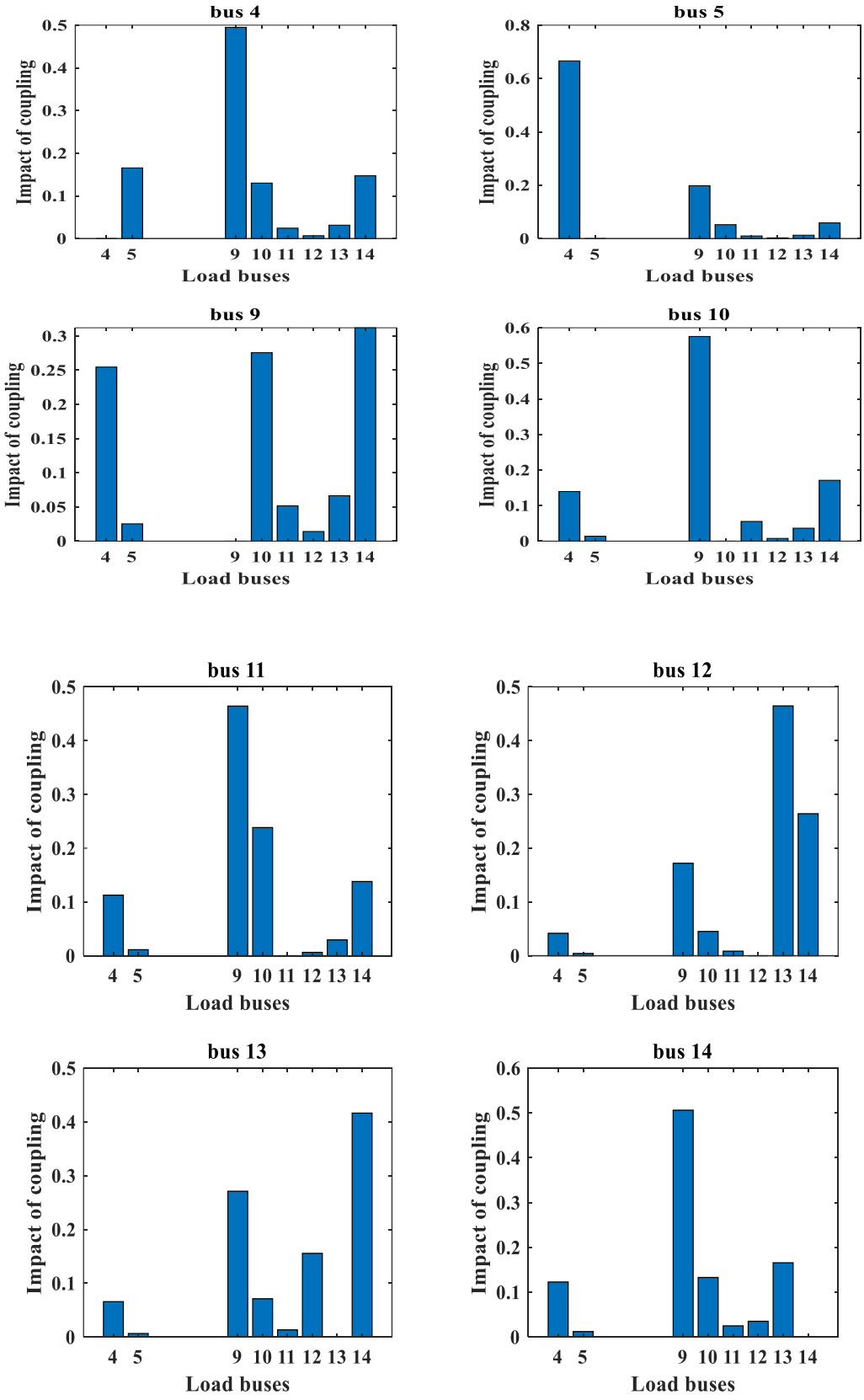

Figure 3.4: Impact of coupling of different load buses

Based on Figure 3.4. the impact of coupling for buses bus 9, bus 13, and bus 4, respectively, comes from large number of buses. On the other hand, the coupling impact for bus 5, bus 10 and bus 12 comes from relatively few buses. The impact of coupling depends on the distance between the influencing bus and target bus, and the load on the influencing bus.

The contribution of a given bus for the system coupling is quantified by the sum of impact of coupling in the following Table 3.3.

Table 3.3: Contribution of load buses for coupling impact

Bus	**Bus 4**	**Bus 5**	**Bus 9**	**Bus 10**	**Bus 11**	**Bus 12**	**Bus 13**	**Bus 14**
Total influence	1.4032	0.2388	2.6820	0.9453	0.1882	0.2282	0.8066	1.5077

The buses contributing much for the coupling are buses 9, 14, and 4, respectively. These buses have high loading in the order bus 4, bus 9 and bus 14. The order of contribution is not maintained based on the loading order due to the other contributor, the impedance matrix Z_{LL}.

3.1.3. Performance of the approximate models under different loading condition

In order to study the performance of the two models mentioned in section 3.1.1, a simple three bus test system, shown in Figure 3.5 below, is used. Our investigation considers load 2 terminal as a target bus. The evaluation of the models is made in comparison with the actual Thevenin impedance.

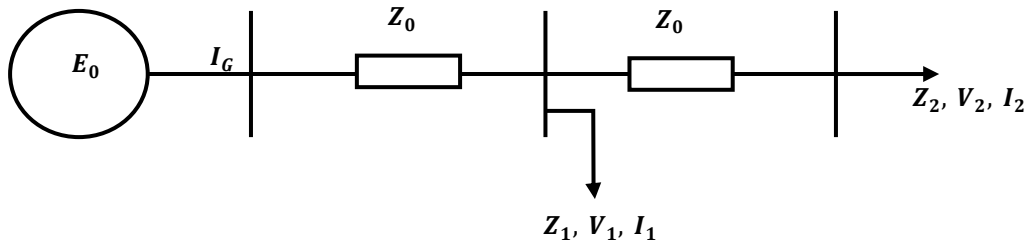

Figure 3.5: Three bus test system

Here below, the performance of the two models under different system loading is studied.

i) **Approximate model 1:**

For the particular simple network of Figure 3.5, the form of (3.1) can be written as;

$$\begin{bmatrix} -I_1 \\ -I_2 \\ I_G \end{bmatrix} = \begin{bmatrix} \frac{2}{Z_0} & -\frac{1}{Z_0} & -\frac{1}{Z_0} \\ -\frac{1}{Z_0} & \frac{1}{Z_0} & 0 \\ -\frac{1}{Z_0} & 0 & -\frac{1}{Z_0} \end{bmatrix} \begin{bmatrix} V_1 \\ V_2 \\ E_0 \end{bmatrix} \quad (3.17)$$

From this matrix the submatrices can be determined as;

$$Y_{LL} = \begin{bmatrix} \frac{2}{Z_0} & -\frac{1}{Z_0} \\ -\frac{1}{Z_0} & \frac{1}{Z_0} \end{bmatrix}$$

$$Y_{LT} = Y_{TL} = Y_{TT} = Y_{TG} = Y_{GT} = Y_{GG} = 0$$

$$Y_{GL} = \begin{bmatrix} -\frac{1}{Z_0} & 0 \end{bmatrix}$$

$$Y_{LG} = \begin{bmatrix} -\frac{1}{Z_0} \\ 0 \end{bmatrix}$$

Hence from (3.5);

$$\mathrm{Z_{LL}} = \mathrm{Y_{LL}}^{-1} = \begin{bmatrix} \mathrm{Z_0} & \mathrm{Z_0} \\ \mathrm{Z_0} & 2\mathrm{Z_0} \end{bmatrix}$$

$$E_{open} = -Z_{LL} Y_{LG} E_0 = \begin{bmatrix} 1 \\ 1 \end{bmatrix} E_0$$

From (3.6) it can be shown;

$$V_2 = E_0 - 2Z_0 I_2 - Z_0 I_1$$

$$V_1 = E_0 - Z_0 I_1 - Z_0 I_2$$

For this study the point of consideration is the terminal for load 2. Hence, the Thevenin equivalent impedance of the model will become;

$$Z_{eq} = 2Z_0 \quad (3.18)$$

It is important to note here that, based on this result, the approximate Thevenin equivalent Z_{eq} is constant for any system loading conditions, i.e. it depends only on transmission impedance.

For comparison purpose, the actual Thevenin equivalent impedance is calculated from circuit analysis techniques as;

$$Z_{th} = Z_0 + \frac{Z_0 Z_1}{Z_0 + Z_1} \tag{3.19}$$

From the two equations (3.18) and (3.19), it can be shown Z_{eq} is the upper limit for Z_{th}. However, to understand the nature of relation for wider ranges of load values we developed the following plots using Matlab.

For this purpose, values $Z_0 = 1 + j0.2\ p.u.$ and $E_0 = 1\ p.u.$ are used. Using (3.18) and (3.19) a Matlab plot is developed on the same axis for various values of Z_1. The approximate Thevenin impedance and the actual Thevenin impedance are shown in figure 3.6 below.

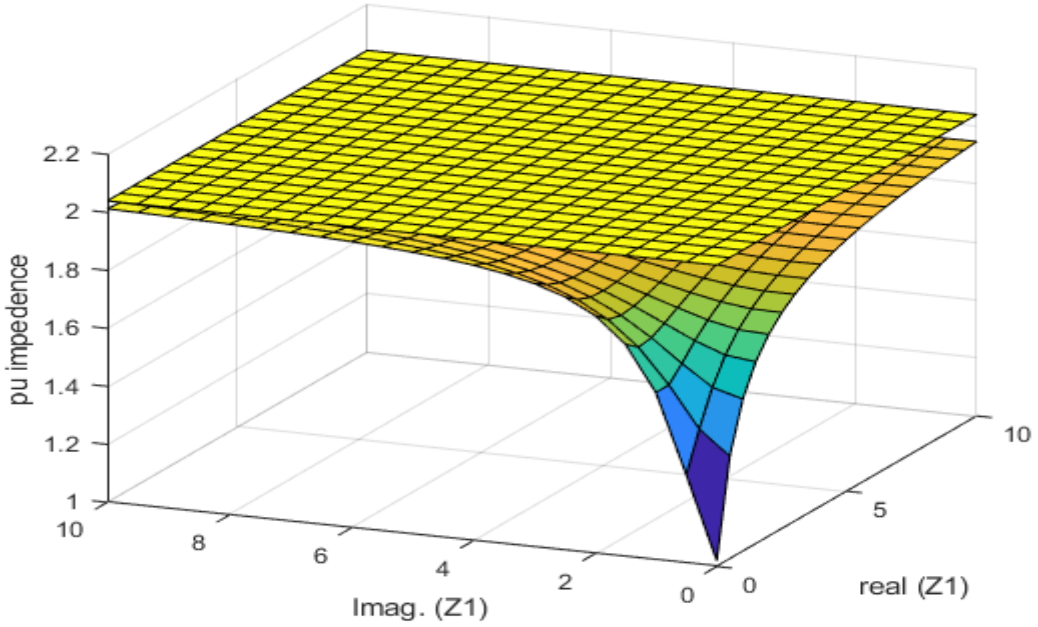

Figure 3.6: Approximate and actual Thevenin impedances for model 1 (top approximate, bottom actual)

From this plot, it is seen, the approximate model 1 produces the upper limit for the actual Thevenin equivalent, as it is noted, previously. For higher values of system impedance, i.e. low system load condition, the model produces a closer value to the actual value.

When the system impedance becomes very low, i.e. high system load condition and the critical case, the discrepancies between the approximate and the actual Thevenin impedances become wide. This time utilizing the approximate Thevenin equivalent for stability assessment could lead erroneous results.

ii) **Approximate model 2**

This approximation relays on (3.13). In this model, the coupling term is taken as part of the Thevenin impedance rather than the Thevenin voltage, as opposing to approximate model 1 above.

For our specific simplified circuit, (3.13) will get the form;

$$V_{L2} = \sum_{j=1}^{1} K_{LG2j} V_{Gj} \; - \left(\sum_{j=1}^{2} Z_{LL2j} \frac{S_{Lj}^*}{S_{L2}^*} \frac{V_{L2}^*}{V_{Lj}^*} \right) I_{L2} \tag{3.20}$$

Computing the network dependent parameters from (3.5);

$$K_{LG} = Z_{LL}(Y_{LT} Y_{TT}^{-1} Y_{TG} - Y_{LG}) = -Z_{LL} Y_{LG} = \begin{bmatrix} 1 \\ 1 \end{bmatrix} \tag{3.21}$$

$$Z_{LL} = {Y_{LL}}^{-1} = \begin{bmatrix} Z_0 & Z_0 \\ Z_0 & 2Z_0 \end{bmatrix}$$

Substituting these values to (3.20);

$$V_{L2} = E_0 \; - \left(Z_0 \frac{S_{L1}^*}{S_{L2}^*} \frac{V_{L2}^*}{V_{L1}^*} + 2Z_0 \right) I_{L2} \tag{3.22}$$

In this case the approximate Thevenin impedance and Thevenin voltage would become;

$$Z_{theq} = Z_0 \frac{S_{L1}^*}{S_{L2}^*} \frac{V_{L2}^*}{V_{L1}^*} + 2Z_0 \tag{3.23}$$

$$E_{th,eq} = E_0$$

Using some computations impedance term Z_{theq} is modified as;

$$Z_{theq} = Z_0 \frac{Z_0 + Z_2}{Z_1} + 2Z_0 \tag{3.24}$$

To see the trend of this approximate value, Z_2 is kept constant since we are interested on the impact of the system impedance, Z_1. For the approximate Thevenin impedance and actual Thevenin impedance the following graph in Figure 3.7. is shown. In similar way with the previous approximate model, the graph shows for higher values of system load (low Z1 value) the approximate and the actual Thevenin impedance show large discrepancy. Hence, this approximate model introduces a more error at these regions.

Despite being popular approaches in the theme, the models presented has the following weaknesses;

1. The first problem with these models is; they show large discrepancy with the actual Thevenin impedance during critical operating points. The critical operating points are high loading conditions, where voltage security problems are much likely to occur. This creates reasonable reservation from using these models for voltage security assessment. However, it is important to note that the models laid an important direction for a more modified method to be researched.

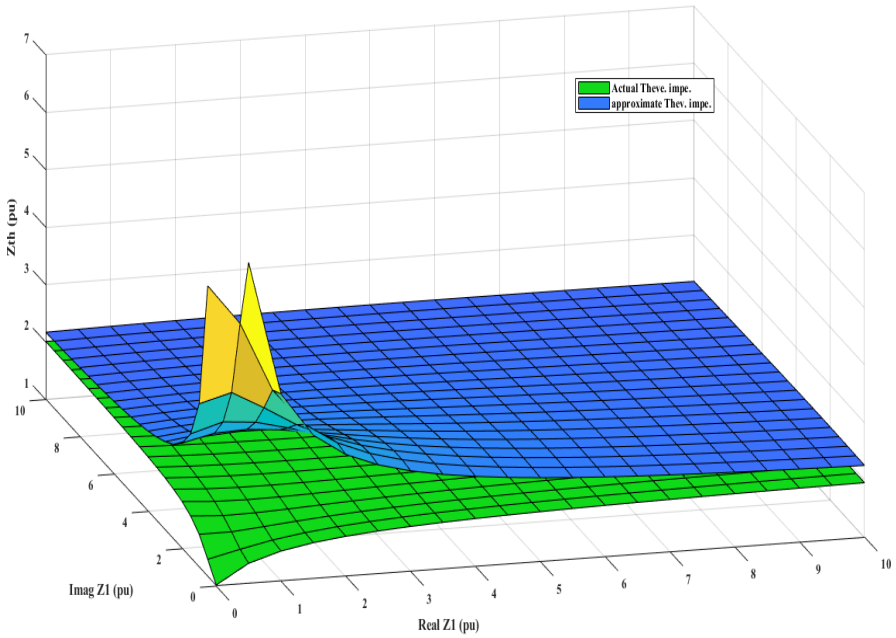

Figure 3.7: Approximate and actual Thevenin impedances for model 2 (top approximate, bottom actual)

2. The Thevenin impedance approximation in the first model fully depends on the system transmission matrix. It excluded system loading for computing the Thevenin equivalents. The exclusion of the loads from calculating the Thevenin equivalent contradicts with what a Thevenin equivalent actually mean. The model should have included loads for the calculation of the Thevenin impedance. In the second model, even if system loading is included, the proportion the system load included is quite erroneous as shown by the previous graphs.
3. Some research works, also show the performance of these models is varying for different bus locations in a system [82]. Some buses show close values to the actual Thevenin equivalents, but for the other buses these approaches show intolerable difference with the actual value. This puts confident utilization of the models in question.

With the view of these identified gaps and the gaps of measurement based Thevenin equivalent determination techniques, the next section is devoted in filling the gaps through producing a more dependable Thevenin equivalent parameters determination technique.

3.2. New Thevenin Equivalent Determination Technique for Online Application

The new Thevenin equivalent determination technique for online application has the following features.

- It requires both the network model and measurements of currents and voltages.
- The measurement required is a single snapshot of current and voltage, improving the requirement of minimum of two sets of readings of the measurement base methods.
- Except the inherent iteration errors that will come from the power flow computations, the new method enables to find accurate Thevenin impedance values.

As it is stated in the previous sections, the coupling term that arise in the process of determining the Thevenin parameters brought a problem to find accurate Thevenin impedance. This is due to the inability to separate the term to Thevenin equivalent impedance and to Thevenin equivalent voltage. Here bellow, the procedure this problem is solved is shown.

The first step in this approach is determining the Thevenin equivalent voltage. The common way of determining Thevenin equivalent voltage is disconnecting a load and measuring the voltage at the terminals where the load was connected. This is adapted from common circuit systems analysis [61]. Hence, the voltage at the load bus when the supplied load is disconnected is the Thevenin equivalent voltage.

When a load is disconnected from the target bus, it becomes a tie bus. Hence (3.1) would get modified in a way the number of load buses decreases by one and the number of tie buses increases by one. Only the number of generator buses remains unchanged.

For this new setup, determining the voltage of the newly added tie bus using power flow analysis is finding the Thevenin equivalent voltage for the target bus.

Now, from the first equation of (3.1) it is found;

$$-I'_L = Y'_{LL}V'_L + Y'_{LT}V'_T + Y'_{LG}V_G \tag{3.25}$$

The primes are the new parameters after converting the load bus to tie bus.

Rearranging this equation;

$$V_L' = -Y_{LL}'^{-1}(I_L' + Y_{LT}'V_T' + Y_{LG}'V_G) \tag{3.26}$$

From the second equation of (3.1) for this setup V_T is expressed as;

$$V_T' = -Y_{TT}'^{-1}(Y_{TL}'V_L' + Y_{TG}'V_G) \tag{3.27}$$

Then substituting (3.27) to (3.26);

$$\begin{aligned} V_T' = {} & (I - Y_{TT}'^{-1}Y_{TL}'Y_{LL}'^{-1}Y_{LT}')^{-1}Y_{TT}'^{-1}Y_{TL}'Y_{LL}'^{-1}I_L' \\ & + (I - Y_{TT}'^{-1}Y_{TL}'Y_{LL}'^{-1}Y_{LT}')^{-1}(Y_{TT}'^{-1}Y_{TL}'Y_{LL}'^{-1}Y_{LG}' \\ & - Y_{TT}'^{-1}Y_{TG}')V_G \end{aligned} \tag{3.28}$$

In a more concise form, (3.28) is expressed as;

$$V_T' = NI_L' \quad + MV_G \tag{3.29}$$

Where: $N = (I - Y_{TT}'^{-1}Y_{TL}'Y_{LL}'^{-1}Y_{LT}')^{-1}Y_{TT}'^{-1}Y_{TL}'Y_{LL}'^{-1}$,

$M = (I - Y_{TT}'^{-1}Y_{TL}'Y_{LL}'^{-1}Y_{LT}')^{-1}(Y_{TT}'^{-1}Y_{TL}'Y_{LL}'^{-1}Y_{LG}' - Y_{TT}'^{-1}Y_{TG}')$

Then the voltage at the target bus (converted to tie) is the Thevenin equivalent voltage at this bus.

Hence;

$$E_{th,i} = \sum_{j=1}^{nl-1} N_{i,j}I_{Lj}' + \sum_{j=1}^{ng} M_{i,j}V_{Gj} \tag{3.30}$$

This calculation is done for every load bus of interest.

Considering all load buses scenario, the first entries of the matrix N and M are taken. The remaining values produce E at the original tie buses. By taking all these first entries, for all load buses new matrices; $nl \times nl$ sized matrix N' and $nl \times ng$ sized matrix M' are formed.

Once the Thevenin voltage is found, resorting to (3.12) and a basic voltage equation of a Thevenin equivalent circuit at (3.9) and equating the two will give;

$$E_{th,i} - I_{Li}Z_{th,i} = \sum_{j=1}^{ng} K_{LGij}V_{Gj} - \sum_{j=1}^{nl} Z_{LLij}I_{Lj} \tag{3.31}$$

Substituting (3.30) to (3.31) and solving for $Z_{th,i}$;

$$Z_{th,i} = \frac{1}{I_{Li}}\left(\sum_{j=1}^{nl-1} N'_{i,j}I'_{Lj} + \sum_{j=1}^{nl} Z_{LLij}I_{Lj} + \sum_{j=1}^{ng}\left(M'_{i,j}V'_{Gj} - K_{LGij}V_{Gj}\right)\right) \tag{3.32}$$

This approach can be used for both online and offline voltage stability assessments. $N'_{i,j}$, $M'_{i,j}$, $Z_{LLi,j}$ and K_{LGij} would be calculated once and would be stored in the processor memory until network configuration change takes place. These once calculated values would greatly reduce the computational effort, hence, making the process time saving.

For offline analysis, I_{Li} and I_{Lj} would be calculated from load flow analysis and for online application these values will be accessed from SCADA measurements. I'_{Lj} will be calculated from load flow analysis. These are the two power flows required for the determination of the Thevenin equivalents.

If network configuration change takes place $N'_{i,j}$, I'_{Lj} and $Z_{LLi,j}$ would be calculated again and the process continues.

Generally, the procedure to calculate the Thevenin equivalent impedance can be summarized as;

1. Formulate the admittance matrix.
2. Rearrange the admittance matrix in the form of (3.1).
3. Formulate the submatrices of (3.1).
4. Using the relations in (3.5) determine Z_{LL} and K_{LG}.
5. Access I_L from system measurement or for offline studies conduct power flow to estimate I_L.
6. Convert target load bus to tie bus (by disconnecting the load) and determine the new submatrices.
7. From (3.29) determine N and M for each load bus.

8. Formulate $N'$and M' from the first row of N and M.
9. Conduct load flow and establish the I_L' matrix, with each column representing the load currents after topology change.
10. If all buses of interest are not addressed go to step 6.
11. Using (3.32) determine the Thevenin Equivalent.

3.3. Voltage Stability Assessment Index Formulation

The method of Thevenin equivalent determination, discussed before, enables the formulation of voltage stability indices, suitable for online application. Next, this work proposes two indices. The first one, which is identified as New Impedance Stability Index (NISI), is formulated based on impedance matching technique and the second is formulated based on active power margin and identified by the name active power margin index (PPMI).

Both the proposed indices in this work relay on measuring the closeness to point of collapse. The first method (NISI) indirectly measures the closeness while the second (PPMI) using the active power margin has a direct measurement to the point of collapse.

3.3.1. New impedance stability index (NISI)

From the basic criterion of voltage stability, using impedance matching technique, a system is;

- voltage stable, when $|Z_{th}| < |Z_l|$. Equivalently;

$$\frac{|Z_{th}|}{|Z_l|} < 1 \tag{3.33}$$

- unstable, when;

$$\frac{|Z_{th}|}{|Z_l|} > 1 \tag{3.34}$$

- at the maximum loading point, when;

$$|Z_{th}| = |Z_l| \tag{3.35}$$

The ratio of Thevenin impedance and load impedance thus can be taken as the stability index. Hence;

$$Index = \frac{|Z_{th}|}{|Z_l|} \tag{3.36}$$

The load impedance can be expressed from basic voltage relation as;

$$Z_{li} = \frac{V_{Li}}{I_{Li}} \tag{3.37}$$

Then substituting (3.32) and (3.37) to (3.36) results the new impedance stability index (NISI) as;

$$NISI_i = \frac{1}{|V_{Li}|}\left|\sum_{\substack{j=1 \\ j\neq i}}^{nl-1} N'_{i,j} I'_{Lj} + \sum_{j=1}^{nl} Z_{LLij} I_{Lj} + \sum_{j=1}^{ng}\left(M'_{i,j} V'_{Gj} - K_{LLij} V_{Gj}\right)\right| \tag{3.38}$$

This index takes values V_{Li} and I_{Lj} from online measurements while $N'_{i,j}$ and $Z_{LLi,j}$ are calculated from the transmission impedance. If offline analysis is needed V_{Li} and I_{Lj} would be calculated from load flow analysis.

Reformulating the stability criterion above using the stability index; a system is voltage stable when $NISI \leq 1$ and voltage unstable when $NISI > 1$. At the maximum loading point $NISI = 1$. This entails NISI value near to 1 indicates a voltage unstable bus and NISI approaching to 0 indicates a voltage stable bus.

3.3.2. Active power margin index (PPMI)

Voltage stability indices measure the closeness of a system to voltage instability. Mostly, this closeness is not interpretive to parameters known by technical system operators [121]. To address this problem, this section, additionally, develops active power transaction-based index. The index is understandable for a system operator who sees and manages

the system in power related terms. Additionally, the index considers the main cause of voltage instability; active power loading margin.

The index, which is termed as active power margin index (PPMI), functions based on the idea of locating the maximum possible active power transfer. Conventionally, in PV based analysis techniques, the location of the maximum active power transfer performed by conducting repetitive power flow calculations through increasing the load until the power flow solution diverges [122-124]. However, this approach consumes considerable processing time and memory which is undesirable for fast operational computations.

A continuation power flow method is also devised for locating the point of collapse [125-130]. However, this too requires considerable number of iterative computations to be performed.

PPMI, like NISI, begins from the determination of the Thevenin equivalent. Next the maximum active power transfer is calculated in a non-iterative way. The non-iterative way avoids the requirement of large number of power flow computations of the former approaches.

For offline analysis, to calculate the PPMI of a given load bus only two power flow computations are required. For online application, maximizing the efficiency, our method requires only one power flow computation, which greatly reduces the effort. These power flows are those used for the computation of the Thevenin equivalent parameters. This low number of power flow computations makes the approach appealing for fast computational requirement of online application.

The index development begins from deriving point of collapse from the PV relation of the system Thevenin equivalent representation as in Figure 2.3. Taking this Thevenin representation of a system, the apparent power delivered to the load is;

$$\boldsymbol{S} = \boldsymbol{V}\boldsymbol{I}^{*} \tag{3.39}$$

Then the current is;

$$\boldsymbol{I} = \frac{E_{th}\angle\phi - V\angle\omega}{Z_{th}\angle\varphi} \tag{3.40}$$

Substituting (3.40) to (3.39);

$$\boldsymbol{S} = V\angle\omega\left(\frac{E_{th}\angle\phi - V\angle\omega}{Z_{th}\angle\varphi}\right)^{*} \tag{3.41}$$

Then the apparent power becomes;

$$\boldsymbol{S} = \frac{VE_{th}\angle(\omega + \varphi - \phi)}{Z_{th}} - \frac{V^2}{Z_{th}}\angle\varphi \tag{3.42}$$

Letting $\alpha = \omega + \varphi - \phi$ and separating (3.42) to active and reactive component;

$$P = \frac{VE_{th}}{Z_{th}}\cos\alpha - \frac{V^2}{Z_{th}}\cos\varphi \tag{3.43}$$

$$Q = \frac{VE_{th}}{Z_{th}}\sin\alpha - \frac{V^2}{Z_{th}}\sin\varphi \tag{3.44}$$

From the trigonometric identity;

$$\sin^2\alpha + \cos^2\alpha = 1 \tag{3.45}$$

Solving for the sine and cosine in (3.43) and (3.44);

$$\cos\alpha = \frac{PZ_{th}}{VE_{th}} + \frac{V}{E_{th}}\cos\varphi \tag{3.46}$$

$$\sin\alpha = \frac{QZ_{th}}{VE_{th}} + \frac{V}{E_{th}}\sin\varphi \tag{3.47}$$

Substituting (3.46) and (3.47) to (3.45);

$$\left(\frac{PZ_{th}}{VE_{th}} + \frac{V}{E_{th}}\cos\varphi\right)^2 + \left(\frac{QZ_{th}}{VE_{th}} + \frac{V}{E_{th}}\sin\varphi\right)^2 = 1 \tag{3.48}$$

Rearranging the terms we come across an equation of quadratic form in V^2 as;

$$V^4 + V^2(2Z_{th}(P\cos\varphi + Q\sin\varphi) - E_{th}^2) + {Z_{th}}^2(P^2 + Q^2) = 0 \tag{3.49}$$

Since the derivation is for PV relation, the reactive power is substituted by the active power using;

$$Q = P\tan\theta \tag{3.50}$$

Substituting this relation to (3.49);

$$V^4 + V^2(2Z_{th}P(\cos\varphi + \tan\theta\sin\varphi) - E_{th}^2) + {Z_{th}}^2P^2\sec^2\theta = 0 \tag{3.51}$$

This equation gives four solutions for the voltage, among which only two are feasible. Solving for V^2;

$$V^2 = \frac{-(2Z_{th}P(\cos\varphi + \tan\theta\sin\varphi) - E_{th}^2) \pm \sqrt{(2Z_{th}P(\cos\varphi + \tan\theta\sin\varphi) - E_{th}^2)^2 - 4{Z_{th}}^2P^2\sec^2\theta}}{2} \tag{3.52}$$

At the maximum active power loading point, the equation under the square root gets zero. Hence,

$$(2Z_{th}P_{max}(\cos\varphi + \tan\theta\sin\varphi) - E_{th}^2)^2 - 4{Z_{th}}^2{P_{max}}^2\sec^2\theta = 0 \tag{3.53}$$

Solving for P_{max} of this equation will give;

$$\begin{aligned} P_{max} &= \frac{E_{th}^2\cos\theta}{2Z_{th}(\cos\varphi\cos\theta + \sin\theta\sin\varphi + 1)} \\ &= \frac{E_{th}^2\cos\theta}{2Z_{th}(\cos(\varphi - \theta) + 1)} \end{aligned} \tag{3.54}$$

The reactive power transferred at the point of maximum loading is also;

$$Q_{@max} = \frac{E_{th}^2\sin\theta}{2Z_{th}(\cos(\varphi - \theta) + 1)} \tag{3.55}$$

The apparent power at the maximum loading point;

$$S_{@max} = \frac{E_{th}^2}{2Z_{th}(\cos(\varphi - \theta) + 1)} \tag{3.56}$$

Resistance of the high voltage transmission lines is negligible as compared with the reactance. Hence, removing the resistive term of the Thevenin impedance, i.e $\varphi = 90$, will give simplest expressions as;

$$P_{max} = \frac{E_{th}^2\cos\theta}{2Z_{th}(\sin\theta + 1)} \tag{3.57}$$

$$Q_{@max} = \frac{E_{th}^2 \sin\theta}{2Z_{th}(\sin\theta + 1)} \tag{3.58}$$

$$S_{@max} = \frac{E_{th}^2}{2Z_{th}(\sin\theta + 1)} \tag{3.59}$$

To calculate the critical voltage equation (3.57) is substituted to (3.52). The term under the square root is zero at the critical point. Then substituting P_{max} value will give;

$$V_{cr} = \frac{E_{th}}{\sqrt{2} * \sqrt{sin\,\theta + 1}} \tag{3.60}$$

Speaking of the power terms at the critical point, the maximum active power transfer at which voltage collapse occurs doesn't change for load increment at constant power factor, provided that the external network stays unaltered. On the other hand, reactive power compensation, i.e. changing the power factor, affects the maximum transferrable active power. When reactive power compensation increases the maximum transferable active power increases.

Reactive power compensation reduces the reactive power transfer via the transmission lines, by locally supplying the reactive power, which is demanded from the transmission network. This reduces congestion and allows more space for active power transfer.

The active and apparent powers at the critical point increases for compensation increment, while reactive power transfer decreases. The response of powers, at the maximum loading, for different power factor is shown in Figure 3.8.

For unity power factor load, the reactive power transfer is zero including at the point of collapse. In this case, talking about reactive power compensation doesn't give sense. Hence, developing an index based on reactive power margin falls short in the case of unity power factor loads. Due to this reason and for active power loading is a determining factor of voltage stability, developing an index based on active power margin is a choice under all power factor conditions.

As a result, the indicator based on active power margin is formulated as margin as;

$$P_{margin} = P_{max} - P_{oper} \tag{3.61}$$

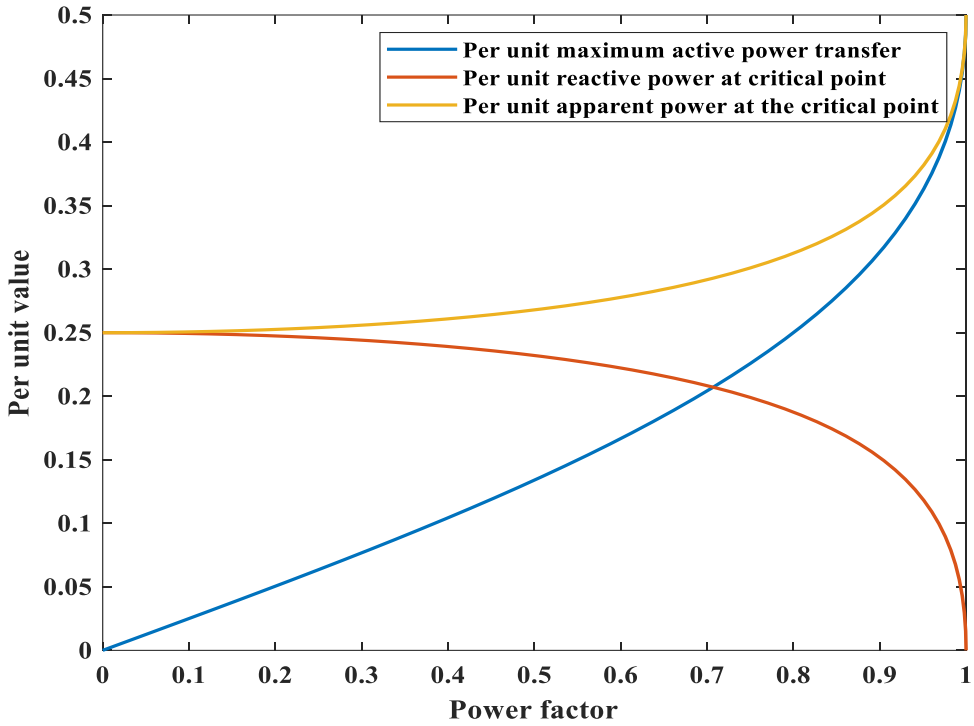

Figure 3.8: The response of power entities at the critical point for power factor change

There are works which takes this loading margin as voltage instability indicator [131]. However, this approach does not take into consideration the capacity of the load bus. High-capacity load buses and low -capacity load buses are weighed on a similar scale. This raises a quest of fairness. Some tests made by other methods prove consideration of bus capacity is required to produce the actual distance from instability. This case is demonstrated latter in section 4.2.2.

The consideration is performed by dividing the difference in (3.61) by the transfer capacity of the load bus. This normalization of power margin measures the relative strength of the load buses. This way, the distance from instability is measured in terms of power reserve to go and according to the capacity of the target load bus. The margin developed by this work is identified as Active Power Margin Index (PPMI) as in (3.62).

$$PPMI = \frac{P_{max} - P_{oper}}{P_{max}} \tag{3.62}$$

Substituting the values of the powers, PPMI comes across the expression;

$$PPMI = 1 - \frac{2VIZ_{th}(\cos(\varphi - \theta) + 1)}{E_{th}^2} \quad (3.63)$$

V and I are the values of voltage and current at the operating point of concern. PPMI takes values from 0 to 1. A value near zero means more voltage unstable bus, while value near to 1 means a more voltage stable load bus.

3.4. QV Curve Analysis and Reactive Power Margin Determination for VSA and FRPM

Maximum active power transfer capability determines the inception of voltage instability. On the other hand, reactive power transaction plays its own role in maximizing or minimizing the maximum active power transfer capability of the load bus. In addition to the devised voltage instability indicators, developed so far, both the PV and QV curves are necessary to analyze the movement of voltage collapse point. For PV curve determination the relation in (3.52) is derived before. Here, below, the expression for the QV curve is derived.

The derivation of QV relation is made for two scenarios. The first is the scenario under constant active power operation and the other is the scenario under constant power factor operating condition.

Commonly, for large power systems, the QV curve is drawn by assuming an ideal, high-capacity reactive compensator being connected to the load bus. The hypothetic reactive power compensation is, then, gradually increased and power flow is run at each reactive power provision, and the corresponding voltage of the bus is recorded. In doing so, the QV set points are plotted to produce the QV curve.

The ability of determining the Thevenin equivalent of a power system, in the previous section, has avoided the need of these many power flow computations and the assumption of fictitious reactive power compensation. Once the Thevenin equivalents at hand, one can determine the QV characteristic curve in a non-iterative way, which is computationally efficient.

3.4.1. Constant active power operation case

This scenario is the common way of investigating the QV characteristics [42, 132]. The assumption, here, in this scenario, is; the active power transfer is kept constant and adjustable reactive compensation is provided at the bus so as to improve the voltage profile. This scenario is, mostly, employed for capacitor sizing, in response to improving the voltage profile of a bus while supporting a given active power load.

In addition, each operating point along a PV curve can be investigated using the QV curve to show how reactive power compensation affects the voltage stability of the specific operating point.

The derivation of QV characteristic at constant active power begins from (3.49) and comes across the following expression;

$$Z_{th}{}^2Q^2 + 2Z_{th}\sin\varphi\, V^2Q + 2Z_{th}P\cos\varphi\, V^2 + Z_{th}{}^2P^2 - E_{th}^2V^2 + V^4 = 0 \tag{3.64}$$

Solving for Q we get;

$$Q = \frac{-\sin\varphi\, V^2 \pm \sqrt{E_{th}^2V^2 - (V^2\cos\varphi + Z_{th}P)^2}}{Z_{th}} \tag{3.65}$$

For demonstration, taking numerical values $Z_{th} = 0.5$, $E_{th} = 0.95$, $\varphi = 90^0$ and for different active power values QV characteristics of Figure 3.9 is drawn.

These graphs demonstrate the effect of compensation on the voltage profile. Beginning from the turning point, when the load bus gets compensated the bus voltage increases. Compensation is interpreted from the graph as a more positive value of Q.

Each QV curve is, basically, divided to two parts. The part left from the maximum reactive power (the turning point of the graph) is the unstable operating region, while the portion right from the maximum reactive power demand is the stable operating region [133].

These graphs also show, as the active power loading increases, the system enters to voltage instability at higher voltages. Additionally, the reactive power transfer capability of the network decreases with active power increment.

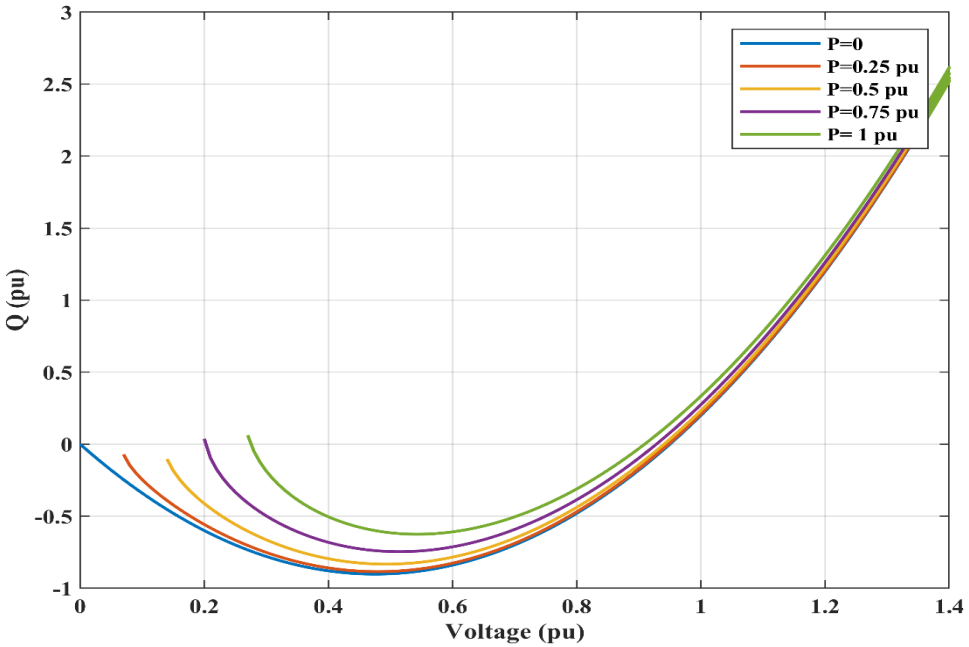

Figure 3.9: QV curves for constant active power

In the graph, in the region below $Q = 0$ the load is consuming reactive power from the external network. Crossing $Q = 0$ point the load is overcompensated and begins to act as reactive power generator, and the voltage of the load bus continues to increase.

3.4.2. Constant power factor operation case

The ability to determine the Thevenin system equivalents, makes the investigation of the second scenario possible, i.e. constant power factor scenario. In reality, when system load increases, usually, it is both the active and reactive power, simultaneously, increasing in a way the power factor is kept constant. This is the case in real power systems. Hence, the QV relation under constant power factor is worth of consideration.

The derivation, here too, begins from (3.49), and substituting active power in terms of reactive power and power factor, gives;

$$V^4 + V^2(2Z_{th}Q(\cot\theta\cos\varphi + \sin\varphi) - E_{th}^2) + {Z_{th}}^2Q^2\csc^2\theta = 0 \qquad (3.66)$$

Some computations and rearrangements will give;

$$V^4 + V^2\left(2Z_{th}Q\frac{\cos(\theta-\varphi)}{\sin\theta} - E_{th}^2\right) + {Z_{th}}^2Q^2\csc^2\theta = 0 \qquad (3.67)$$

Solving for Q;

$$Q = \frac{-V^2 \cos(\theta - \varphi) \pm V\sqrt{V^2 \cos^2(\theta - \varphi) - V^2 + E_{th}^2}}{Z_{th} \csc \theta} \tag{3.68}$$

Taking the values in section 3.4.1 and different power factor values, the following QV curves in Figure 3.10 are plotted for demonstration of the characteristics.

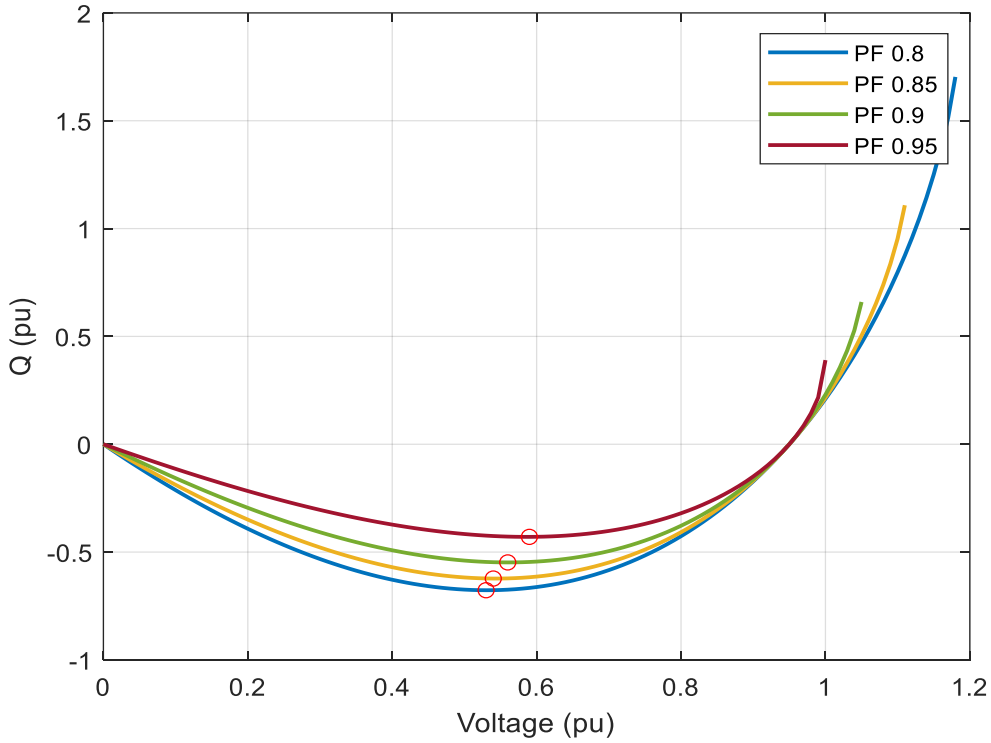

Figure 3.10: QV curves for constant power factor

These characteristic curves show each characteristic is dependent on the power factor. As the power factor goes to 1, the graph closes to zero, finally, QV curve getting flattened at power factor of 1. This entails QV methods cannot be used for evaluating voltage stability for a purely resistive load.

On the graph the maximum reactive power that can be delivered to the load is shown by the red circles. This maximum reactive power is used for the calculation of the reactive power margin whenever necessary. The reactive power margin is calculated as a difference between Q_{max} and the current reactive power, operating. The more the power factor goes to 1 the margin gets narrow. The voltage at which the point of collapse occurs also gets higher.

The maximum reactive power that can be delivered by the system can be computed from (3.68). The maximum reactive power would become;

$$Q_{max} = \frac{E_{th}^2 \sin\theta}{2Z_{th}(1+\cos(\theta-\varphi))} \tag{3.69}$$

The critical voltage at which this maximum reactive power occurs is;

$$V = \frac{E_{th}}{\sqrt{2(1+\cos(\theta-\varphi))}} \tag{3.70}$$

The derivation is given at Appendix I.

Here, an important result is, under constant power factor operation, the maximum reactive power that can be delivered is the reactive power delivered at the maximum active power transfer. This can be seen from equations (3.47) and (3.69). The voltage at which this max occurs is also the same, as it can be inferred from equations (3.60) and (3.70).

3.4.3. Voltage stability assessment based on the QV relation

The VSA scheme is made to provide different ways of voltage security assessment. One of the capabilities is using QV relation curves. Voltage stability assessment methods of a load bus based on QV curve, commonly, falls on two class. These are sensitivity analysis and the reactive power margin [133] .

a) Sensitivity analysis

The QV graph is employed for voltage stability analysis by determining sensitivity of voltage for reactive power change. The sensitivity is determined as;

$$S = \frac{dQ}{dV} \tag{3.71}$$

The basics behind the sensitivity analysis is when the system is in voltage stability state the direction of change for V is the same as the direction of changes in Q. This operating point lays right of the Q_{max} operating point on the QV curve. On the other hand, under voltage instability the direction of change for V is opposite to the direction of change for Q, i.e. S is negative, which is left part of the QV curve from the Q_{max}.

The sensitivity analysis method identifies only two states, i.e. the stable and unstable states. This method cannot show how far the system is from voltage instability. Hence, ranking is not possible in sensitivity analysis.

b) Reactive power margin

This approach measures how much reactive power can the system supply to the load before it comes to the voltage instability. The margin is computed as the difference between current operating reactive power and the maximum reactive power that can be delivered at constant active power [134]. The difference is given as;

$$Q_{\ margin} = \mathrm{Q_{max}} - \mathrm{Q_{oper}} \tag{3.72}$$

3.5. Constructing the VSA Scheme

By bringing together the above derivations, the VSA scheme is realized. The construction of the VSA scheme relays on the process flow of the voltage security assessment. This is shown in Figure 3.11 next. The scheme has two major process loops. The outer loop and the inner loop.

The outer loop is the process that interacts with the external measurement environment. It begins from accessing system topology data. Then proceeds to the computation of the network topology dependent matrices, i.e. Z_{LL}, K_{LL}, N, M, N' and M'. These matrices get stored and will be used for the next inner loop computation until the next topology change takes place. If system topology change takes place this loop is recomputed. The other data accessed by this loop are the load currents and voltages, $\boldsymbol{I_L}$ and $\boldsymbol{V_L}$**.** For offline voltage security analysis, $\boldsymbol{I_L}$ and $\boldsymbol{V_L}$ are computed from power flow. This power flow is one of the two power flows mentioned in earlier sections.

The inner loop is mandated for tracking system load changes. Whenever system loading is changed, this inner loop is initiated. This loop computes the capabilities of the scheme, which are determining the Thevenin equivalent of a system, determination of maximum active and reactive power transfer, voltage stability assessment indices, PV curve determination, QV curve determination, QV sensitivity analysis, and reactive power margin determination. The inner loop initiates the second power flow which is used to compute $I_{Lj}^{'}$, which is the load currents vector computed after removal of the targeted bus load during the computation of the Thevenin equivalent voltage.

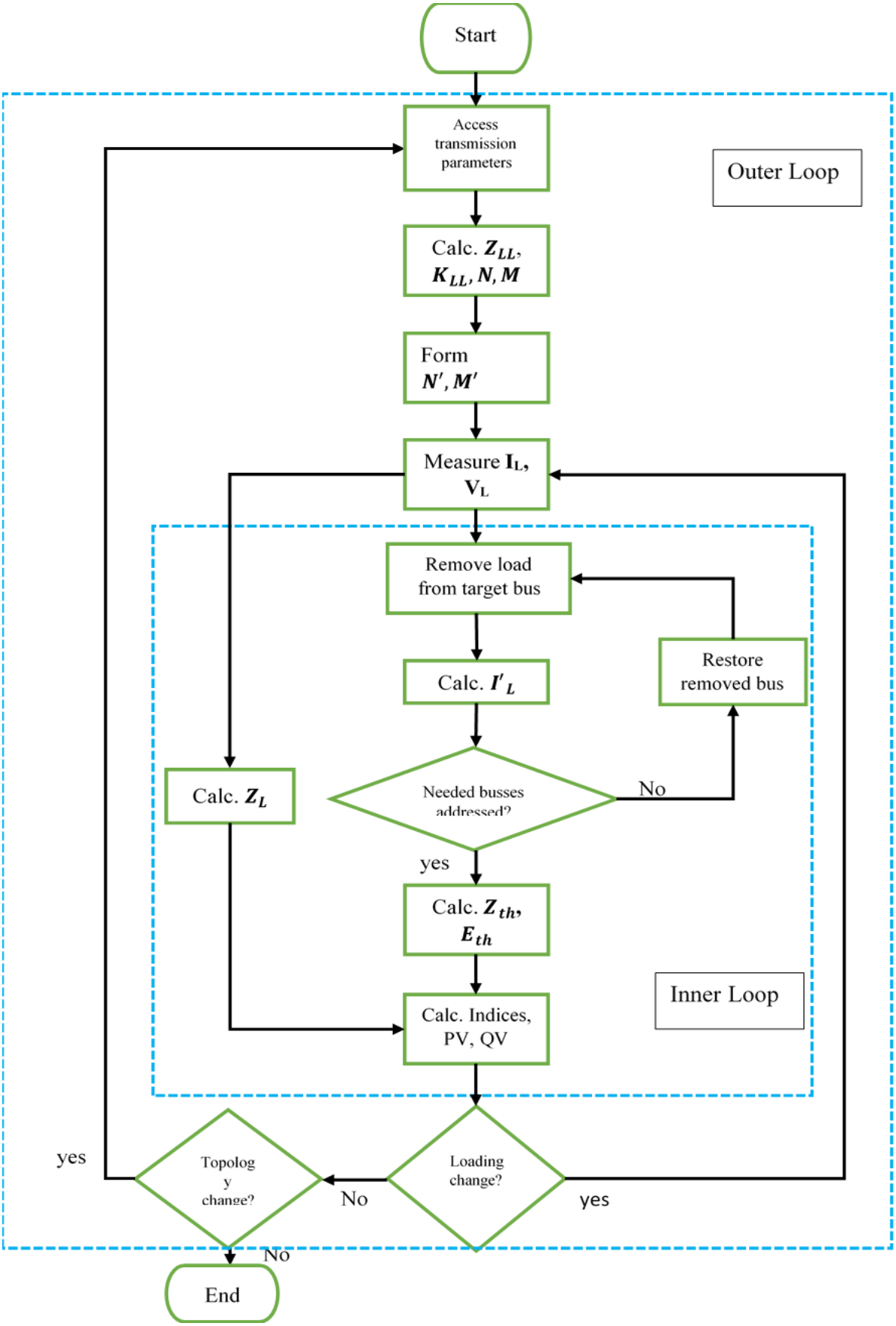

Figure 3.11: The voltage security assessment scheme

3.6. Improved Multi Objective Particle Swarm Optimization Based Reactive Power Optimization

FRPM is voltage security assessment while reactive power is provided. The reactive power provision brings changes in $\boldsymbol{I_L}$ and $\boldsymbol{V_L}$ of figure 3.11. Hence, FRPM is done through using voltage security analysis using VSA indices. Hence, every step of the VSA is the step of FRPM.

Hence, without repeating the VSA process for FRPM, the next discussion is devoted to discussing the other component of RPM scheme, CRPM based on IMOPSO. In coming sections, the formulation of the IMOPSO algorithm is discussed.

3.6.1. Multi objective reactive power optimization problem formulation

Multi objective optimization problem is characterized by having more than one objective. The objectives can be going along each other or conflicting.

A multi objective problem can be formulated as;

$$minimize\ f_i(x) \qquad i = 1 \ldots . n_o \tag{3.73}$$

Subject to the equality and inequality constraints;

$$h_j(x) = 0\ ;\quad j = 1 \ldots n_{ec} \qquad l_k(x) \leq 0\ ;\quad k = 1 \ldots n_{ic} \tag{3.74}$$

Where n_o is the number of objective functions, n_{ec}- number of equality constraint, n_{ic}- number of inequality constraint.

In our specific problem of reactive power optimization, the objective is formulated as a two-objective problem. This formulation begins from the basic voltage security definition, which contains both voltage stability and voltage limit maintenance.

i) Voltage stability index based objective function

The voltage stability-based objective is formulated using active power margin index (PPMI) of (3.63). Based on this index, when the value of PPMI closes to 1 the load bus is more voltage stable, while nearing to zero the bus is getting more unstable. Hence, the

nature of the index entails a maximization problem. In order to avoid contradiction with the second objective function, which is clearly a minimization problem as discussed in the next section, the objective is converted to a minimization problem by finding the complement of PPMI.

For the objective is to improve the whole system voltage stability, the objective function is formulated as the average of this complement of all load buses as in (3.75). The average is taken in order not to have large values of the function due to summation effect, in case of large power systems who have many hundreds of load buses.

$$\min f_{PPMI} = \frac{1}{n_{lb}} \sum_{i=1}^{n_{lb}} (1 - PPMI_i) \tag{3.75}$$

n_{lb} -is the total number of load buses.

ii) Voltage deviation based objective function.

The second objective function is based on the bus voltage deviation. System load buses are expected to operate at a unity per unit value of voltage. System operator strives to maintain this standard. Whenever the voltage deviates from this standard, the operator adjusts the reactive power resources to minimize the deviation from this standard. There are variations among literature in objective function formulation for the voltage deviation. Some approaches include the sum of absolute valued difference [99, 100], sum of squired difference in [94], squired normalized difference [135], square root of the sum of squire of deviations [136]. For this work the last approach is chosen. The need for absolute valuation or squaring is to avoid the cancellation effect upon the sum of the differences. The choice avoids cancellation by squaring each difference and reduces magnitude increment, that come with squaring, by taking the square root of the sum.

$$\min f_{VD} = \left[\sum_{i=1}^{n_{lb}} (V_{li} - 1)^2 \right]^{1/2} \tag{3.76}$$

iii) **Constraints.**

The constraints represent the various limits imposed on the system. The first set of constraints is the equality constraints, which contains the active power and reactive power

balance equations at each bus. The system operation is governed by these power flow equations.

Power flow constraints;

$$P_i = V_i \sum_{j=1\ldots nl} V_j\left(G_{ij}\cos\theta_{ij} + B_{ij}\sin\theta_{ij}\right) \tag{3.77}$$

$$Q_i - \nabla Q_{ci} = V_i \sum_{j=\cdots nl} V_j\left(G_{ij}\sin\theta_{ij} - B_{ij}\cos\theta_{ij}\right) \tag{3.78}$$

The control variables, also, should operate within the limits which constitute the inequality constraint set. These are given as;

$$Q_{ci}^{min} \le Q_{ci} \le Q_{ci}^{max} \text{ (Reactive compensation limit)} \tag{3.79}$$

$$V_{gi}^{min} \le V_{gi} \le V_{gi}^{max} \text{ (Generator output voltage limit)} \tag{3.80}$$

$$T_i^{min} \le T_i \le T_i^{max} \text{ (Transformer tap changer limit)} \tag{3.81}$$

State variable limits;

$$Q_{i\,min} \le Q_i \le Q_{i\,max} \text{ (Generator reactive power limit)} \tag{3.82}$$

$$S_i \le S_{limit} \quad \text{(Transmission line thermal limit)} \tag{3.83}$$

$$V_{Li}^{min} \le V_{Li} \le V_{Li}^{max} \quad \text{(Bus voltage limit)} \tag{3.84}$$

$$P_{gi}^{min} \le P_{gi} \le P_{gi}^{max} \text{ (Active power generation limit)} \tag{3.85}$$

The equality constraints and the state variable limits are imposed during power flow computation. The control variable limits are imposed on the computation of the algorithm during the initialization of the position and during position updates.

3.6.2. IMOPSO algorithm formulation

IMOPSO is established on a MOPSO platform. The main modification made is in creating positions additional to the set created by the standard MOPSO algorithm. This affects the normal trend of PSO position search mechanism. In turn, this prevents convergence to false optimal positions.

The additional positions are created using adapted binary crossover (ABX). Crossover is a genetic operation common to genetic based evolutionary algorithms. To implement ABX to MOPSO, potential positions are selected based on dominance and crowding

distance. The crowding distance helps for maintaining the diversity of the solution and the dominance principle gears the solution towards the true pareto front.

In the next sub sections, the major components of the algorithm are discussed, and finally the algorithm is put as a whole.

i) Updating speed and position.

This is the position assignment step of the PSO algorithm class. In our algorithm, also, it is the core position producing step through position and velocity updating equations as;

$$V_{i,j}^{k+1} = wV_{i,j}^{k} + c_1 r_1\left(Pbest_{i,j}^{k} - X_{i,j}^{k}\right) + c_2 r_2\left(h - X_{i,j}^{k}\right) \qquad (3.86)$$

$$X_{i,j}^{k+1} = X_{i,j}^{k} + V_{i,j}^{k+1} \qquad (3.87)$$

The constants c_1 and c_2 in (3.86) determines the weight of exploitation and exploration in the search space. c_1 is the exploitation constant while c_2 is the exploration constants. h- is the leader selected from the pareto set on a probabilistic selection approach. Equation (3.87), using the velocity vector and old positions, creates the new positions.

ii) Principle of Dominance

The dominance determination step is the core process of pareto based multi objective optimizations. A given position x_2 is dominant over the other position x_1 when:

i) For all objective functions f_i , $f_i(x_1) \leq f_i(x_2)$ and
ii) At least there exists one objective function for which $f_i(x_1) < f_i(x_2)$.

Commonly, the positions resulting from (3.87) get subjected to dominance determination and the pareto front is determined directly from this set.

In our approach, however, the pareto front is determined at latter stages. But the potential positions, on which ABX is going to be applied, is selected from the result of (3.87). This selection is made based on dominance and crowding distance calculation.

iii) Ranking of the population and crowding distance (CD) computation.

These features are common in genetic algorithm based algorithms [137]. In our algorithm ranking and crowding distance are used for selecting potential positions for ABX

operation. Ranking measures the closeness of the solution set to the true pareto front while CD measures the dispersion of the solution. A more dispersed solution is favoured for it contains a more diverse solution, which gives a more varied choice of solutions. The utilization of CD in our algorithm helps to maintain the diversity of the pareto front.

The crowding distance is measured as a distance between consecutive neighbouring solutions normalized to the maximum range of the objective values [137, 138]. This is given as;

$$CD_i = \sum_{m=1}^{M} \frac{f_m(x_{i+1}) - f_m(x_{i-1})}{f_m max - f_m min} \tag{3.88}$$

Where f is the fitness function, M the number of objective functions and x is the particle position.

Once the rank and crowding distance of positions is computed potential positions are selected for implementing the crossover operation. The selection is made in favour of large crowding distance so as to enhance diversity and in favour of dominating groups according to the rank.

iv) Application of ABX to MOPSO algorithm.

The disturbance introduced to the MOPSO algorithm is adapted from the crossover operation, simulated binary crossover, which is used in genetic algorithm [112, 113]. In this operation two potential parents are taken and the genetic information is exchanged to produce two new offspring. In our case, the two parents are two positions np_1 and np_1 selected based on rank and crowding distance. The offspring are identified as intermediate positions nip, in our case.

The new intermediate positions (nip) are computed as;

$$nip_1 = 0.5 * \left((1 + \beta) * np_1 + (1 - \beta) * np_2\right) \tag{3.89}$$

$$nip_2 = 0.5 * \left((1 - \beta) * np_1 + (1 + \beta) * np_2\right) \tag{3.90}$$

β - is a distribution index and determines degree of exploration and exploitation. β close to 0 the new intermediate position becomes similar with the np's. This means the

exploitation is more intensive. β close to 1 the operation explores the search space much more. Hence, this approach adds a more exploration and exploitation effort to the PSO equation of (3.86).

β is computed as;

$$\beta = (2 * u)^{\frac{1}{\mu+1}} \quad \text{if u<0.5} \tag{3.91}$$

$$\beta = \frac{1}{(2(1-u))^{\frac{1}{\mu+1}}} \quad \text{otherwise} \tag{3.92}$$

μ is the distribution index for cross over, u is the random number generated between 0 and 1.

The intermediate positions then get mingled with the original positions to produce larger size position set. This increases the originally planned size of positions. To maintain the planed size, next, positions are selected from this large population based on dominance and crowding distance. This gives the new position set with planed size.

The utilization of crowding distance for the selection of resulting positions improves the diversity of the algorithm.

Now, the algorithm for the IMOPSO can be generalized as follows.

1. Initialize position and velocity.
2. Compute the fitness function values and determine the dominant positions for the initial positions.
3. Select a leader from the dominant set on a probabilistic approach.
4. Update speed and position using equations (3.86) and (3.87).
5. Perform power flow with the new position and compute the fitness functions.
6. Select potential positions using ranks and crowding distance for crossover.
7. Perform crossover on the selected position and produce intermediate positions.
8. Merge intermediate positions to the population from step 4.
9. Select the new position set based on dominance and CD respectively, with intended size of positions.
10. Check if the constraints are respected, if not make adjustments for over/under_the_limit quantities.

11. Update the set of the dominant front.
12. If the maximum iteration is reached or the minimum error is achieved terminate the search. Else go to step 3.

3.6.3. Performance measure of IMOPSO

The performance of the IMOPSO is measured based on two criteria. The first criterion is the quality of the pareto front and the second is the diversity of the solution. In this work, the quality of the pareto front is measured using inverted generational distance (IGD) and the diversity of the solution is measured using crowding distance.

By quality of the pareto front it is meant the closeness of the solution to the true pareto front. A given algorithm should produce a pareto front as close as the true pareto front. The discrepancy between the actual pareto front and the resulting pareto front is used as the measure of the quality of the pareto front. In this study, this quality is quantified using the inverted generational distance (IGD).

The inverted generational distance measures the closeness of the pareto front to the true pareto front [118-120, 139]. The IGD is given as;

$$IGD_i = \frac{\sum_{j=1}^{N} \min(\mathrm{d(i,j)})}{N} \tag{3.93}$$

N- is the number of non-dominated vectors. $\mathrm{d(i,j)}$ is a Euclidean distance between the i^{th} solution of existing pareto front and the j^{th} element of the true/reference pareto front. The lower the value of the IGD indicate the closer the pareto front to the true pareto front.

The IGD is the first line of the performance evaluation tool. CD would apply as a performance measure, if the pareto fronts are the same or approximately the same in terms of the IGD. If two pareto fronts are different in terms of IGD, applying CD for comparison leads to erroneous result. The reason is a low quality pareto front may have higher values of CD, due to the position of the PF at high values in the objective space.

3.7. Construction of the RPM Scheme

Total setup of the scheme is shown in Figure 3.12 below. The process begins from system data scanning. The system scanning provides the data about system topology, existing system loading, existing power generation and reactive power resource allocation.

Based on this accessed data the system is identified if contingency has occurred. The contingencies include transmission line outages, generator outages and significant load centre disconnections. If a contingency takes place, FRPM will be initiated. The FRPM reads the voltages and currents of the system and computes the VSA indices and identifies weakest buses. If the VSA index value of the weakest buses are not fairly far from voltage instability reactive resources will be switched on and the voltages and currents of the load buses get read and VSA will be conducted to see if the voltage stability of the weakest buses is improved. If not improved the cycle repeats itself. If the stability is improved next system scanning is conducted.

If contingency has not occurred the system will be investigated for system loading change. If loading change takes place, CRPM will be conducted. The system loading and the existing topology data will be taken by the CRPM component and IMOPSO will be conducted. Since the IMOPSO uses the stability indices as the objective function, IMOPSO interacts with the VSA scheme continually for the objective function computation. Once, the optimization gets over the reactive power resources will get switched based on the optimization results. In this aspect FRPM and CRPM differs. FRPM switches reactive resources and computes if improvements are made while CRPM first conduct computations and last switches the reactive resources.

Once one cycle of CRPM gets conducted the system will get scanned for system loading changes. If system loading change has not occurred the process terminates.

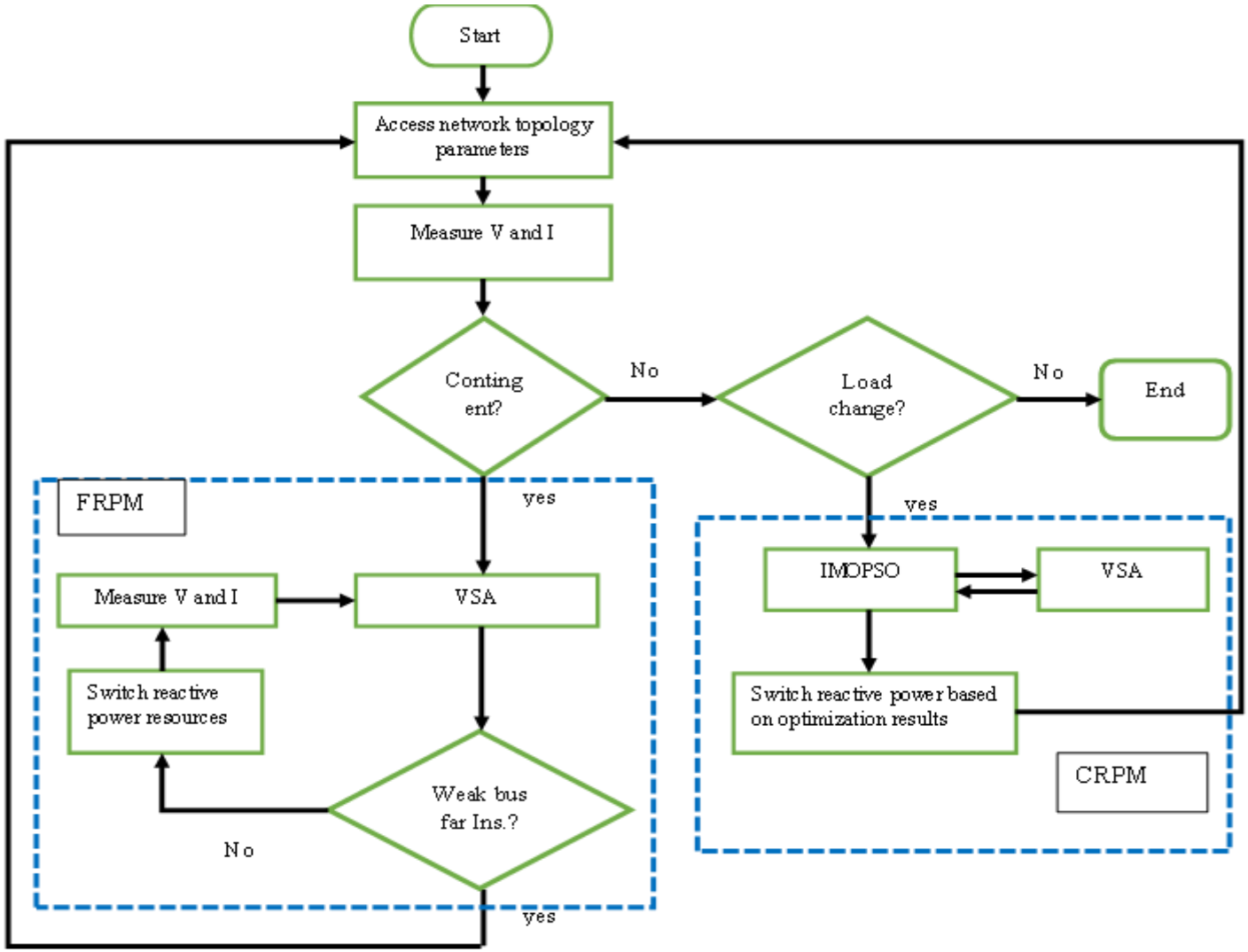

Figure 3.12: The reactive power management scheme

3.8. Test Setup of VSA and RPM Schemes

Regarding to the test of the schemes both Matpower 7.1 and Matlab 2021 version software are utilized. Matpower is an open-source power simulation software, used for power flow analysis and runs on a Matlab environment. This power system analysis software doesn't employ a graphical representation of a power system. Instead, the power system data is prepared in a table format specific to Matpower [140].

In our simulation case, functions regarding to Thevenin equivalent calculation, maximum power calculation, index calculator, PV and QV plotters and the IMOPSO are developed on Matlab editor and power flow analysis is performed using Matpower. The interaction between the software is shown here below in Figure 3.13.

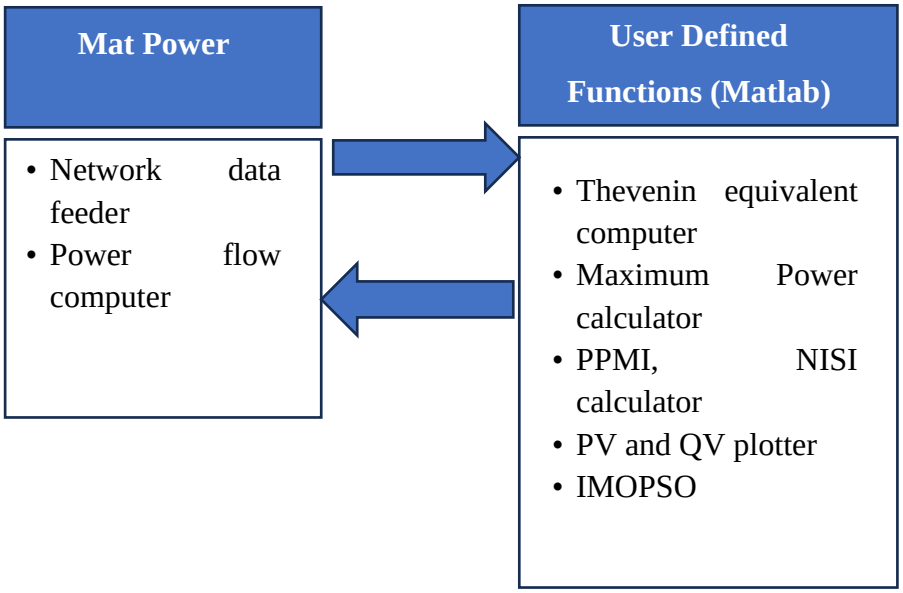

Figure 3.13: The interaction of the software employed for testing the schemes

For testing the schemes IEEE 14 bus system, IEEE 30 bus system and the EEP system are utilized. The data for these systems is provided at Appendix II. This data is prepared in a format suitable for Matpower software. Additionally, the graphical representation for the IEEE test cases, based on [141] is added.

CHAPTER 4 PERFORMANCE EVALUATION OF BASIC CAPABILITIES OF VSA AND RPM SCHEMES

This chapter is devoted for the test of the major capabilities of the VSA and RPM schemes. The capabilities considered for the test in this chapter are those that are related with the major findings of this research work and which the other capabilities base on. These are Thevenin equivalent determination, the two indices (NISI and PPMI) and the IMOPSO. The rest capabilities are demonstrated in the next application chapter. In this chapter, the tests begin from the test of the Thevenin impedance determination technique. Then it proceeds to the test of the two voltage stability assessment indices. Then the test terminates by evaluating the performance of the IMOPSO.

4.1. Performance Evaluation of the New Thevenin impedance Determination Technique

First, the accuracy of the technique is tested using simple four bus system shown in Figure 4.1. A four-bus test system is selected for its simplicity, so that, the actual Thevenin equivalent impedance can be calculated analytically for comparison purpose. Then the Thevenin impedance determined in the new method is compared with the models of coupled single port approach. Finally, for IEEE 14 bus system, Thevenin equivalent impedance seen by each bus is computed under different loading condition.

4.1.1. Accuracy of the New Thevenin impedances

The accuracy of the Thevenin impedances determined by the new method is tested using four bus radial system shown below in Figure 4.1. The check is made against the result from the analytical computation that uses circuit system rules.

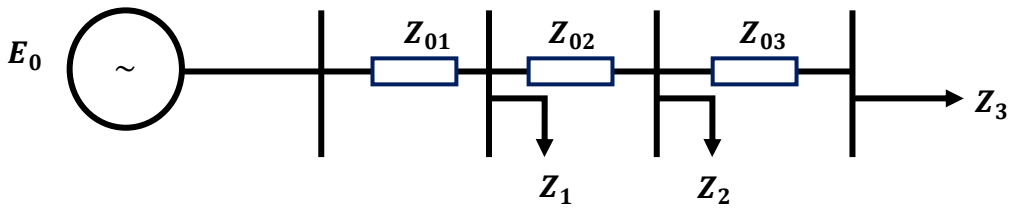

Figure 4.1: Four bus test system

The following numerical values are taken for the impedances. $Z_{01} = 0.01 + 0.5j$; $Z_{02} = 0.02 + 0.45j$; $Z_{03} = 0.015 + 0.7j, Z_1 = 1.2 + 2j$, $Z_2 = 1.5 + 3j$; $Z_3 = 1 + 4$j; These values are own proposed values. Some considerations are made in choosing the values to create similar condition with the actual power grid conditions. The considerations are;

- Transmission line resistance is much smaller than the transmission line reactance.
- Load impedance is much larger than the transmission impedance.

Using the procedures the new method in section 3.2. the Thevenin impedance seen by the terminal at Z_3 is determined to be:

$$Z_{th3} = 0.1228 + 1.3910i$$

Using circuit systems rules, the actual Thevenin impedance is calculated for this test system as;

$$Z_{tha3} = \frac{Z_{01}Z_1Z_2 + Z_{02}Z_{01}Z_2 + Z_1Z_{02}Z_2}{Z_{01}Z_1 + Z_{02}Z_{01} + Z_1Z_{02} + Z_2Z_{01} + Z_2Z_1} + Z_{03} \quad (4.1)$$

Substituting the values, similar result is obtained as;

$$Z_{tha3} = 0.1228 + 1.3910i$$

Thevenin equivalents are calculated for the remaining buses and tabulated here below in Table 4.1.

Table 4.1: Thevenin impedance values from the new method as compared with the actual values

Load Bus	Z_{th} **actual**	Z_{th} **with the new method**
1	$0.0283 + 0.4159i$	$0.0283 + 0.4159i$
2	$0.0713 + 0.7341i$	$0.0713 + 0.7341i$
3	$0.1228 + 1.3910i$	$0.1228 + 1.3910i$

The result from the new method is similar with the actual Thevenin value. This shows the accuracy of our method is high. In this case the voltages and currents, which are normally expected from power flow analysis, are calculated from circuit analysis due to small size of the system. This enabled a 100 % match between the two impedances.

Here it is worth mentioning; when larger system is considered it is clear 100 % accuracy cannot be achieved. This is due to the fact that our method employs power flow computations for the determination of load bus voltages and currents. Power flow methods are themselves numerical methods which operate within allowed level of errors. This shows our method cannot produce results with 100 % accuracy as analytical calculations. But it is worth mentioning that the errors that can come with our method are errors in power flow methods. But the accuracy is higher than any other method proposed so far in this theme.

4.1.2. Comparison of Thevenin impedance from the new method with those from coupled circuit models

Next, the Thevenin impedance from our new method is compared with the result from the two approximate models of coupled single port circuit approach discussed in section 3.1.1., under all bus load increment of IEEE 14 bus test system. This is shown in Figure 4.2.

From the diagrams, Thevenin impedance from Model 1 is independent of system loading. This is shown by the constant value graphs of the model. Thevenin impedance determined by the new method always lies above the Thevenin impedance from the first model of the coupled network.

Model 2, similar to the new method, gives load dependent Thevenin impedance. The results depend on unique system loading and network configuration. Model 2 shows values, sometimes above and sometimes below the Thevenin impedance of the new method and other times very near to the actual values produced by our method. At some loading point they are seen producing exactly the same results as can be inferred from the crossing points.

The other important finding is for all the load buses the Thevenin impedance from the new method shows increment near the maximum loadability point. However, model 2 is seen decrementing near the maximum loadability point for some buses. This shows an increasing discrepancy between model 2 and the new method near the maximum loadability point, which is the critical method.

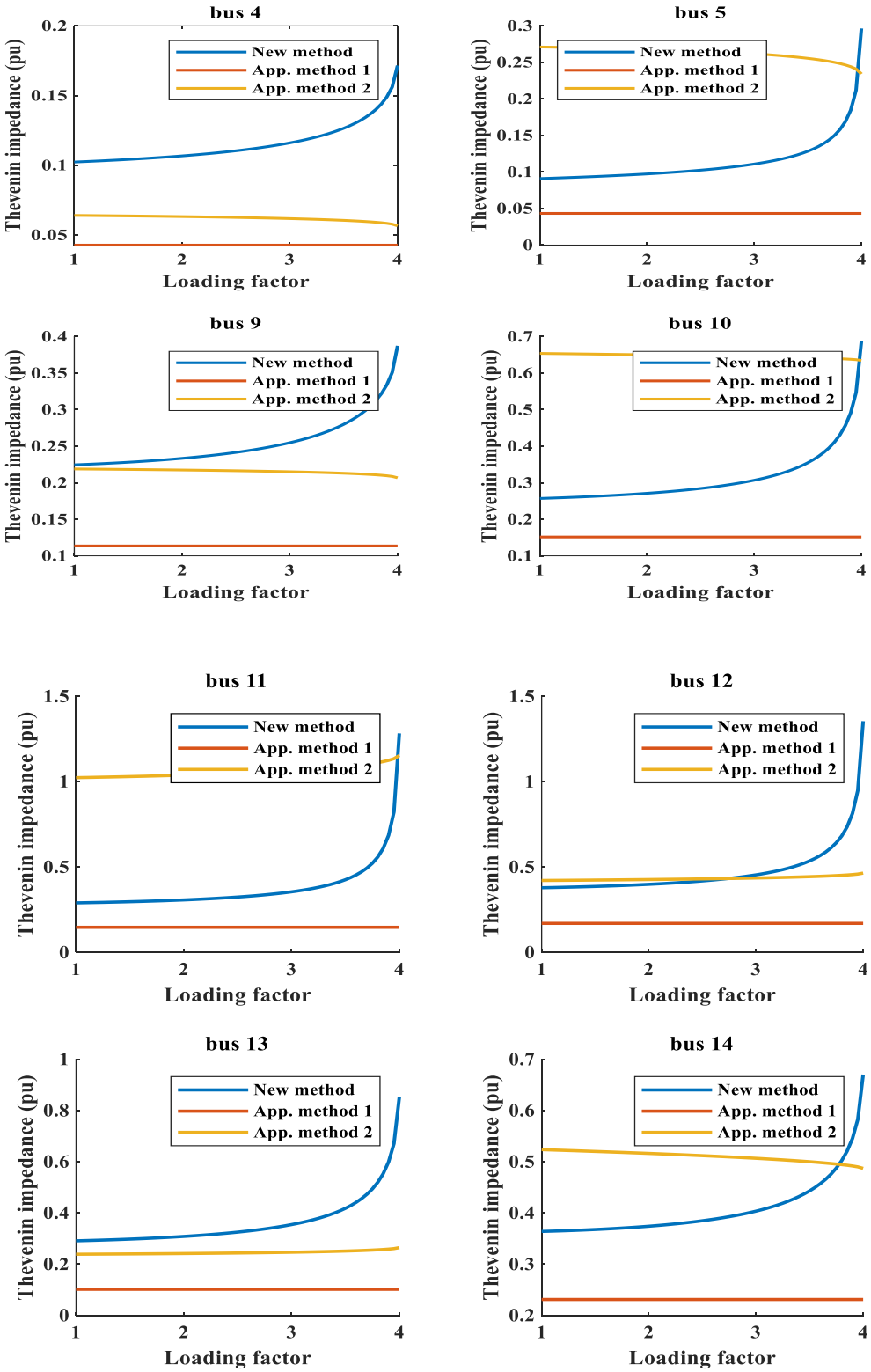

Figure 4.2: Comparison of Thevenin impedances from the new method and from models of coupled network

4.1.3. Z_{th} determination of IEEE 14 bus test system

Each operating point of a power system results different Thevenin equivalent impedance as seen from the load points. The investigation here, next, takes this fact into consideration and the Thevenin impedances are calculated under different system loading condition. This is also a case during online application, where the system loading constantly varies.

Two extreme loading scenarios are considered. The first condition is all load increment. This loading condition is an approximation of the peak loading condition. The other loading condition is a single load bus increment, which is the simplest form of loading increment.

i) Z_{th} under all load increment

In this scenario all system loads are incremented and the corresponding plots are shown below in Figure 4.3. The figure contains Thevenin impedance plots seen by all load buses, combined in a single diagram, for comparison purpose.

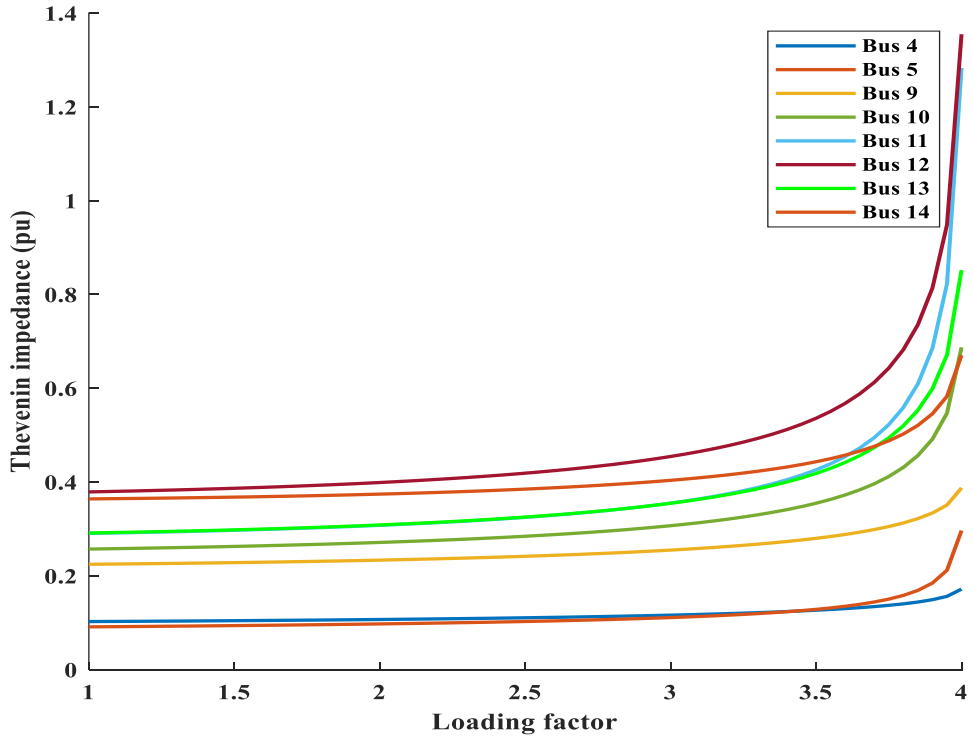

Figure 4.3: Thevenin impedances seen by the load buses for all load increment

For the wide loading ranges, largest Thevenin impedances are seen by buses 12 and bus 14 and the least Thevenin impedances are seen by bus 5 and bus 4 respectively. For this specific case, the load buses near to the generator buses see the lowest Thevenin impedance.

ii) Single bus loading increment

For investigating this scenario bus 4 and bus 14 are selected for load increment. Bus 4 is the bus near to the generating area and bus 14 is a bus on a distant location from generation. The Thevenin impedances seen by the system buses are shown in Figures 4.4 and 4.5 at different loading factor.

For bus 4 load increment all load buses see increasing Thevenin impedance. This is according to the rule governed by (3.32). The rate of Thevenin impedance increment for single bus load increment is smaller than that of total load increment. Incrementing more loads results higher rate Thevenin impedance increment. All Thevenin impedances seen by the load buses are plotted on a single diagram in Figure 4.4 and Figure 4.5, for the two buses. These diagrams tell the Thevenin impedances for single bus load increment are minimum.

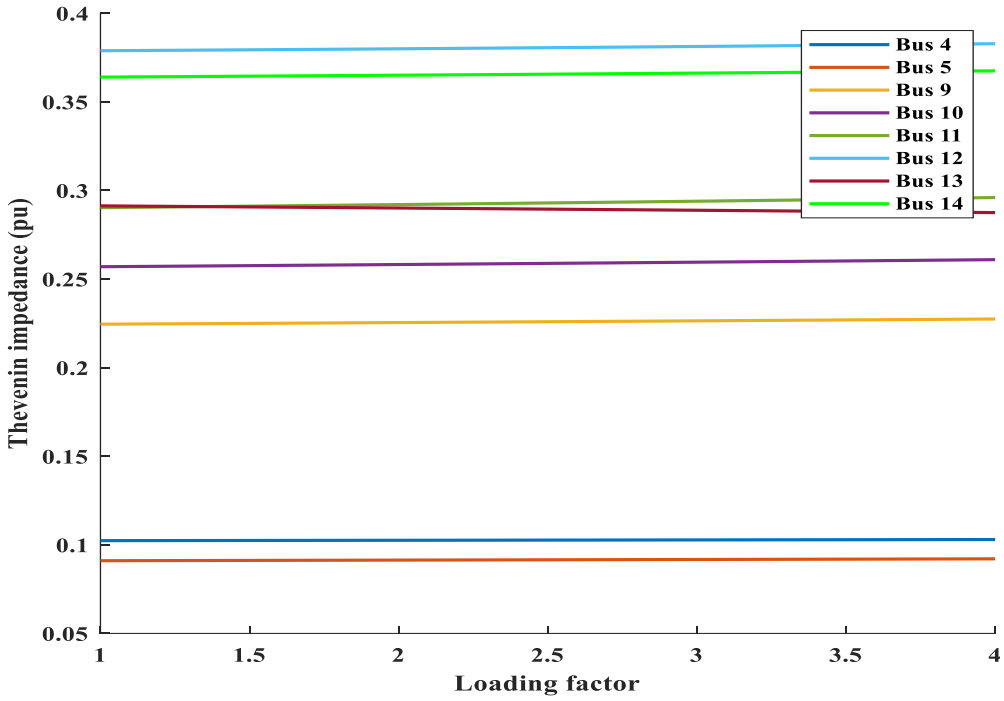

Figure 4.4: Thevenin impedances seen by the load buses for load increment at bus 4

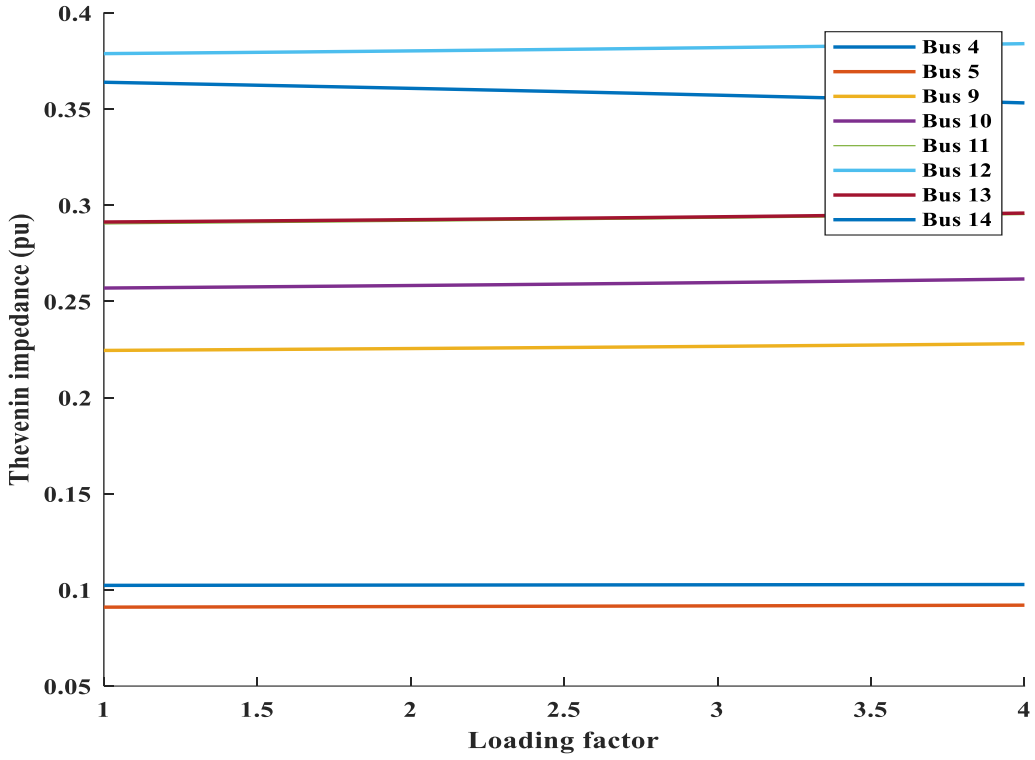

Figure 4.5: Thevenin impedances seen by the load buses for load increment at bus 14

Next the Thevenin impedance seen by the buses for load increment at other different buses is demonstrated in Figures 4.6 and 4.7. Buses 4 and bus 14 are selected for this demonstration.

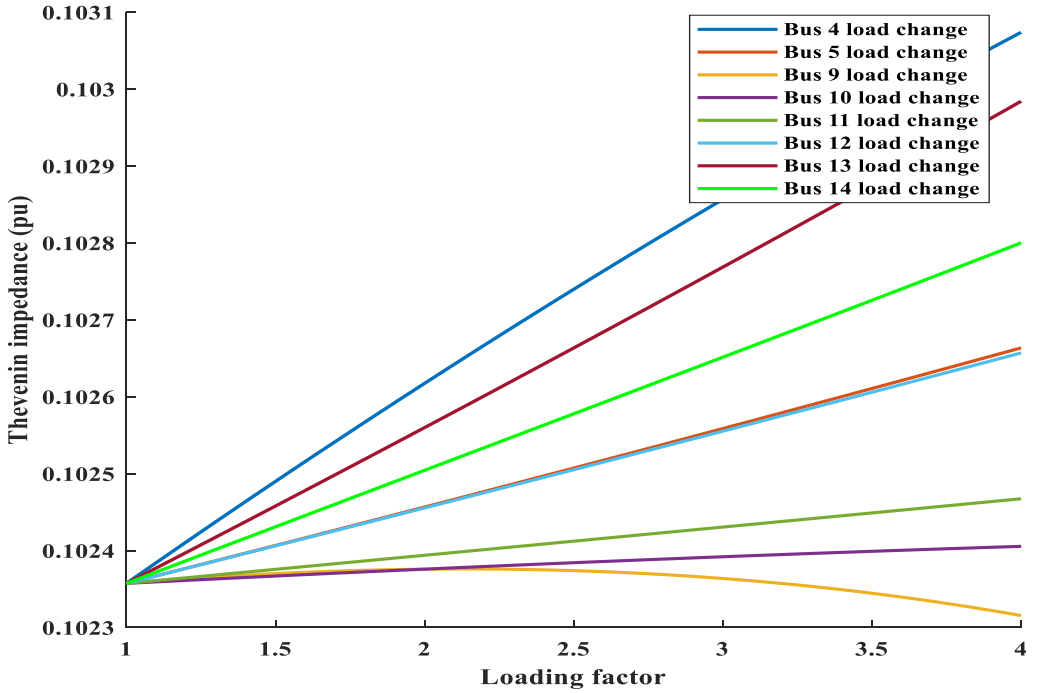

Figure 4.6: Thevenin impedance seen by bus 4 for load increment at other buses

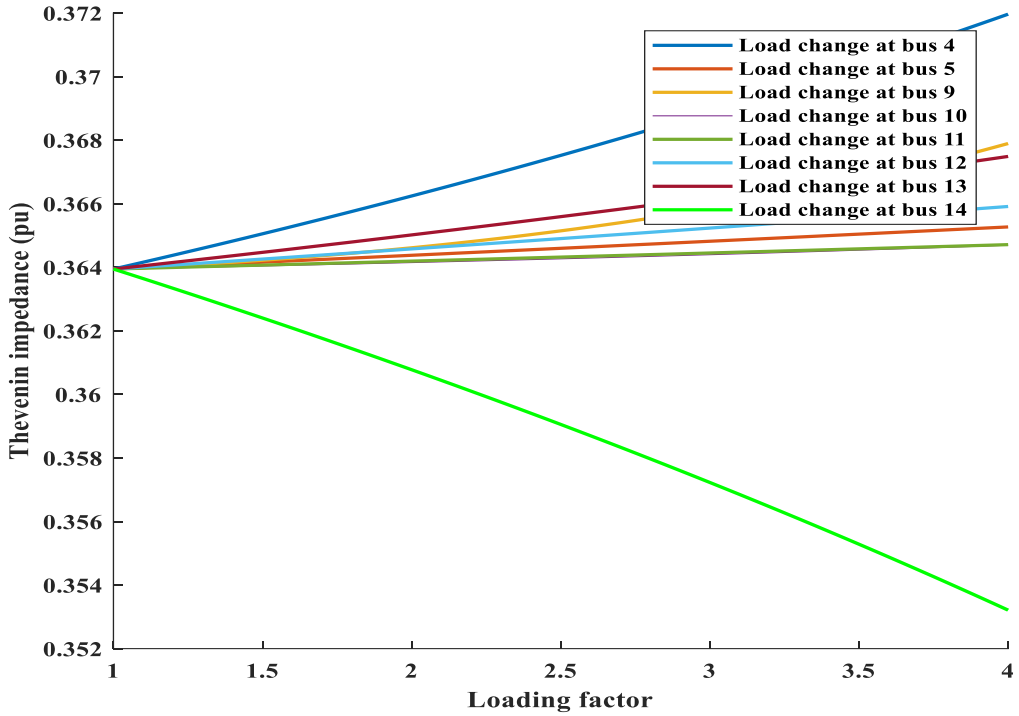

Figure 4.7: Thevenin impedance seen by bus 14 for load increment at other buses

These two Figures show, the Thevenin impedance seen by the load buses behave differently for different buses load increment. For some buses load increment, the Thevenin impedance shows decrement. But for the majority load increments the Thevenin impedance shows increment with load increment. This differing relation between loading and Thevenin impedance depends on the network setup and the impact of power flow in the network as it is governed by (3.32).

The important conclusion that can be drawn from these experiments is that for system load increment the Thevenin impedance doesn't always show increment. Sometimes buses see reducing Thevenin impedances for some system load increments. Hence, in these cases, which are accompanied by Thevenin impedance reduction, the voltage instability can be seen delayed than the normally anticipated.

4.2. Performance Evaluation of the Developed Indices

As it is discussed in section 3.3, two indices are developed to assess voltage stability. The first index shows the relative closeness of the system operation to voltage instability, while the second index in addition to showing closeness to voltage instability, it can be easily interpreted in power related terms, that are easily understandable for operating

personnel. Here, next the performance of these indices is evaluated under different scenarios.

4.2.1. Test on the new impedance stability index (NISI)

i) All bus load increment

In figure 4.8, below, the trend of Thevenin impedance, load impedance and NISI changes are plotted for load increment at each load bus of IEEE 14 bus system. As the system loading increases the Thevenin impedance and the stability index increase, while the load impedance drops fast. Rate of drop for load impedance is high as compared with the rate of increment of both Thevenin impedance and the stability index.

At the point of maximum system loading, the Thevenin impedance and the load impedance meets and the stability index gets a value of 1. All load buses enter instability beyond the loading factor of 4.

These graphs, additionally, show the NISI near the collapse point increases at higher rates. The graphs demonstrate different behaviour based on the characteristic of individual load buses.

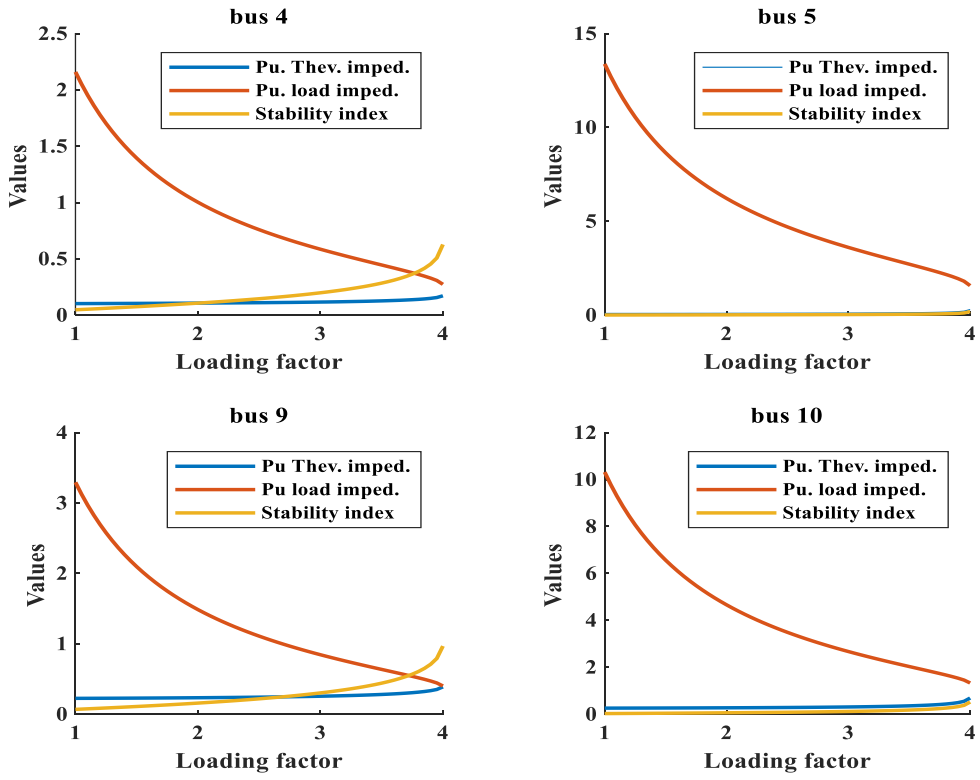

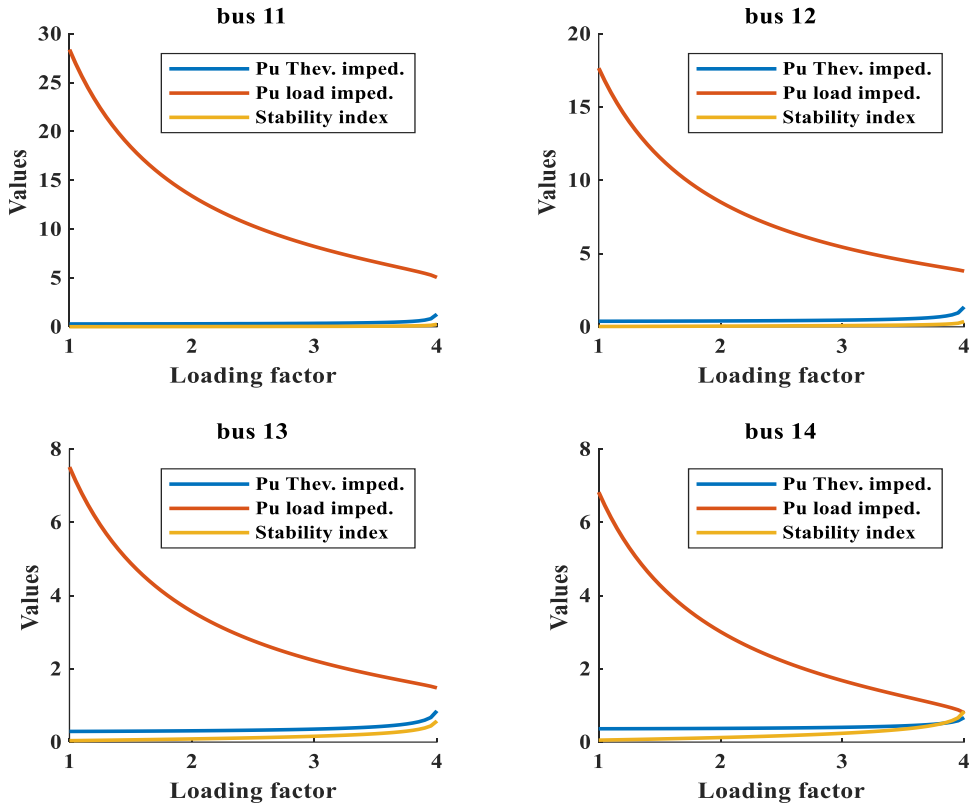

Figure 4.8: Load impedance, Thevenin impedance and NISI of load buses of IEEE 14 bus system

ii) Weakest bus identification

Most weak bus identification techniques base their computation by taking only the rated system loading. However, on a continually varying system loading speaking about fixed weakness leads wrong conclusion. A weakest bus under nominal system loading may not be the weakest under other system loading conditions, among the infinite system operating point options [125, 142].

To go in line with the above reasons and with the demand of online voltage stability assessment, continuous bus weakness identification is adopted in this work. For IEEE 14 bus test system the weakness under different system loading is plotted in Figure 4.9.

In this figure, except near the maximum loading point, for different loading factors the ranks of the buses maintain the same order. According to this order, bus 9 is weakest bus followed by bus 14.

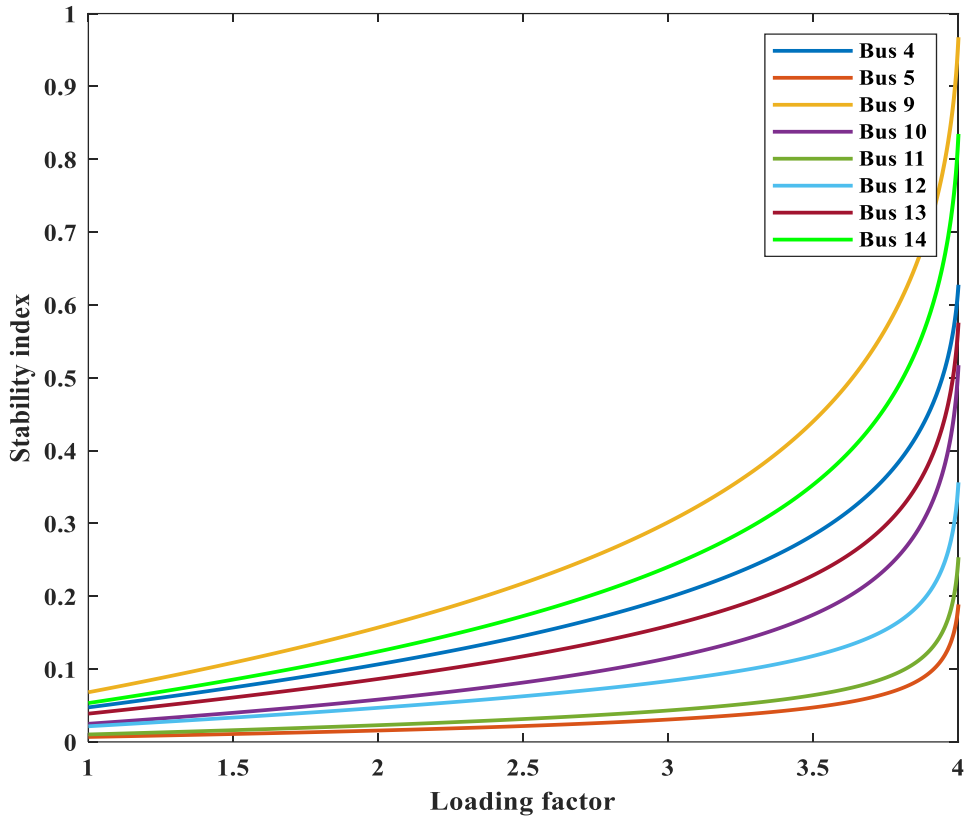

Figure 4.9: NISI under different system loading level for IEEE 14 bus system

iii) Reactive power loading and NISI response

Reactive power loading or compensation affects the system voltage stability. When the load consumes more reactive load the system gets close to instability. Here, below, two scenarios of reactive loading increment are depicted in the following Figure 4.10 and Figure 4.11. The active load is maintained constant while the reactive load increases.

The two figures demonstrate that NISI increases more for system wide load change. In the case of single bus reactive power increment, the NISI increment is low.

According to figures from 4.9-4.11 the results show the weakest bus to be bus 9 followed by bus 14 and bus 10. These buses are located around the vicinity of each other. The strongest buses are bus 5, bus 11 and bus 12 respectively. These buses are too located on the same vicinity. These situations indicate area weakness identification using NISI is possible.

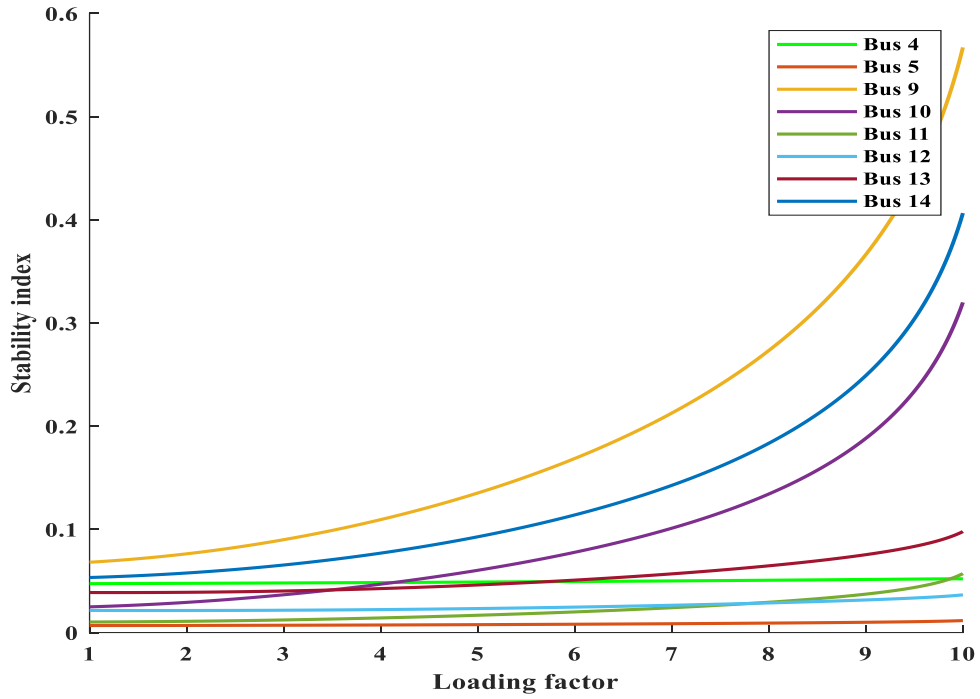

Figure 4.10: The response of NISI for all load reactive load increment

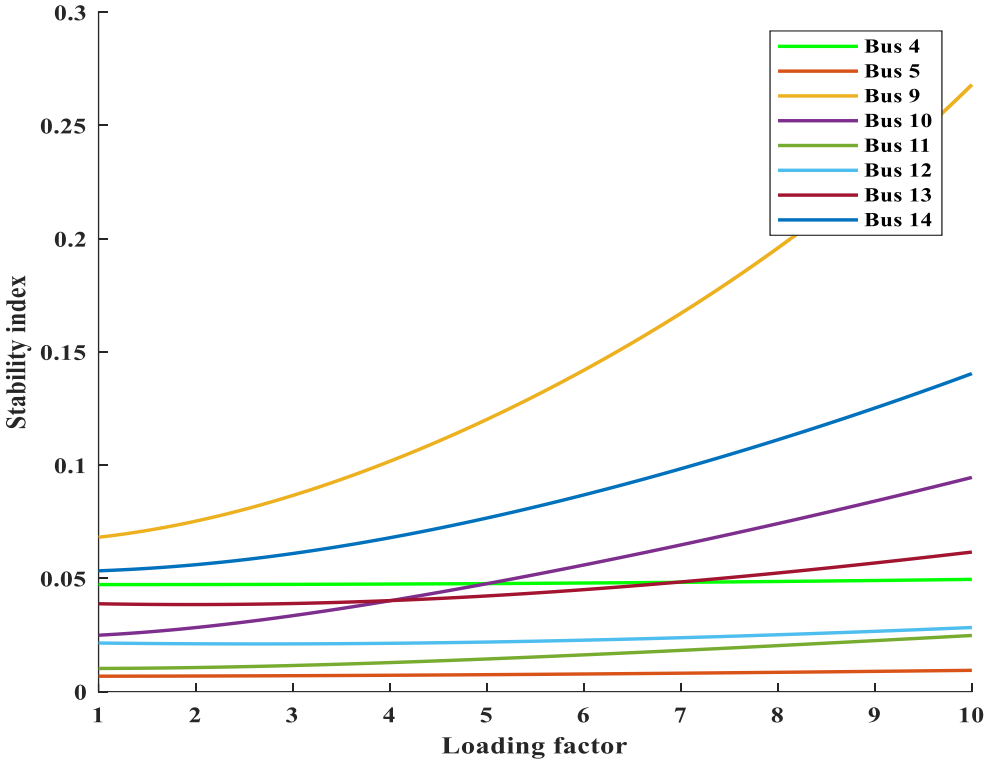

Figure 4.11: The response of NISI for self-reactive load increment

4.2.2. Testing PPMI and comparison with other indices

Next, the performance of the active power margin index (PPMI) is tested. PPMI is important for the power system operator who needs actual power values for decision making. This index is tested using IEEE 14 bus and IEEE 30 bus test systems.

i) PPMI test using IEEE 14 bus system

IEEE 14 bus system is used for calculating the index at rated system loading condition. Using the expressions derived in section 3.3, the Thevenin equivalent parameters, the maximum active power transfer, and reactive and apparent powers at the point of collapse are calculated for system load buses. The results are shown in Table 4.2 here below.

Table 4.2: The per unit Thevenin parameters and per unit powers at the maximum loading point

Bus no	E_{th}**(pu)**	Z_{th} **(pu)**	φ	θ	P_{max} **(pu)**	$Q_{@max}$ **(pu)**	$S_{@max}$ **(pu)**	$V_{@max}$ **(pu)**	**Prated (pu)**
4	1.0237	0.1024	79.4502	-4.6644	4.6280	-0.3776	4.6434	0.6894	0.4780
5	1.0213	0.0910	86.8060	11.8887	4.4490	0.9366	4.5466	0.6433	0.0760
9	1.0805	0.2245	101.267	29.3670	1.7287	0.9728	1.9836	0.6673	0.2950
10	1.0630	0.2569	96.0121	32.7995	1.2742	0.8211	1.5159	0.6241	0.0900
11	1.0611	0.2903	94.7939	27.2161	1.2485	0.6421	1.4039	0.6384	0.0350
12	1.0627	0.3788	85.9631	14.6973	1.0912	0.2862	1.1282	0.6537	0.0610
13	1.0614	0.2913	98.5778	23.2498	1.4178	0.6091	1.5431	0.6704	0.1350
14	1.0593	0.3639	84.4000	18.5502	1.0372	0.3481	1.0941	0.6310	0.1490

Based on Table 4.2, the highest per unit Thevenin equivalent impedance is seen by bus 12 followed by bus 14. This is also confirmed in section 4.1.2. At constant power factor the highest maximum active power transfer can be made at bus 4 with 4.628 pu active power and critical voltage of 0.6894, whilst the minimum P_{max} can be made by bus 14 at pu active power of 1.0372 and critical voltage of 0.6310 pu. The lowest critical voltage occurs at bus 10 with a value of 0.6241.

Here, it is worth mentioning this maximum active power transfer occurs when the external system stays unchanged and the target bus load increases at constant power factor. If either of these parameters changed, a change in P_{max} occurs. Hence, the calculation needs to be recomputed.

Next PPMI is calculated as in Table 4.3. For comparison purpose the result from new impedance stability index (NISI) and SPMI from [78] are also included in the table as shown.

Table 4.3: Power margin indices and NISI at rated loading of IEEE 14 bus system

Bus	$P_{max} - P_{rated}$ **(pu)**	**PPMI**	**SPMI**	**NISI**
4	4.1500	0.8967	0.8967	0.0474
5	4.3730	0.9829	0.9829	0.0068
9	1.4337	0.8294 (1^{st})	0.8294(1^{st})	0.0682 (1^{st})
10	1.1842	0.9294	0.9294	0.0249
11	1.2135	0.9720	0.9720	0.0102
12	1.0302	0.9441	0.9441	0.0215
13	1.2828	0.9048	0.9048	0.0388
14	0.8882	0.8563(2^{nd})	0.8563(2^{nd})	0.0533(2^{nd})

NISI and PPMI are designed to work in a reverse mode. The nearer to value 1 is unstable for NISI and stable for PPMI. The same reversal occurs to zero.

PPMI and SPMI are equivalents, they produce exactly the same result. Accordingly, the weakest bus is bus 9 followed by bus 14. This result matches with the result obtained with NISI. To get the active power needed to go before instability one can multiply the index by the maximum power. This is shown in column 2 of Table 4.3.

ii) Test using IEEE 30 Bus System

IEEE 30 bus test system is utilized for testing the performance at rated condition and to test the response of the index for load increment. For the 30-bus test system, the Thevenin parameters are determined using the procedure mentioned before. For not congesting the space for all load bus data, the results are demonstrated using bar graphs in Figure 4.12.

It can be observed from the diagram the highest Thevenin impedance is seen by bus 30 followed by bus 26. The minimum Thevenin impedance is seen by bus 4. It is important to remember that the Thevenin impedance depends on the admittance matrix and the load current as shown by (3.32). The difference among load buses arises from difference in these parameters. The per unit Thevenin voltage doesn't show large variations. The highest maximum active power transfer can be made at bus 4 with the value of 4.1577 at a critical voltage of 0.6182 pu. The lowest maximum active power transfer is of bus 26

with a value of 0.3188 at a critical voltage of 0.5330 pu. The lowest critical voltage is also shown by this bus.

Then the indices are shown in the bar chart in Figure 4.13.

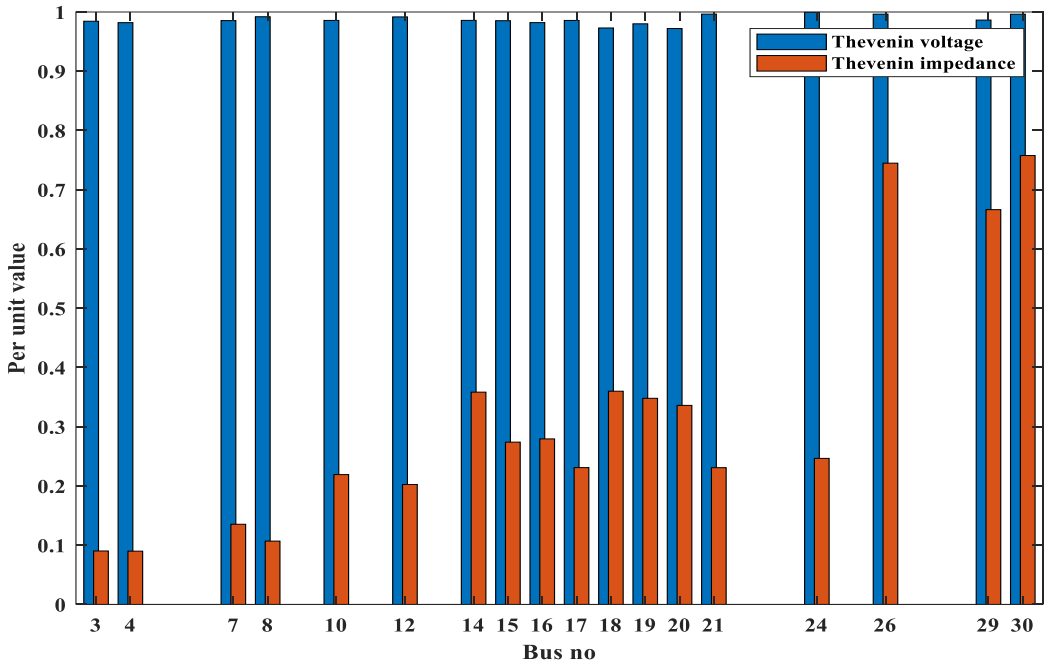

Figure 4.12: Thevenin equivalent parameters seen by the load buses of IEEE 30 bus system

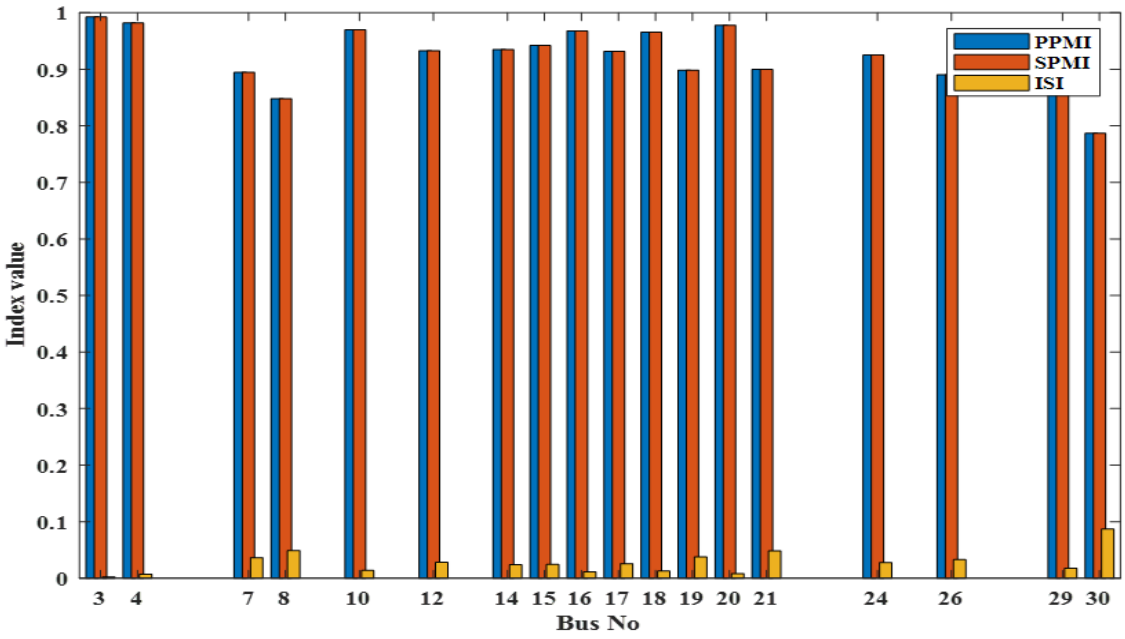

Figure 4.13: Stability indices of IEEE 30 bus test system

For verification of the results, SPMI and NISI are also included in this diagram. Bus 30 is the weakest bus followed by bus 8. Bus 3 is the strongest bus. Both SPMI and NISI

show the same result. This result is also proved by other studies made on the same system [143].

In real-time operation, system loading constantly varies. This variation affects the Thevenin impedance seen by the load bus. The variation in Thevenin impedance, in turn, affects the stability indices. Here, below, in Figure 4.14, the response of PPMI for load increment is plotted for the weakest buses.

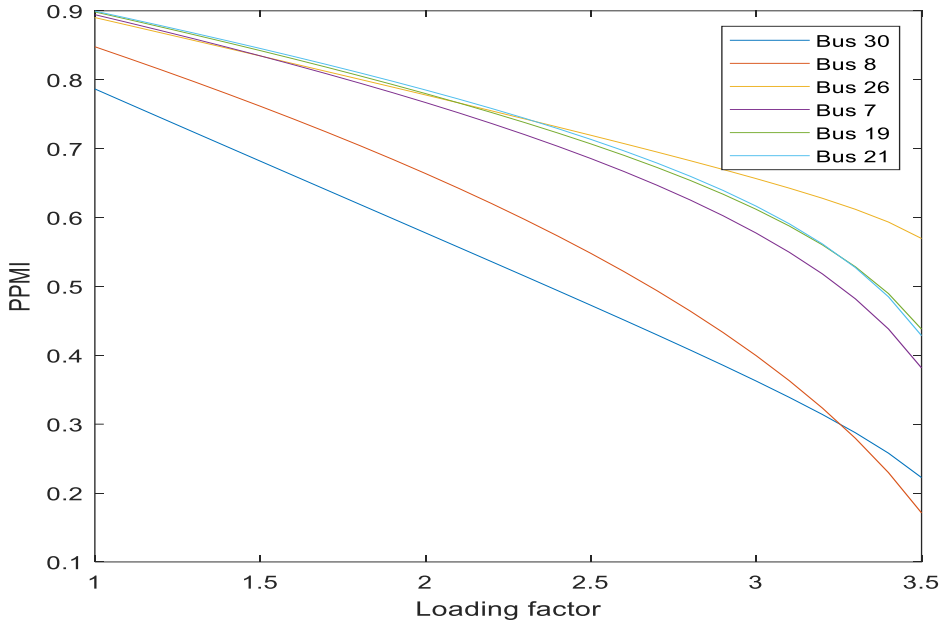

Figure 4.14: The response of PPMI for load increment for weakest buses

Figure 4.14 shows, for some buses, the rank of the buses varies when system loading changes. For all load increment, under constant power factor, until the loading factor of 3.3, bus 30 is the weakest bus. Beyond this point bus 8 takes over to become the weakest bus.

This condition shows, determining the index from the rated system loading condition only may give wrong proximity to the point of collapse. Hence constant tracking and determining proximity based on current operating point is necessary to have the actual status.

iii) PPMI as FRPM tool

As mentioned in chapter two, reactive power compensation plays two roles in voltage security ensuring activities. The first is improving the voltage profile so that system

voltage limit is respected. The second importance is increasing maximum power transfer capability, and hence improving voltage stability.

Here below, the effect of reactive power compensation is demonstrated in Figure 4.15. The weakest bus of IEEE 30 bus system, i.e. bus 30, is chosen for demonstration.

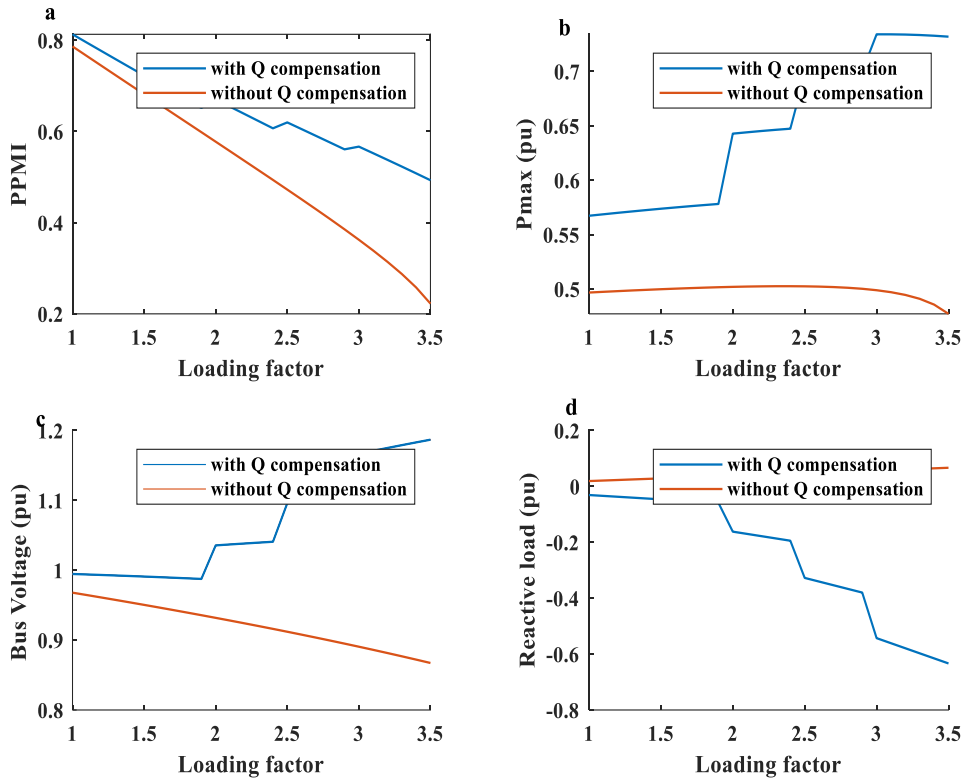

Figure 4.15: Response for reactive power compensation (a) PPMI, (b) maximum transferable active power, (c) Bus voltage profile (d) Reactive power compensation

In this test, the reactive power compensation at the load bus is increased in 5 MVar steps. The compensation is made at factors of 1, 2, 2.5, and 3 reaching a total compensation of 20MVar. This compensation is shown in Figure 4.15 (d). The compensation increased the maximum deliverable active power, and hence PPMI got increased. As an illustration, initial compensation of 5MVar increased the maximum deliverable active power from the uncompensated 0.4967 pu to 0.5673 pu. The PPMI increased from 0.7866 to 0.8131. This shows widening of the margin from instability and makes the system more voltage stable.

The reactive power compensation also improves the voltage profile. As in figure 4.15. (c) the initial compensation of 5 MVar has increased the voltage profile from 0.9679 pu to 0.9946 pu. This shows both voltage profile and voltage stability have got improved.

4.3. Performance Evaluation of IMOPSO

In this test, for the first phase, test functions ZDT1, ZDT2 and ZDT3, which are common test functions of AI algorithms, are utilized. The pareto fronts are also graphically depicted for elaborating the meaning of the IGDs and CDs.

In the second phase of the test the IMOPSO is applied to IEEE 14 bus reactive power optimization.

4.3.1. Test of IMOPSO for standard test functions

This scenario tests the algorithm as applied to the standard test functions; ZDT1, ZDT2 and ZDT3. These functions are widely employed in the literature for the test of different algorithms. In the performance evaluation, IMOPSO is evaluated against standard MOPSO and NSGA-II algorithms. The comparisons are made based on the quality of the pareto front and the diversity of the pareto front. The quality is measured using the inverted generational distance (IGD) and the diversity is measured using the crowding distance (CD).

i) Quality of the pareto front

In order to understand the results from IGD, first the pareto fronts are visualized on the solution space graphically in Figure 4.16. Then, the IGDs of the pareto fronts are calculated and they are shown in Figure 4.17. For discussion of the results ZDT1 is chosen. Not to make redundancy of discussions, only the results from ZDT2 and ZDT3 are depicted in Figure 4.18.

Based on Figure 4.16, MOPSO produces the less dominant pareto front of all. NSGA II shows the next less dominant front, while IMOPSO is producing the dominant front of all. For a narrow range, NSGA II shows dominance comparable to IMOPSO, but IMOPSO is seen generally dominating.

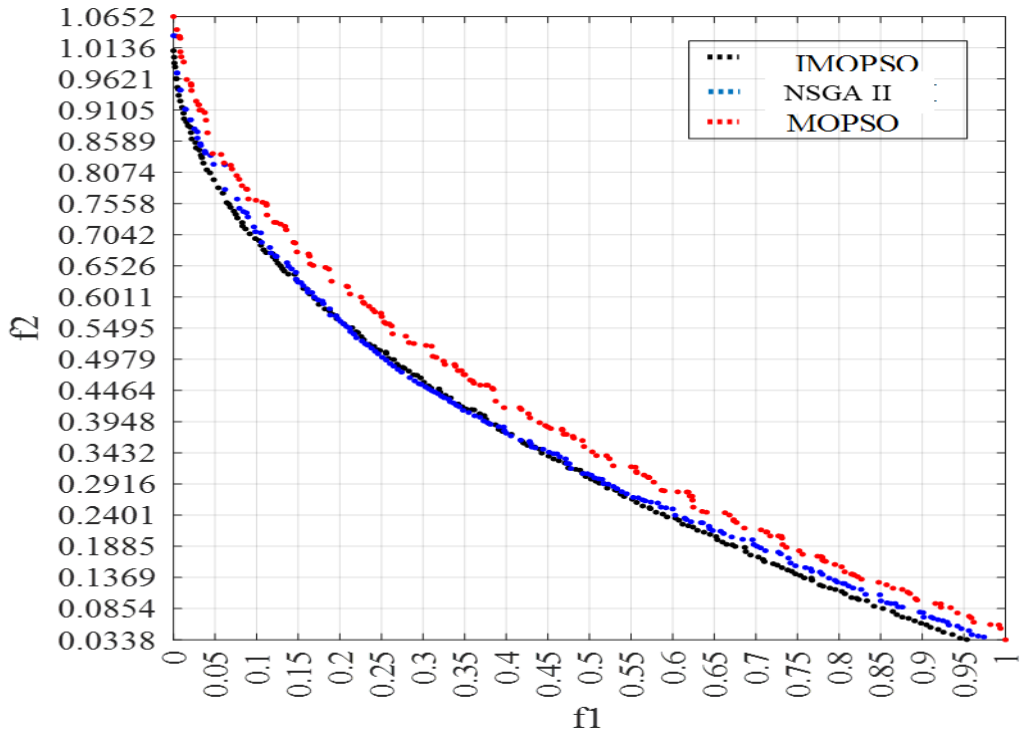

Figure 4.16: Pareto fronts from IMOPSO, NSGA II and MOPSO for ZDT 1 test function

Further, the IGDs are shown in Figure 4.17. The graph of the IGDs reveals two things. The first is the quality of the pareto front in coming closer to the true pareto front. The second thing revealed is the speed of convergence. The method that settles to its best front in earlier iterations has fast convergence.

The IGD graphs show the dominance of IMOPSO over MOPSO and NSGA II algorithms in terms of closeness to the pareto front and speed of convergence. IMOPSO settles to its minimum distance at earlier iterations.

Seeing the magnitude of IGDs, the result from Figure 4.17 consolidates the result in Figure 4.16. The IGD value of IMOPSO is the smallest as compared to the counter parts. This means the pareto front of IMOPSO is nearest to the true pareto front. NSGA II and MOPSO come in the next order.

Comparing MOPSO and NSGA II, MOPSO shows faster convergence at early iterations than NSGA II. This result go in line with the findings of the literature, which speak about the fast convergence of PSO [107]. But, though slower, NSGA II, finally, achieves lower IGD than MOPSO, which makes it more preferable in terms the quality of the pareto

front. These results show the superiority of IMOPSO over the other methods used for the comparison, in terms of closing up to the true pareto front and speed of convergence.

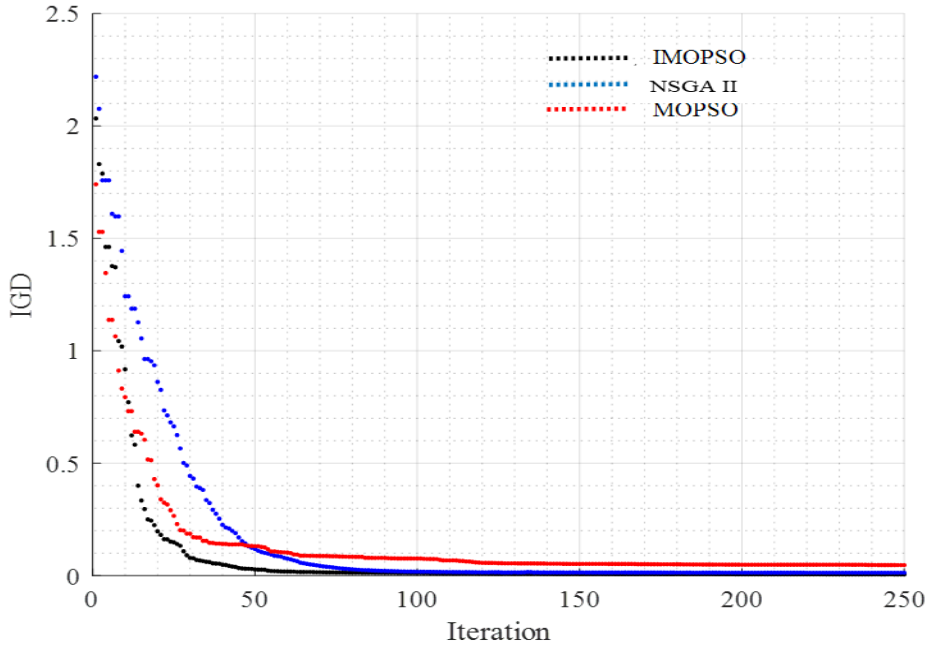

Figure 4.17: Inverted generational distance of the Algorithms

The results from the test function ZDT2 and ZDT3 are shown in Figure 4.18 next. The results show the same improvement is made, as in the case with ZDT1 test function.

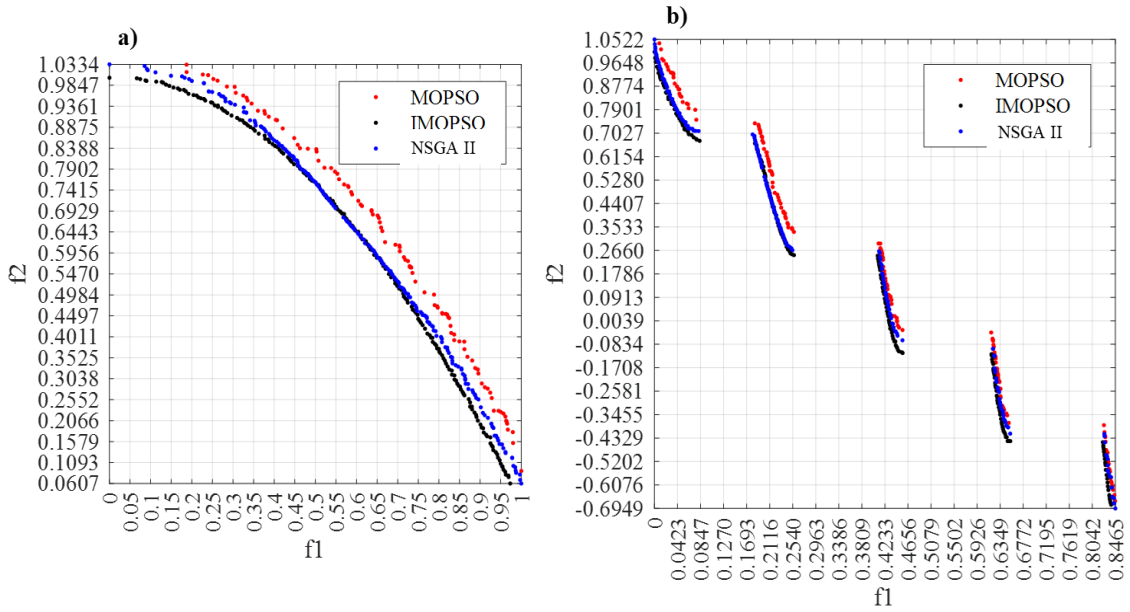

Figure 4.18: Pareto fronts of test functions a) ZDT 2 b) ZDT3

ii) Diversity of the pareto fronts

In this section, the diversity of the pareto fronts is measured in terms of the crowding distance (CD). Larger value of CD means a more diverse pareto front which is highly favoured. Smaller value of CD indicates a less diverse pareto front. The crowding distance of the pareto fronts from the three algorithms for the three test functions is shown in Table 4.4, below.

Table 4.4: Crowding distance computation of the pareto fronts from the three algorithms

Function	ZDT1		ZDT2		ZDT3	
	Mean	Standard deviation	Mean	Standard deviation	Mean	Std. deviation
MOPSO	0.0335	0.0173	0.0384	0.0213	0.0244	0.0401
NSGA II	0.0199	0.0075	0.0191	0.0150	0.0202	0.0391
IMOPSO	0.0201	0.0053	0.0198	0.0063	0.0202	0.0336

From Table 4.4 MOPSO seems to produce a more diverse front as the mean value of CDs is the highest. However, it is important to note that the PF from MOPSO is situated in the less dominant solution space as discussed and depicted by the previous section. This means MOPSO fails the first line of performance check when compared with IMOPSO and NSGA II algorithms.

In this analysis, despite IMOPSO produces a more dominant PF than NSGA II, this difference doesn't result in a larger impact on the CD computation. Hence, the computation takes this into consideration.

Table 4.4 contains the mean value of the CDs and the distribution of CDs around the mean as measured in terms of the standard deviation. Larger values of mean indicate higher crowding distance values. Larger value of the standard deviation means a large deviation from the mean. Larger mean value and smaller standard deviation is needed, for the PF to be diverse. Larger mean and smaller standard deviation indicate individual CDs are at higher values and are close to the mean.

Hence, comparing NSGA II and IMOPSO, IMOPSO owns higher mean values and smaller standard deviation for the three functions. This indicates the CDs are at higher values which shows a more diverse position is obtained using IMOPSO.

4.3.2. Test of IMOPSO on IEEE 14 bus system

Once the algorithm gets tested using standard test functions, next, it is tested on IEEE 14 bus test system. The IEEE 14 bus system is a simplest test system containing the necessary control parameters for voltage security study. These control parameters are generator voltage outputs, reactive power compensations and tap changing transformers.

The IEEE 14 bus test system data is taken from Matpower simulation software [140]. Accordingly, the test system contains five generators, five transformers (this includes two winding representations of three winding transformers), one reactive power compensation as control variables. Additionally, the system contains 9 load buses.

In this implementation, the control variables are set as follows. The generator voltages are allowed to vary between the range minimum 0.9 pu and maximum 1.1 pu. The transformer tap positions are allowed in the range 0.95 and 1.05. The reactive power compensation is allowed to vary between the minimum value of 0 MVAR to the maximum value of 20 MVAR.

The iteration is run for 200 iterations. After, the final iteration the pareto front, in Figure 4.19, is obtained.

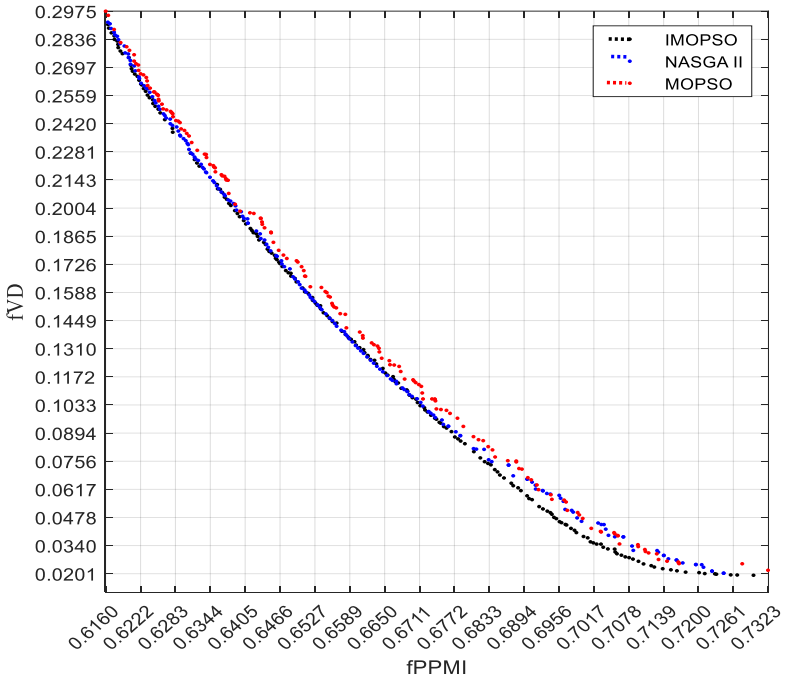

Figure 4.19: Pareto front of voltage security determining objectives

For comparison purpose the result from NSGA II and standard MOPSO algorithms are also shown. These depictions consolidate the result from the previous section 4.3.1. In this specific application, for lower f_{PPMI} and higher f_{VD} IMOPSO and NSGA II show similar performance. But, moving towards lower f_{VD} IMOPSO continues to dominate both NSGA II and standard MOPSO.

Enough being said about the comparison of the algorithms, the discussions afterwards, are based on the pareto front from IMOPSO.

The pareto front of IMOPSO in Figure 4.19 contains 200 possible operating points meeting the objectives, the equality constraints and inequality constraints. The voltage deviation objective function (f_{VD}) goes from a minimum of 0.0188 to the maximum of 0.3059 while the voltage stability index objective function (f_{PPMI}) goes from a minimum of 0.6131 to the maximum of 0.7281.

Interpreting these functions in terms of voltage deviation and individual bus index, each bus will have average minimum voltage deviation of 0.0457 pu and average maximum voltage deviation of 0.1844 pu, in this optimal front. The deviation is measured from the nominal voltage of 1pu. Based on the standard, i.e. IEC 60038, load buses are allowed to vary $\pm$ 5 % (0.5 pu value) from the nominal voltage setting. Hence, the variations resulted from IMOPSO well respect this standard.

In terms of the stability index PPMI, using the relation in (3.83), the index varies from average minimum PPMI value of 0.9191 to the average maximum PPMI index of 0.9319. Based on (3.81) these values indicate large gap between current operating power (P_{opr}) and the maximum possible active power transfer (P_{max}). This means the system is far enough from voltage instability under these optimal operating points.

From the set of optimum values, the selection depends on the specific need of the system operator. Whether to incline to voltage deviation or voltage stability, within this optimum set, is up to the operator's specific preference.

Below, the value of the control variables for the 200 optimal positions, in the pareto front, are revealed in Figure 4.20. The control variables are generator output voltages, transformer tap positions and the value of the reactive power compensation. For more elaboration of the discussion, Table 4.5 shows important features of the data set.

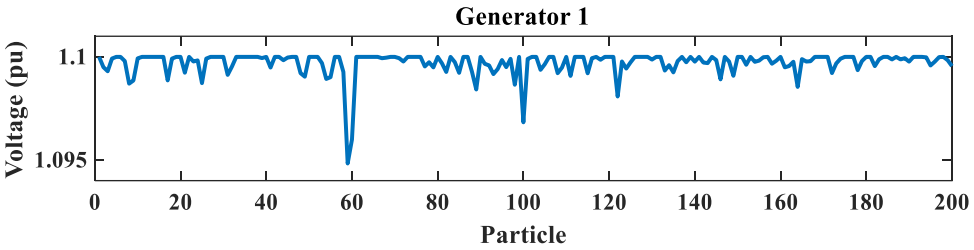
Generator 1
Voltage (pu)
1.1
1.095
0
20
40
60
80
100
120
140
160
180
200
Particle

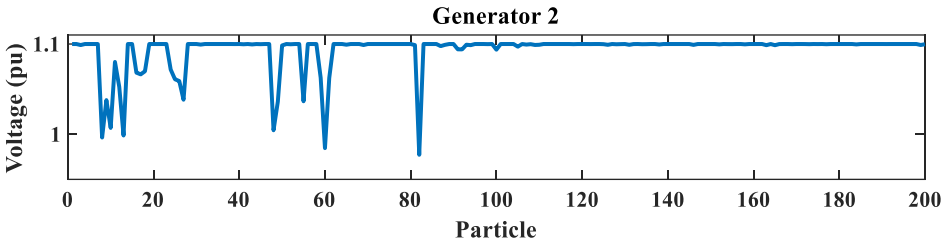
Generator 2
Voltage (pu)
1.1
1
0
20
40
60
80
100
120
140
160
180
200
Particle

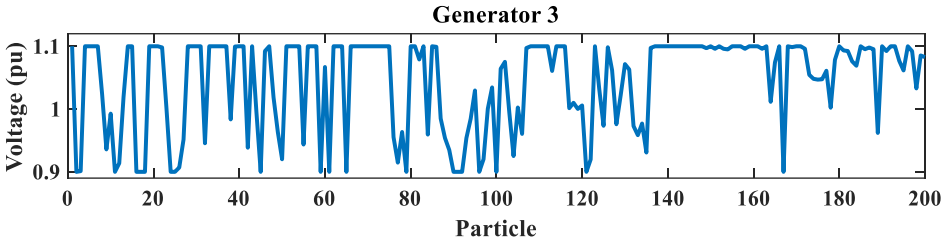
Generator 3
Voltage (pu)
1.1
1
0.9
0
20
40
60
80
100
120
140
160
180
200
Particle

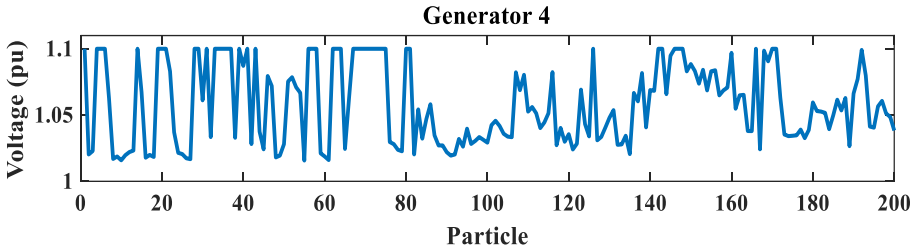
Generator 4
Voltage (pu)
1.1
1.05
1
0
20
40
60
80
100
120
140
160
180
200
Particle

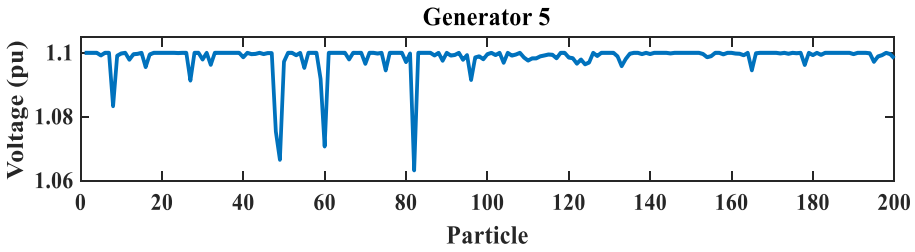
Generator 5
Voltage (pu)
1.1
1.08
1.06
0
20
40
60
80
100
120
140
160
180
200
Particle

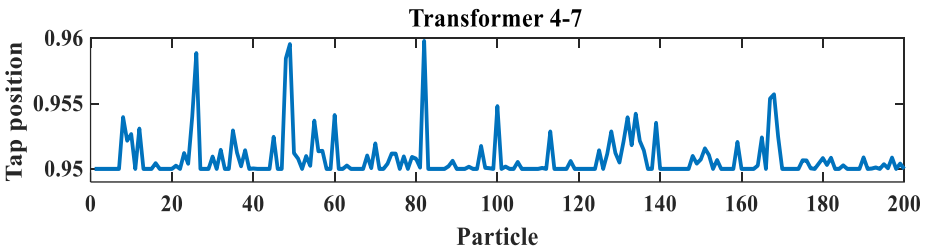
Transformer 4-7
Tap position
0.96
0.955
0.95
0
20
40
60
80
100
120
140
160
180
200
Particle

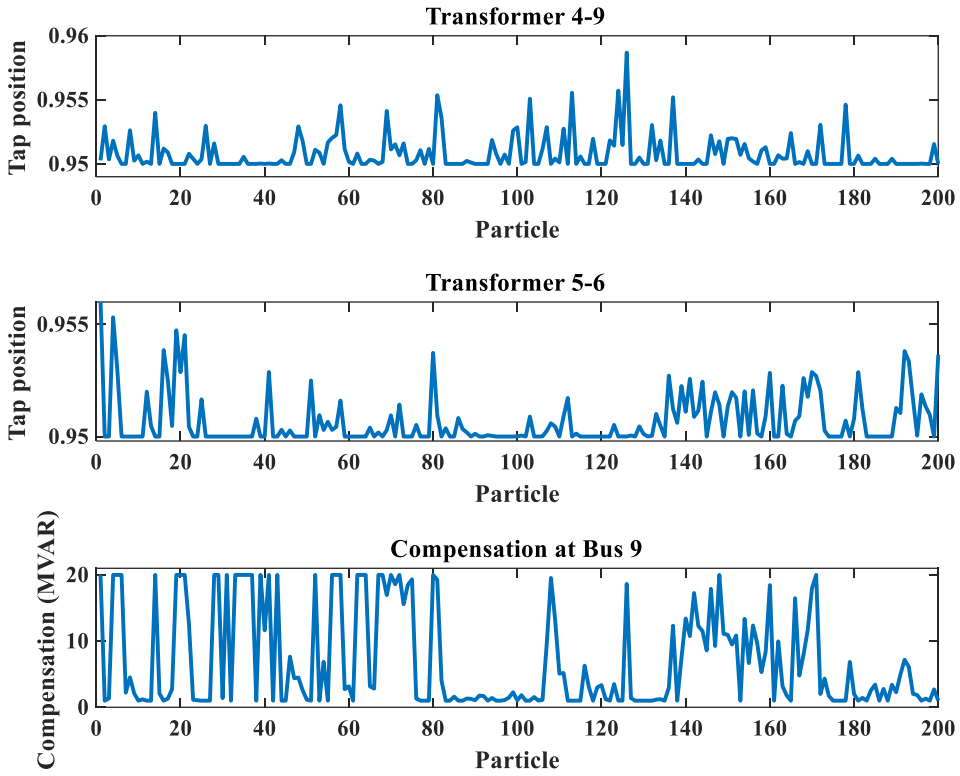

Figure 4.20: The control variable values at the optimum operation of IEEE 14 bus system

Table 4.5: The variation of the control variables

Control variable	Minimum	Maximum	Mean	Standard deviation
Vg1	1.0948	1.1000	1.0997	0.0006
Vg2	0.9773	1.1000	1.0936	0.0210
Vg3	0.9000	1.1000	1.0447	0.0733
Vg4	1.0157	1.1000	1.0584	0.0299
Vg5	1.0632	1.1000	1.0986	0.0047
Transformer 4-7	0.9500	0.9598	0.9508	0.0016
Transformer 4-9	0.9500	0.9587	0.9508	0.0014
Transformer 5-6	0.9500	0.9561	0.9507	0.0011
Transformer 7-8	0.9500	1.0500	1.0428	0.0116
Transformer 7-9	0.9500	1.0500	1.0371	0.0251
Compensation at bus 9	1.0000	20.0000	7.0300	7.4922

Discussing the generator output voltages; based on Figure 4.20 and Table 4.5, the highest generator output voltage hits are the same for all generators. The minimum generator output is recorded for generator 3. The highest among minimum generator output voltage is made by generator 1. This attributes to the stabilizing capacity of this generator and its service as a slack bus. The highest mean value goes to generator 1. The standard deviation from the mean value is minimum for this generator too. That means generator 1 is

operated at higher voltage values almost for all pareto front points, with minimum deviation.

Continuing speaking of generator output voltages, the lowest mean value is owned by generator 3. This means for the majority of the pareto points generator 3 is operated at relatively lower voltage output. The standard deviation for this generator output voltage is also the largest. That means generator 3 owns a large set of operating voltage output values.

The maximum limit of the generators, i.e 1.1 pu, is hit by all the generators but the minimum limit 0.9 pu is hit by only one generator. This infers optimum operating points favour high generator output voltages. This, indirectly, indicate the system is prone to under voltage insecurity.

Coming to the transformer tap changer position, the minimum tap changer position 0.95 is hit by all the transformers. Whilst, the maximum tap changer position is hit by 2 transformers out of 5 transformers. This indicates the optimum operating points favour the lower tap changer position.

Figure 4.20 contains only the positions of 3 transformers out of five. This selection is made for the selected elements are enough for the discussion purpose.

Transformer 5-6 shows a minimum variation in values around the mean, for the standard deviation is the smallest. The mean is also the smallest for this transformer. Transformer 5-6, Transformer 4-7 and Transformer 4-9 are operated at lower tap changer positions, as revealed by lower maximum and average values of the tap positions.

Coming to the reactive power compensation at bus 9, the compensation goes from the minimum 1MVAR to the maximum 20 MVAR. However, the mean value 7.03 MVAR, which is less than the median 11 MVAR, shows the reactive power compensation favours lower amount of compensation.

CHAPTER 5 APPLICATION OF THE VSA AND RPM SCHEMES ON THE EEP SYSTEM

5.1. Setup of the EEP System Used for the Study

For the application study, only in-service components of the EEP, as of 2022, are taken into consideration. Components temporarily or permanently down due to maintenance issue and new components waiting future connectivity are not considered.

The makeup of the system used for the study consists of the following components as listed in Table 5.1 below.

Table 5.1: EEP system makeup used for the analysis

Component	**Type**	**Amount per type**	**Total amount**
Buses	Load buses	283	798
	Generator bus	47	
	Intermediate buses	468	
Transmission lines	500 kV	4	372
	400 kV	30	
	230 kV	130	
	132 kV	160	
	66 kV	34	
	45 kV	13	
	15 kV	1	
Transformers	2 winding	354	575
	3 winding	221	
Generators	Generating units	64	64
Reactive power auxiliary supplies	Shunt capacitors	9	77
	Shunt reactors	68	

These components fall into 11 areas, which are used by the EEP for technical and institutional administration. The areas are:

- Addis Ababa region, area 01
- Central region, area 02

- Eastern region, area 03
- Western region, area 04
- Southern region, area 05
- Northeastern regions, area 06
- Northwestern region, area 07
- Southwestern region, area 08
- Northern region, area 09
- The Djibouti supplying buses, area 10 and,
- Republic of Sudan supplying buses, area 11

These areas are used by this study, too, to understand areal distribution of voltage security problems.

5.2. VSA Scheme Applied to the EEP System for Voltage Security Assessment and FRPM

The capabilities of the VSA scheme, demonstrated in this section, are computations of Thevenin impedance, maximum power transfer, PPMI index, PV curves and QV curves. The EEP system is analysed using these capabilities in the following sections.

From the two voltage stability assessment indices the PPMI is taken for analysis. This is for two reasons. The first reason is the two indices produce a matching result, as shown in chapter 4. Hence, the approach plans to avoid repetitions. The second reason is PPMI gives an advantage in providing the necessary information on power transfer capacities, which enables detailed discussion in power related terms.

In this analysis, procedures of the voltage stability assessment are discussed, for each step provides supportive evidence for the results on system vulnerability to voltage security problems. These procedures are determining Thevenin equivalent parameters, determining the maximum active power transfer limit, PPMI computation, vulnerability ranking, PV curve analysis and QV curve analysis.

This study is made for the following four scenarios;

(i) Heavy load uncompensated system
(ii) Heavy load compensated system
(iii) Light load uncompensated system
(iv) Light load compensated system

The reason for the inclusion of compensation scenarios is to reveal the utilization of PPMI as FRPM tool.

5.2.1. Thevenin equivalent impedance seen by EEP load buses

The four scenarios reveal the dependency of Thevenin impedance on the system unique loading condition and the reactive power compensation level. This is shown in diagrams of Figure 5.1 below. The names of the load buses at each number are provided in Appendix II. Area-wise, bus numbers 2-50 fall in Area 1, 51-119 in Area 2, 120-140 in Area 3, 141-158 in Area 4, 159-193 in Area 5, 194-210 in Area 6, 211-237 in Area 7, 238-257 in Area 8, 258-281 in Area 9.
Load increment and reactive power compensation show differing impacts on high value and low value Thevenin impedances. For a closer investigation of Figure 5.1, top ten and least ten values owning buses are screened out in Table 5.2.

In the case of high value Thevenin impedance, compensation reduces Thevenin impedance while system load increment increases it. These changes also affect the order of values among the load buses. All the top ten high Thevenin impedance seeing buses are supplied from the 66 kV transmission line. Area-wise, 70 percent of these load buses are from area 7 or area 6. According to the data from the EEP, the 66 kV transmission lines have highest impedance per km as compared to other transmission lines. This contributes to the high impedance value seen by the load buses, which are supplied from these lines. Buses PAWIE 15 and PAWIE 33, consecutively, are buses seeing high Thevenin impedance value. These two buses are located on the Two terminals of a three-winding transformer. This is an indication of buses near to each other see a closer Thevenin impedance values.

In the low Thevenin impedance value seeing buses, for the majority, compensation increases Thevenin impedance while load increment decreases the Thevenin impedance value. This incidence is opposing the case with high Thevenin impedance seeing buses. The least Thevenin impedances are seen by buses DIRE DAWA 33 and ADIGALA 33, consecutively. The buses, seeing low Thevenin impedance, are those supplied from either 132 kV or 230 kV transmissions. With some exceptions, as in the least three, low Thevenin impedance seeing buses are dominantly from Addis Ababa region, i.e area 1. This can be seen by screening least 20 values. This attributes to the high connectivity of the transmission buses in this area.

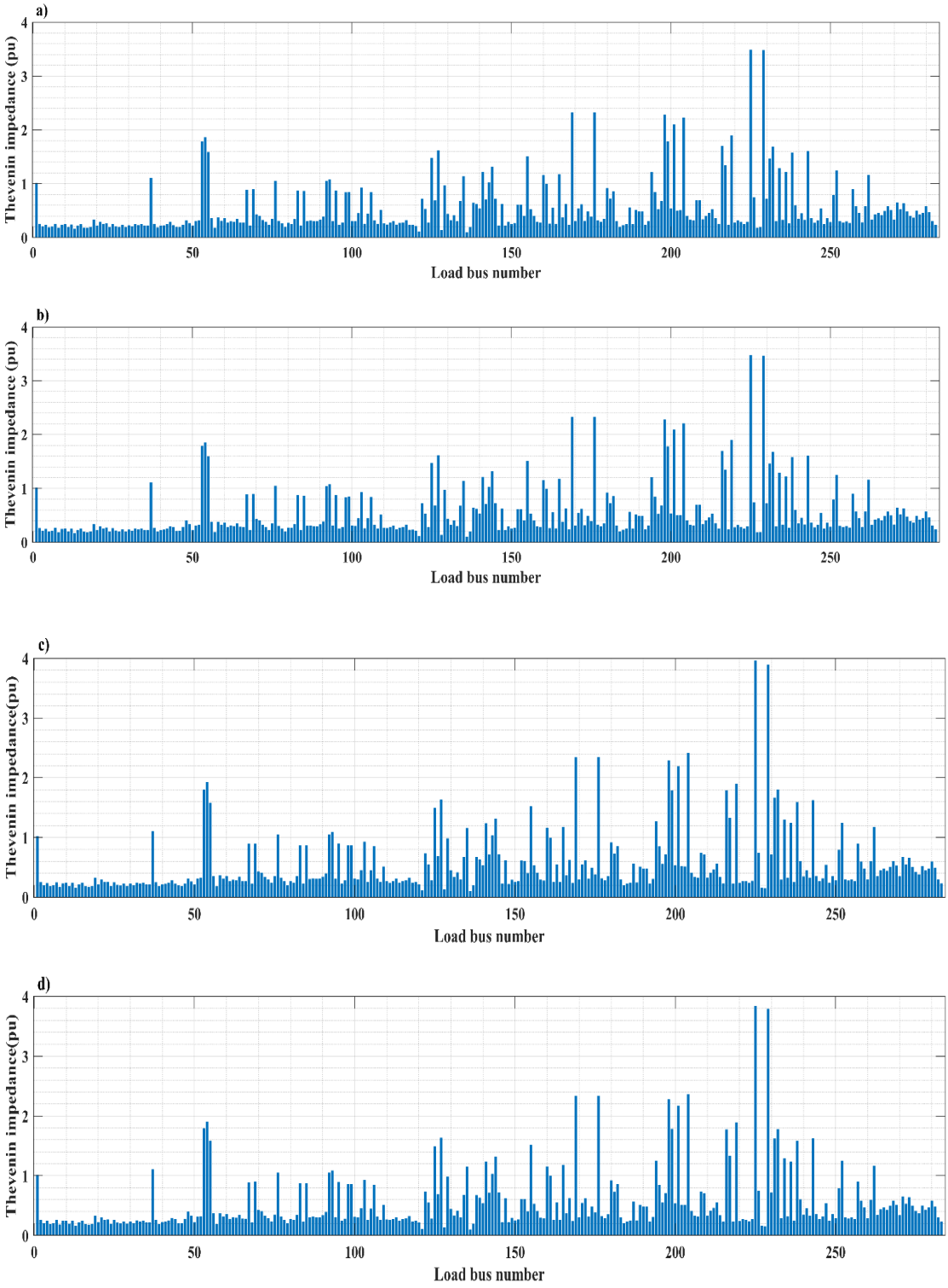

Figure 5.1: Thevenin impedance seen by the load buses a) Light load uncompensated system b) Light load compensated system c) Heavy load uncompensated system d) Heavy load compensated system

Table 5.2: High value and low value Thevenin impedances

	Light load uncompensated system			**Light load compensated system**			**Heavy load uncompensated system**			**Heavy load compensated system**		
High value Thevenin impedance	Load bus	Area	Zth (pu)	Load bus	Area	Zth (pu)	Load bus	Area	Zth (pu)	Load bus	Area	Zth (pu)
	PAWIE 15	7	3.4929	PAWIE 15	7	3.4779	PAWIE 15	7	3.9563	PAWIE 15	7	3.8436
	PAWIE 33	7	3.4808	PAWIE 33	7	3.4672	PAWIE 33	7	3.8902	PAWIE 33	7	3.7923
	NG-BORNA 15	5	2.3271	NG-BORNA 15	5	2.3261	WOLDIA 33	6	2.4127	WOLDIA 33	6	2.3686
	NG-BORNA 33	5	2.3261	NG-BORNA 33	5	2.3251	NG-BORNA 15	5	2.3419	NG-BORNA 15	5	2.3399
	LALIBEL 15	6	2.2829	LALIBEL 15	6	2.2800	NG-BORNA 33	5	2.3412	NG-BORNA 33	5	2.3392
	WOLDIA 33	6	2.2237	WOLDIA 33	6	2.2097	LALIBEL 15	6	2.2885	LALIBEL 15	6	2.2840
	WOLDIA 15	6	2.0995	WOLDIA 15	6	2.0919	WOLDIA 15	6	2.1958	WOLDIA 15	6	2.1745
	FT-SELAM 15	7	1.9014	FT-SELAM 15	7	1.9017	FITCHE 33	2	1.9273	FITCHE 33	2	1.9050
	FITCHE 33	2	1.8625	FITCHE 33	2	1.8519	FT-SELAM 15	7	1.8958	FT-SELAM 15	7	1.8965
	FITCHE 15	2	1.7867	FITCHE 15	2	1.7858	DANGLA 15	7	1.8049	FITCHE 15	2	1.7958
Low value Thevenin impedances	DIRE DAW 33	3	0.1004	DIRE DAW 33	3	0.1008	DIRE DAW 33	3	0.1004	DIRE DAW 33	3	0.1004
	ADIGALA 33	3	0.1122	ADIGALA 33	3	0.1122	ADIGALA 33	3	0.1124	ADIGALA 33	3	0.1123
	DIRE DAW 15	3	0.1354	DIRE DAW 15	3	0.1360	DIRE DAW 15	3	0.1348	DIRE DAW 15	3	0.1350
	AYAT GIS 15	1	0.1615	AYAT GIS 15	1	0.1654	GONDAR2 15	7	0.1517	GONDAR2 15	7	0.1554
	TORHYL G 15	1	0.1792	B. DAR-2 15	7	0.1823	AYAT GIS 15	1	0.1599	AYAT GIS 15	1	0.1637
	SULULTA-33	1	0.1812	TORHYL G 15	1	0.1861	B. DAR-2 15	7	0.1631	B. DAR-2 15	7	0.1648
	B. DAR-2 15	7	0.1829	SULULTA-33	1	0.1884	TORHYL G 15	1	0.1750	TORHYL G 15	1	0.1824
	GINCHI 15	2	0.1855	GONDAR2 15	7	0.1902	SULULTA-33	1	0.1767	SULULTA-33	1	0.1843
	GEFRSA-3 15	1	0.1868	GINCHI 15	2	0.1903	GINCHI 15	2	0.1819	GINCHI 15	2	0.1873
	B-LION 15	1	0.1878	GEFRSA-3 15	1	0.1931	GEFRSA-3 15	1	0.1826	GEFRSA-3 15	1	0.1894

5.2.2. Maximum active power transfer (P_{max}) of EEP load buses

For a given load bus, P_{max} changes with variation of load and compensation. Under the four scenarios, the maximum active power transfer capability of the load buses is shown in Figure 5.2 below.

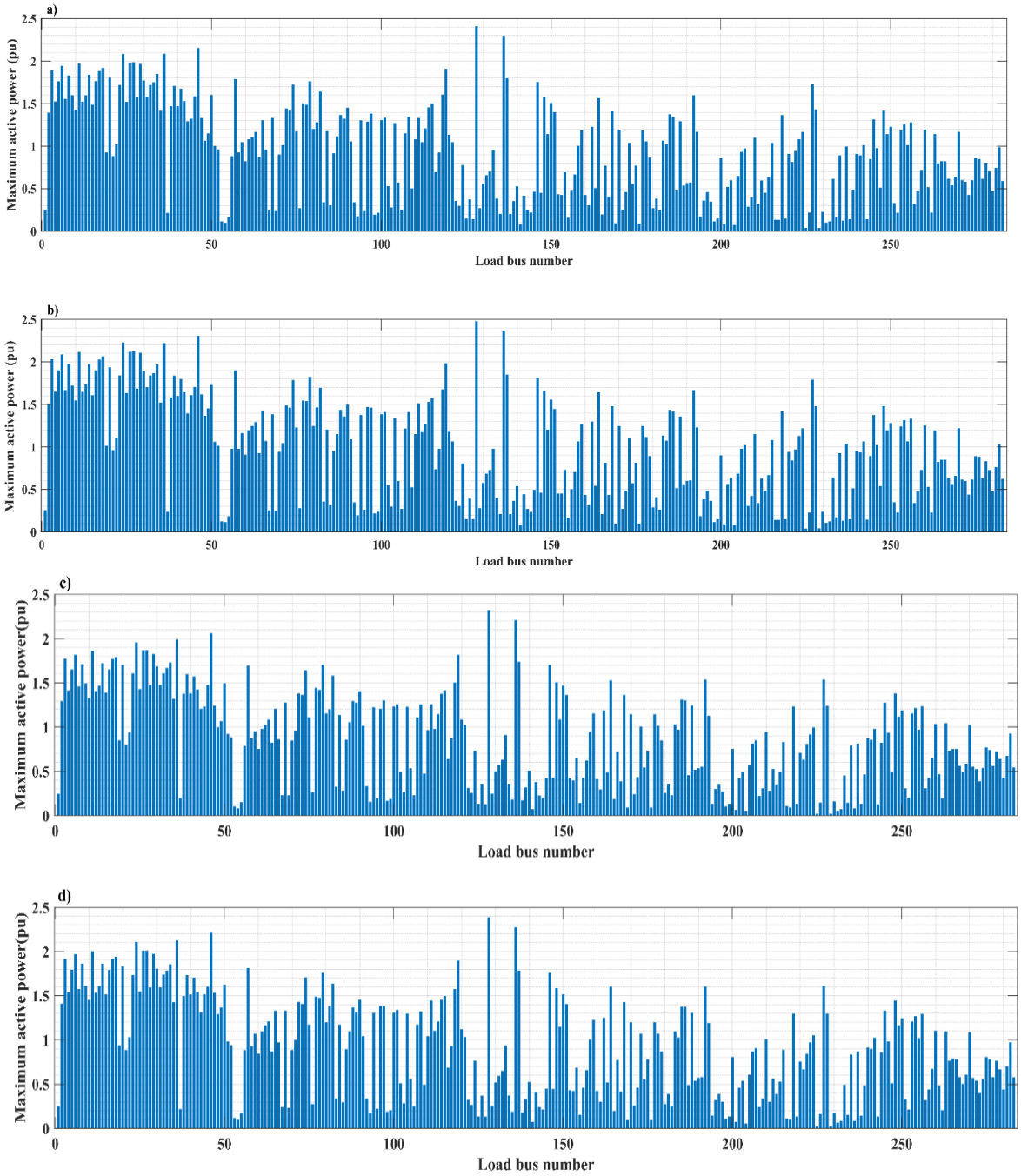

Figure 5.2: Maximum active power transfer limit of the load buses a) Light load uncompensated system b) Light load compensated system c) Heavy load uncompensated system d) Heavy load compensated system

Top ten P_{max} values and least ten P_{max} values are screened for demonstration, below in Table 5.3. The results show, as system loading increases, the maximum possible power transfer decreases. This is due to the reduction of the Thevenin equivalent voltage and the relative increase of Thevenin impedance. On the other hand, reactive power compensation, i.e. increase in power factor, increases the maximum active power transfer. Both compensation and load increment, affect the order of P_{max} values among load buses.

Buses sharing the same node, show a close value. This is due to the dependency of the maximum active power transfer on the network representation, as viewed from the load bus. Buses sharing the same node see the same network, i.e. see the same Thevenin equivalent representation. This can be seen from DIRE DAWA 15 and DIRE DAWA 33, PAWIE 15 and PAWIE 33, NEGELE BORENA 15 and NEGELE BORENA 33 and other buses. These buses are located at the terminals of a three-winding transformer.

Buses with top P_{max} values are supplied from 132 kV or 230 kV transmission lines. These buses are characterized by higher Thevenin voltage and lower Thevenin impedances. More than 80 % of the top ten buses are from the Addis Ababa region, area 1. Close investigation of Figure 5.2 trends confirms these results. DIRE DAWA 15 and DIRE DAWA 33 buses respectively have the highest P_{max} values.

On the other hand, 90 % of the least ten P_{max} values, are buses supplied from 66 kV transmission lines. As shown in the discussion of section 5.2.1, these buses are characterized by higher Thevenin impedance and lower Thevenin equivalent voltage. Buses with lowest P_{max} value are frequent in area 7 and area 6. This is due to the high concentration of the 66 kV transmission lines in these areas. PAWIE 15 and PAWIE 33 are buses with the least P_{max} value from all the system load buses. These buses are remembered from previous discussions, having highest Z_{th} value.

Table 5.3: Highest and lowest P_{max} values under the four scenarios

	light load uncompensated system			**light load compensated system**			**heavy load uncompensated system**			**Heavy load compensated system**		
High P_{max} values	Load bus	Area	P_{max}	Load bus	Area	P_{max} (pu)	Load bus	Area	P_{max} (pu)	Load Bus	Area	P_{max} (pu)
	DIRE DAW 15	3	2.4085	DIRE DAW 15	3	2.4762	DIRE DAW 15	3	2.3206	DIRE DAW 15	3	2.3858
	DIRE DAW 33	3	2.3006	DIRE DAW 33	3	2.3677	DIRE DAW 33	3	2.2094	DIRE DAW 33	3	2.2739
	SEBETA-2 36	1	2.1555	SEBETA-2 36	1	2.3066	SEBETA-2 36	1	2.0598	SEBETA-2 36	1	2.2113
	ADDIS-W1 15	1	2.0869	KLTI-NRTH 15	1	2.2288	ADDIS-W1 15	1	1.9892	ADDIS-W1 15	1	2.127
	KLTI-NRTH 15	1	2.0853	ADDIS-W1 15	1	2.222	KLTI-NRTH 15	1	1.9577	KLTI-NRTH 15	1	2.1062
	YESU 15	1	1.9890	YESU 15	1	2.1245	YESU 15	1	1.8695	YESU 15	1	2.0093
	NEFASILK 15	1	1.9824	NEFASILK 15	1	2.1210	NEFASILK 15	1	1.8661	NEFASILK 15	1	2.0091
	LEGETAFO 15	1	1.9739	LEGETAFO 15	1	2.1146	LEGETAFO 15	1	1.8604	LEGETAFO 15	1	2.0057
	KALITI GIS 15	1	1.9660	KALITI GIS 15	1	2.1058	KALITI GIS 15	1	1.8277	KALITI GIS 15	1	1.9727
	ADIS-EST 215	1	1.9450	ADIS-EST 215	1	2.0875	ADIS-EST 215	1	1.8194	ADIS-EST 215	1	1.9673
Low P_{max} Values	PAWIE 15	7	0.0395	PAWIE 15	7	0.0419	PAWIE 15	7	0.0201	PAWIE 15	7	0.0235
	PAWIE 33	7	0.0401	PAWIE 33	7	0.0425	PAWIE 33	7	0.0211	PAWIE 33	7	0.0244
	WOLDIA 33	6	0.0749	WOLDIA 33	6	0.0805	WOLDIA 33	6	0.0528	WOLDIA 33	6	0.0591
	ASSOSA 33	4	0.0777	ASSOSA 33	4	0.0828	DANGLA 33	7	0.0568	ASSOSA 33	4	0.0650
	WOLDIA 15	6	0.0851	WOLDIA 15	6	0.0907	WOLDIA 15	6	0.0659	WOLDIA 15	6	0.0722
	NG-BORN 15	5	0.0923	NG-BORN 15	5	0.0984	ASSOSA 33	4	0.0691	ASSOSA 33	4	0.0744
	NG-BORN 33	5	0.0936	NG-BORN 33	5	0.0998	DANGLA 33	7	0.0740	DANGLA 33	7	0.0824
	FITCHE 33	2	0.1001	DANGLA 33	7	0.1072	DABAT 33	7	0.0775	DABAT 33	7	0.0847
	DANGLA 33	7	0.1014	FITCHE 33	2	0.1130	FITCHE 33	2	0.0836	NG-BORN 15	5	0.0917
	FITCHE 33	2	0.1138	LALIBELA 15	6	0.1176	NG-BORN 15	5	0.0855	NG-BORN 33	5	0.0929

5.2.3. Active power margin index (PPMI) of the load buses

The active power margin index of load buses is determined after calculating the maximum active power transfer. The results are depicted in Figure 5.3 below.

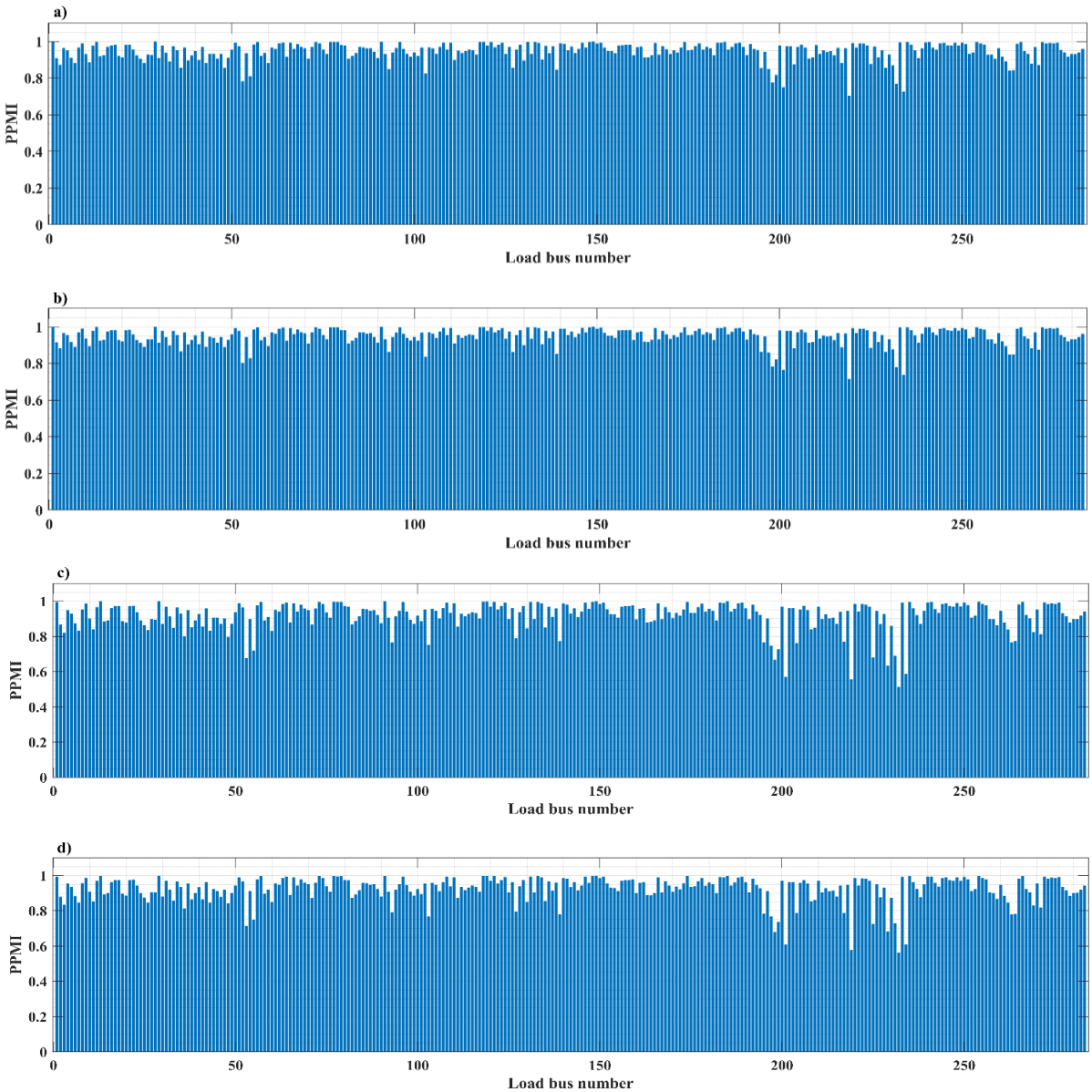

Figure 5.3: Active power margin index under different loading condition; a) Light load uncompensated system b) Light load compensated system c) Heavy load uncompensated system d) Heavy load compensated system

As loading increases the PPMI decreases, while compensation increases the PPMI. Loading changes ranks of strength and weakness of load buses. Ranking depends on each unique system loading condition. Upon system loading change, there are buses who maintained their rank while others change. Here below, the weakest buses are shown in Table 5.4.

Table 5.4: Weakest buses under different system loading condition

Light load uncompensated system			**Light load compensated system**			**Heavy load uncompensated system**			**Heavy load compensated system**		
Load bus	area	PPMI	Load bus	area	PPMI	Load bus	area	PPMI	Load bus	area	PPMI
FT-SELAM 15	7	0.7038	FT-SELAM 15	7	0.7154	DANGLA 15	7	0.5145	DANGLA 15	7	0.5638
BITCHENA 33	7	0.7276	BITCHENA 33	7	0.7385	FT-SELAM 15	7	0.5555	FT-SELAM 15	7	0.578
WOLDIA 15	6	0.7502	WOLDIA 15	6	0.7658	WOLDIA 15	6	0.5702	WOLDIA 15	6	0.6078
DANGLA 15	7	0.7689	DANGLA 15	7	0.7804	BITCHENA 33	7	0.5871	BITCHENA 33	7	0.6086
LALIBELA 15	6	0.777	LALIBELA 15	6	0.7834	PAWIE 33	7	0.6333	LALIBELA 15	6	0.6805
FICHE 15	2	0.7825	FICHE 15	2	0.8044	LALIBELA 15	6	0.6676	PAWIE 33	7	0.6833
ADIS ALM 15	2	0.8092	SEKOTA 15	6	0.8224	FICHE 15	2	0.6771	FICHE 15	2	0.7131
SEKOTA 15	6	0.817	ADIS ALM 15	2	0.8279	PAWIE 15	7	0.6794	PAWIE 15	7	0.7252
WOLISO 15	2	0.825	WOLISO 15	2	0.8358	DANGLA 33	7	0.6905	DANGLA 33	7	0.7293
MEKELE 15	9	0.841	MEKELE 15	9	0.8471	ADIS ALM 15	2	0.7202	SEKOTA 15	6	0.7378

Based on the 10 weakest buses shown in Table 5.4 above, the majority of load buses under light load and all the load buses under heavy load condition are supplied from the 66 kV transmission line. Based on the data obtained from the EEP, the 66kV transmission lines are oldest lines with higher line resistances per km as compared with other transmission lines. This condition of the transmission lines assures the result from PPMI to be reasonable.

From previous discussions, we have seen these buses having large Thevenin impedance and lower P_{max} values. These two conditions are also indicators of the possibility for these buses to be weak buses.

Speaking area-wise area 7 is the weakest area constituting 60 % of the 10 weakest buses. This area is known not being the most loaded area. Hence, the problem is from the network setup of the area. The high concentration of the 66 kV transmission lines in this area is one of the causes. Hence, considering upgrading these transmission lines is vital for the system voltage stability. Here below in Figure 5.4, the PV curves of the top four weakest buses are shown

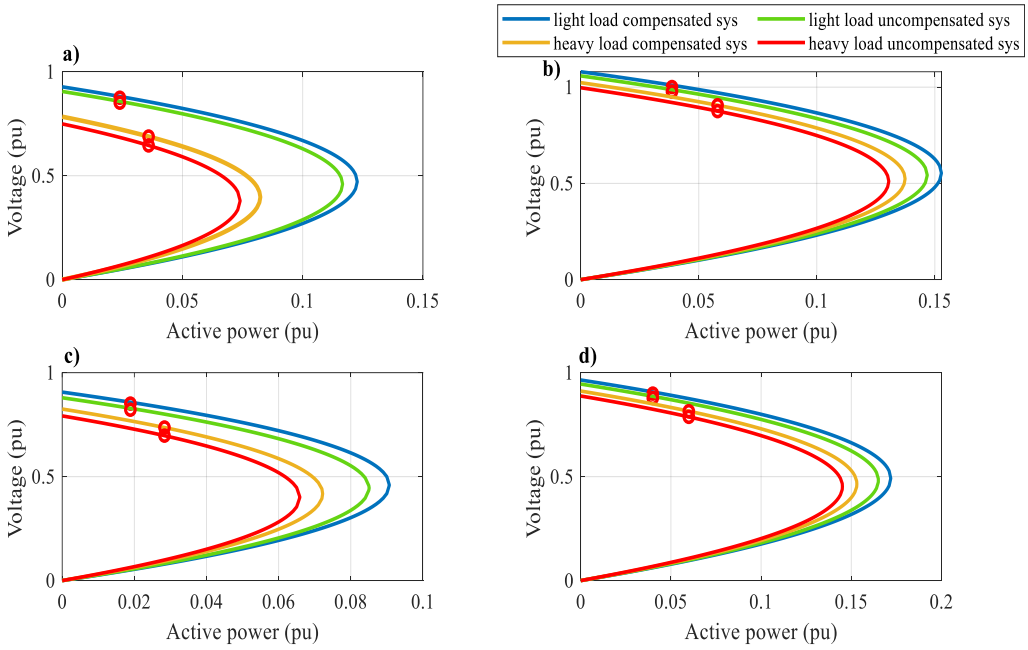

Figure 5.4: PV diagrams of the weakest buses a) DANGLA 15 b) FT-SELAM 15 c) WOLDIA 15 d) BITCHENA 33

In the PV diagrams, current operating active power-voltage value is shown by red circles. The top four buses have different maximum active power value and current operating

values. From the four buses BITCHENA 33 has the highest P_{max} value followed by FENOTE SELAM 15, while WOLDIA 15 own the least value. Both BITCHENA 33 and FENOTE SELAM 15 have the highest operating power among the four. The operating power is almost a similar for these two buses. The difference in P_{max} created the difference in weakness rank. WOLDIA 15 is the bus with the least operating power among the four.

The PV plots also reveal, system reactive power compensation is improving the voltage profile at current operating active power and seen maximizing the maximum active power transfer. This indicates the utilization of VSA for the implementation of FRPM. High system loading reduces both bus voltage profiles and the maximum active power transfer. Decreasing maximum active power transfer against increasing bus loading, results in further reduced active power margin, i.e reduced PPMI.

As it can be seen from Figure 5.4, for some buses like BITCHENA 33 and FENOTE SELAM 15, both loading and reactive power compensation bring similar magnitude impact on the voltage profile and voltage stability level. While for other buses, like DANGLA 15 and WOLDIA 15, loading produces more impact than reactive power compensation, in moving the maximum active power in the direction of higher or lower values.

Here, it is important to mention PV diagrams cannot be used for bus ranking, as each bus has its unique current operating state and unique maximum active power transfer capability. This is why the index development is necessary.

The most stable buses based on the index are shown here below in Table 5.5. Top ten buses are selected for demonstration. For the strongest buses, the rank change that comes from compensation and loading variation is little. The majority of buses are supplied from 132 kV transmission lines. GHEDO 33 and KALITI GIS 15 are the strongest buses, consecutively. The majority of the most stable buses are located in area 2. Addis Ababa region, area 1, despite having buses with the highest P_{max} and lowest Thevenin impedance, it is not the area with the most stable buses. This is due to the fact the centre being the most loaded area. High system loading mean operating close to the maximum active power transfer and hence narrow active power margin.

Table 5.5: The most stable buses under different system loading condition

Light load uncompensated system			**Light load compensated system**			**Heavy load uncompensated system**			**Heavy load compensated system**		
Load bus	Area	PPMI	Load bus	Area	PPMI	Load bus	Area	PPMI	Load bus	Area	PPMI
KALITI GIS 15	1	0.9995	GHEDO 33	4	0.9996	GHEDO 33	4	0.9994	GHEDO 33	4	0.9994
GHEDO 33	4	0.9995	KALITI GIS 15	1	0.9995	KALITI GIS 15	1	0.9993	KALITI GIS 15	1	0.9993
WON SUG 11	2	0.9992	WON SUG 11	2	0.9992	WON SUG 11	2	0.9988	WON SUG 11	2	0.9989
AYAT GIS 15	1	0.9989	AYAT GIS 15	1	0.9990	AYAT GIS 15	1	0.9984	AYAT GIS 15	1	0.9985
KOKA 15	2	0.9987	SHASHEMN 33	5	0.9987	SHASHEMN 33	5	0.9982	SHASHEMN 33	5	0.9983
SHASHEMN 33	5	0.9986	KOKA 15	2	0.9986	KOKA 15	2	0.9980	KOKA 15	2	0.9981
AWASH-2 15	2	0.9984	AWASH-2 15	2	0.9985	AWASH-2 15	2	0.9977	AWASH-2 15	2	0.9979
AGARO 33	8	0.9983	AGARO 33	8	0.9983	AGARO 33	8	0.9976	AGARO 33	8	0.9977
KOKA 15	2	0.9982	KOKA 15	2	0.9983	KOKA 15	2	0.9975	KOKA 15	2	0.9976
AWASH-2 15	2	0.9981	AWASH-2 15	2	0.9982	AWASH-2 15	2	0.9974	AWASH-2 15	2	0.9974

5.3. QV Curve Analysis of EEP System for VSA and FRPM

5.3.1. Constant active power operation

For constant active power operation, since the objective is to investigate the impact of compensation, only the uncompensated system operation scenarios, for both light load and heavy load operation, are taken. The objective is to see the impact of compensation for both the voltage profile improvement and voltage stability of these uncompensated states. The QV curve results of weakest buses are shown in Figure 5.5 next.

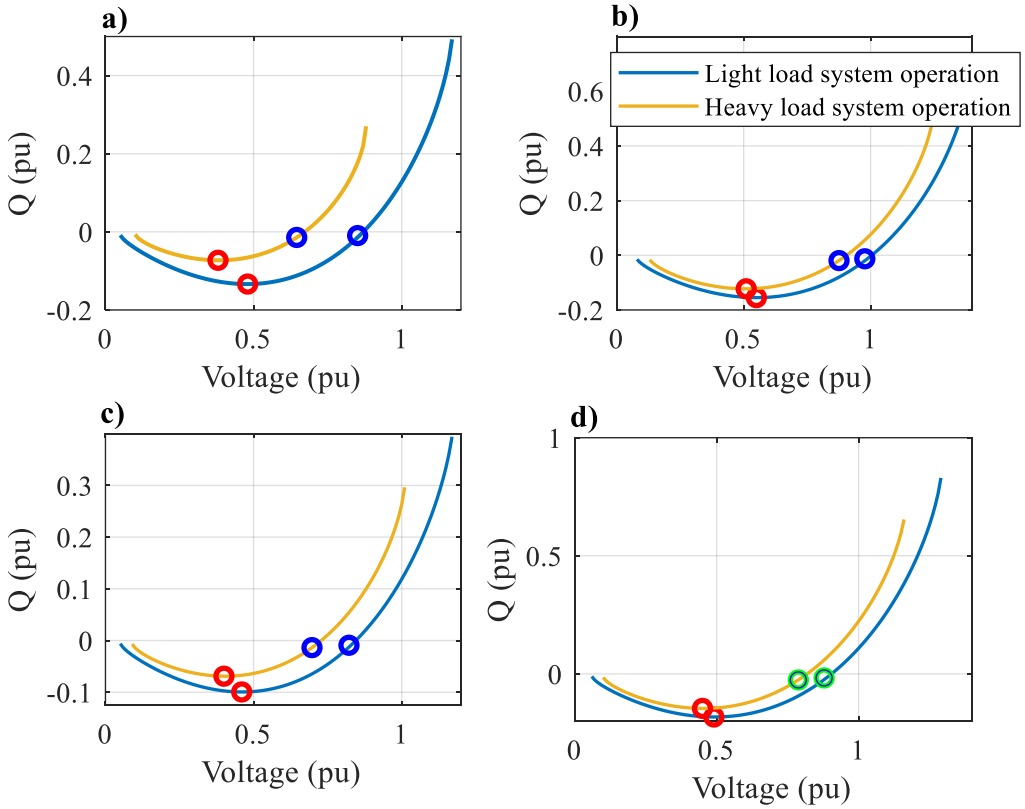

Figure 5.5: QV characteristics of EEP weakest buses for constant P: a) DANGLA 15 b) FT-SELAM 15 c) WOLDIA 15 d) BITCHENA 33

According to the results in this figure, as loading increases the reactive power margin decreases. This means as we proceed towards the maximum active power transfer point, the reactive margin of the operating points gets smaller and smaller. This entails the operating points near the maximum loadability can easily pushed to voltage instability with little reactive power loading increment. The margin indicates the bus enters to voltage instability with minimum reactive load increment. This means the bus needs high

reactive power compensation to keep the operating point far from instability. On the other interpretation, the system cannot make sufficient reactive power transfer and the bus needs reactive power compensation. The less the margin the more the operating point is near to voltage instability.

In figure 5.5. the maximum reactive powers that is possible to compensate are shown by red circles and the current operating reactive load, i.e. the reactive power being supplied to the load, is shown by blue circles. For more clarity the values are extracted here below in Table 5.6. For the given operating scenarios WOLDIA 15 shows the lowest reactive power margin followed by DANGLA 15. However, it is important to mention here that DANGLA 15 operates at relatively higher rating than WOLDIA 15.

The rest two buses FT-SELAM 15 and BITCHENA 33 takes the next ranks respectively in terms of reactive power margin for the given operating conditions.

Table 5.6: The reactive values of the maximum possible value and the current operating point.

Bus	**Operation Scenarios**	**Q_{max} (pu)**	**Q operating (pu)**	**Qmargin (pu)**
DANGLA 15	Light load operation	0.1337	0.0096	0.1241
	Heavy load operation	0.073	0.0144	0.0586
FT-SELAM 15	Light load operation	0.1549	0.0129	0.142
	Heavy load operation	0.1227	0.01935	0.10335
WOLDIA 15	Light load operation	0.1	0.009	0.091
	Heavy load operation	0.069	0.014	0.055
BITCHENA 33	Light load operation	0.1825	0.0257	0.1568
	Heavy load operation	0.1462	0.0171	0.1291

The rank changes, here in Q margin, doesn't alter the meaning of the rank identified by PPMI index so far. PPMI measures the maximum active power transfer the system

supports at a given load bus, while the reactive power margin, at constant active power, measures the robustness of a single active power operating point, which is located anywhere along the PV characteristic, for reactive power loading.

On the other hand, in terms of sensitivity analysis, all current operating points lay right from the maximum reactive power transfer point, which is the stable region. Hence, all operating points of interest are under voltage stability condition. More reactive power loading pushes the system towards the unstable region. Similarly, more active power loading brings the $\mathbf{Q_{max}}$ towards the operating point, which results the close up of the voltage instability region.

5.3.2. Constant power factor operation

Under constant power factor operation, when the reactive power loading changes, the active power also changes to keep the power factor constant. Here too, since the objective is to investigate the impact of system reactive power compensation, only the uncompensated system operation scenarios are taken. The constant power factor characteristic of the weakest buses is shown in Figure 5.6 next.

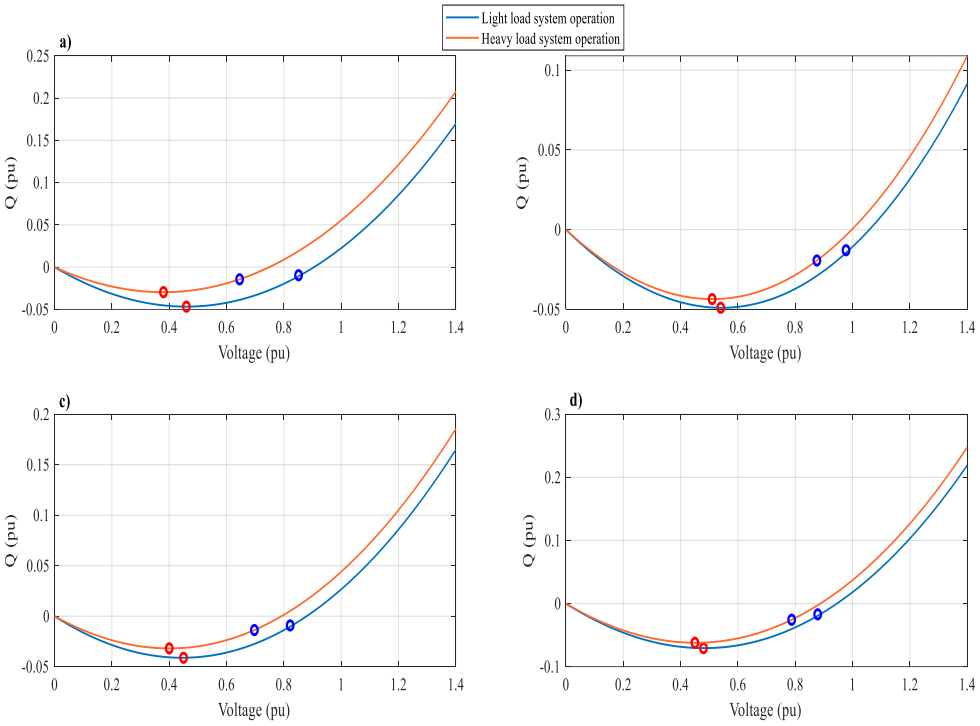

Figure 5.6: QV characteristics of weakest buses for constant power factor operation a) DANGLA 15 b) FT-SELAM 15 c) WOLDIA 15 d) BITCHENA 33

In this figure, the possible maximum reactive power that can be delivered to the load is given by red circles, and the current operating point under the scenarios are shown with blue circles. For better observation these values are screened out in Table 5.7 below.

Taking heavy load operation, i.e. the worst case scenario, the least reactive power margin is owned by DANGLA 15. Whilst, the highest margin among the weakest buses is owned by BITCHENA 33.

Table 5.7: Maximum and operating reactive powers of the weakest buses

Bus	**Operation Scenarios**	**Q_{max} (pu)**	**$Q_{operating}$ (pu)**	**Q_{margin} (pu)**	**Normalized Q_{margin}**
DANGLA 15	Light load operation	0.047	0.0096	0.0374	0.7957
	Heavy load operation	0.03	0.0144	0.0156	0.52
FT-SELAM 15	Light load operation	0.049	0.0129	0.0361	0.7367
	Heavy load operation	0.0435	0.01935	0.02415	0.5551
WOLDIA 15	Light load operation	0.0412	0.00915	0.03205	0.7779
	Heavy load operation	0.0319	0.0137	0.0182	0.5705
BITCHENA 33	Light load operation	0.0706	0.0171	0.0535	0.7578
	Heavy load operation	0.0621	0.0257	0.0364	0.5861

In this case when the reactive power loading changes, the active power also changes. The plots sense this change in active power.

Due to this fact, constant power factor QV curves are better indicator of total proximity to voltage instability than QV curves of constant active power operation. QV curves of constant active power are voltage instability indicators of a single operating point. That is why we get, here, a result that matches with our PPMI index in identifying the weakest bus to be DANGLA 15. At heavy load case scenario, the normalized $\mathbf{Q_{margin}}$ produces fully matching results with the PPMI index.

In Table 5.7, it can be seen the maximum reactive power possible to be delivered is relatively less than its equivalent in the case of constant active power in section 5.3.1. The reason is, in the case of constant power factor scenario, at maximum reactive power

condition the active power loading, also, increases in amount. This results in reduced maximum reactive power transfer.

Based on QV sensitivity all the operating points of all buses are to the left of the maximum reactive power transfer point. Hence all operating points are under voltage stability state.

In conclusion, these two scenarios present two analysis needs of a system operator. The first is to quantify the reactive power provision plan, needed to improve both the voltage profiles and voltage stability of a given load bus while operating at a fixed active power delivery. On the other hand, the second scenario is proposed to envision the QV characteristics during the expected, simultaneous change of active power and reactive power while keeping the power factor constant.

5.4. Continuous Reactive Power Management (CRPM) of the EEP System

The application of CRPM to the EEP system is done through optimization of the reactive power resources using IMOPSO algorithm. As mentioned in the previous discussions, every system loading needs an optimized settings of reactive resources meeting the objectives. From an infinite operating point options on which optimization can be applied, in this case, optimization of light load operation is taken for demonstrating the application of IMOPSO for the reactive power optimization of the EEP system. Here, next the results from the analysis are shown.

5.4.1. The pareto front

The pareto front for the EEP system voltage security ensuring reactive power optimization is shown in the following Figure 5.7. The iteration is run up to 50 iterations. The simulations show the values of the objective functions being constant after the 50^{th} iteration. This is an indication of closeness of the optimization to the true pareto front.
The values of the objective functions at the pareto front are shown in Table 5.8 following. The voltage stability index function goes from a minimum of 12.8977 to the maximum of 13.2527. The voltage deviation objective function, on the other hand, goes from a minimum of 0.6228 to the maximum of 0.7776.

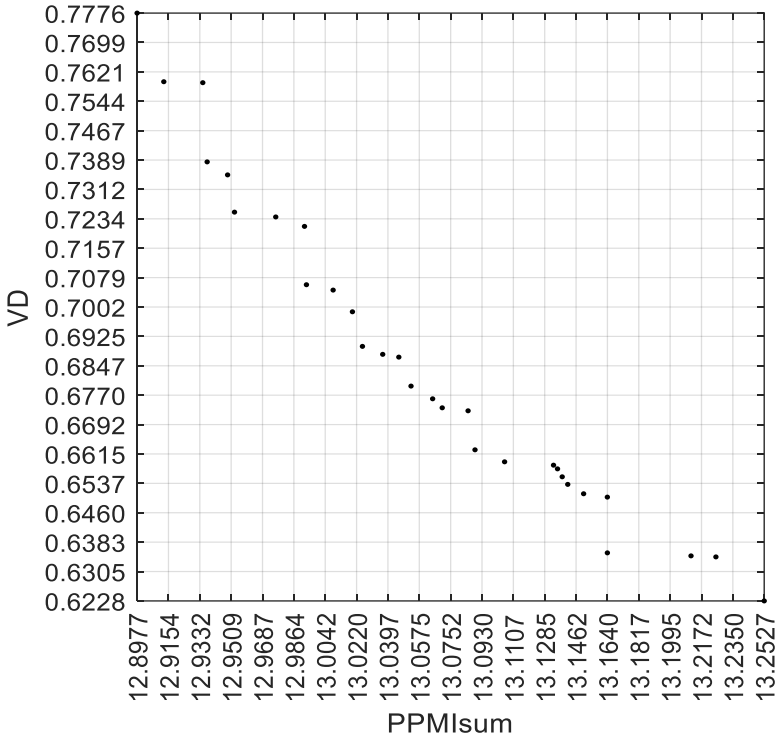

Figure 5.7: Pareto front of the objectives for EEP system optimization

Table 5.8: Dominant positions in the pareto front

PPMIsum	**Vdsum**	**PPMIsum**	**Vdsum**
12.8977	0.7776	13.065	0.676
12.9128	0.7595	13.0704	0.6736
12.9349	0.7593	13.0851	0.6729
12.9373	0.7384	13.089	0.6626
12.9489	0.735	13.1057	0.6594
12.9528	0.7252	13.1335	0.6585
12.9762	0.7239	13.1357	0.6576
12.9925	0.7214	13.1384	0.6555
12.9936	0.7061	13.1415	0.6535
13.0087	0.7047	13.1505	0.651
13.0196	0.6989	13.1639	0.6501
13.0253	0.6898	13.1639	0.6354
13.0367	0.6877	13.2113	0.6346
13.0459	0.687	13.0528	0.6344
13.0528	0.6794	13.2527	0.6228

These values are sum of average values of voltage security indicators of individual load buses. Interpreting these values to individual bus values, on average, the load buses experience a minimum PPMI of 0.9532 and a maximum PPMI of 0.9544 after optimization.

At this point it is important to mention the result from the unoptimized computation of PPMI values discussed in section 5.2.3. In this unoptimized compensation the average PPMI value of the load buses is 0.9494, which is well below the minimum average value, i.e. 0.9539, and the maximum average PPMI, i.e. 0.9544, achieved through the optimization. This shows the optimization has improved the voltage stability of the system.

While coming to the voltage deviation from the 1 pu value each bus experiences on average from minimum deviation of 0.0022 pu to the maximum average deviation of 0.0027 pu. In this respect, the unoptimized compensation of this scenario produced an average voltage deviation of 0.0071, which is well above the deviations resulted from the optimization. Additionally, these deviations well respect the IEC standard, IEC 60038, which allows a ± 0.5 pu deviation. This indicates the improvements coming with the optimization employed.

5.4.2. Optimal settings of generating units

The operating generating units within the EEP system under consideration are 47. Based on the optimization the lowest average output voltage is achieved by unit 1 of AWASH 3 hydro power station. The five lowest average output voltage owning generators are shown in Table 5.9 following.

Table 5.9: The lowest average output voltage producing generation units.

Generator	**AWASH 3 unit 1**	**G. Gibie 3 unit 2**	**SUDAN-GADARIF 230 (4^{th} connection)**	**GENALE-III unit 2**	**ADAMA WF I unit 1**
Output Voltage avg	0.9003	0.9223	0.9361	0.9391	0.9391

The high average value owning units are also shown in Table 5.10 below. These high voltage producing units are owning lowest standard deviations of all. This indicates these

units are striving to maintain high voltages for the optimized operation. Here, below, the rank of the standard deviation for the high voltage producing buses is also shown.

Table 5.10: High average output voltage producing units

Generator	**BELES unit 4**	**GADARIF TIE 1**	**REPPIE WF unit 2**	**KOKA unit1**	**G. GIBIE 3 unit 1**
Output Voltage avg	1.1000	1.0999	1.0999	1.0998	1.0997
Std deviation	3.8021e-05	3.4249e-04	2.6803e-04	3.3863e-04	4.4173e-04
Rank of the std (lowest)	2^{nd}	7^{th}	5^{th}	6^{th}	8^{th}

Table 5.10 shows, the top five high voltage producing generators are also the buses showing the least variations. This is, clearly, showing the EEP system seeking high voltage profiles to ensure the voltage security.

Among the top five high voltage producing generators the three, i.e. G. GIBIE 3 unit 1, BELES unit 4 and the GEDARIF tie connections are high-capacity generators. This means they are clearly playing crucial role in stabilizing the system voltage. The real practice of the EEP system goes in line with this fact. The units at BELES and G. GIBIE 3 power stations are used by the EEP for system stabilizing demands.

The other generators REPPIE WF and KOKA 1 appear on the stabilizing importance. The reason is highly probable to be due to their closeness to the high loading area of the grid, area 1 and area 2. It is important to mention here that capacity and electrical distances of reactive resources play a crucial role on the voltage security of the system.

The voltage profiles of these top five generators are shown here below in Figure 5.8 for the 30 positions of the dominant front.

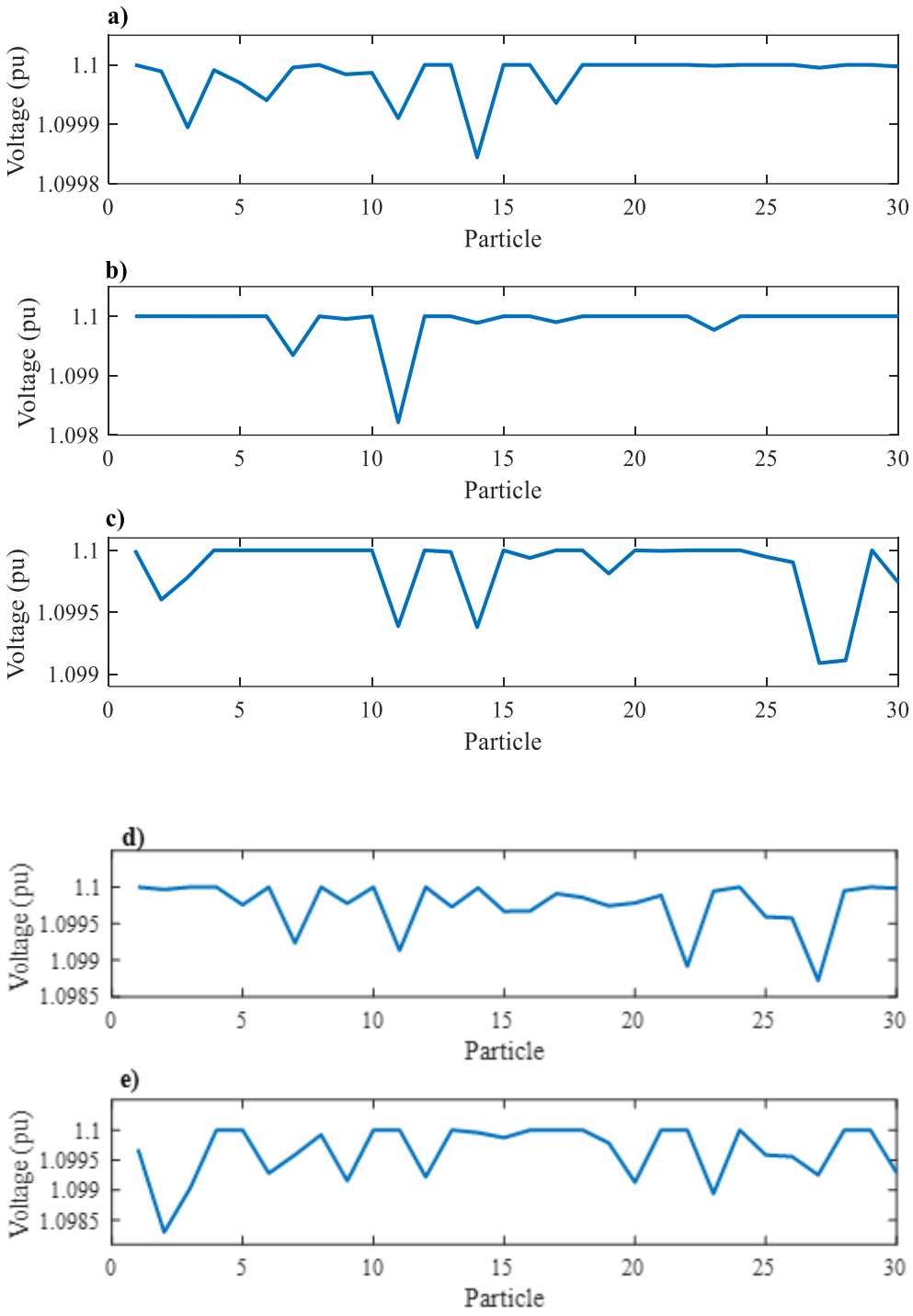

Figure 5.8: Output voltages of the five top generators producing high avg. output voltage a) BELES unit 4 b) GADARIF TIE 1 c) REPPIE WF unit 2 d) KOKA unit1 e) G. GIBIE 3 unit 1

5.4.3. Capacitor optimal settings within the system

Here below Table 5.11, shows the capacitor settings for the optimal operating points. Out of service capacitors during the time the data taken are not considered.

Table 5.11: Capacitor settings for the optimal positions

Capacitor location	Min MVAR	Max MVAR	Average MVAR	Standard deviation
GELAN 400	18.9962	20	19.7988	0.2363
BOLE LEMI 33	16.2192	18.8933	17.6818	0.6440
KILINTO 33	6.3703	20	18.3537	3.2444
KOYO ABO 1 15	1.3777	3.4444	2.4713	0.5340
KOYO ABO 2 15	1	9.3813	3.8134	2.0973
D.ZEIT3 15	4.0917	10.4345	6.7232	1.9612
HOLETA-33-1	18.0873	20	19.0139	0.5431
HOLETA-33-2	17.9517	19.9119	19.2998	0.4604
HOLETA-33-3	19.3480	20	19.8496	0.1761

From the above table the majority of the capacitors choose to operate near the maximum limit set. This includes capacitors at GELAN 400 and HOLETA -33 buses, which owns high average value. These results mean the system needs high reactive power provision to maintain the voltage security.

On the other hand, capacitors at KOYO ABO 15 and D. ZEIT 3 operate at lower values. This means their impact is very minimum for the voltage security maintenance.

5.4.4. Optimal transformer tap-changer positions

Five transformers own the lowest limit set for the tap changer positions, i.e 0.95. These transformers are shown in Table 5.12 next.

Among the transformers WERETA 66-33-15 three winding transformer is with the minimum tap changer position on the majority of the pareto points. Among the lowest tap changer position having transformers, this transformer is also with the lowest standard deviation. This shows the lowest tap position demand of the area around this transformer. This means the area is experiencing lowest voltage profile.

With their respective ranks the transformers mentioned in Table 5.12 experience the same condition. The highest tap position maintaining buses are also shown in Table 5.13 next. Highest tap position maintaining buses come from different areas.

Table 5.12: Lowest tap position maintaining transformers

Transformer	**WERETA 66-33-15**	**HURSO 132-33-15**	**ADDIS EAST-II 132-15 T1**	**COTEBEI-I 132-15 T2**	**KALITI TWO 132-15 T2**
Avg tap changer position	0.9500	0.9500	0.9500	0.9500	0.9500
Std deviation of Tap changer position ($\times 10^{-4}$)	0.1577	0.1933	0.5811	0.2508	0.6401

The values of avg tap changer positions in Table 5.12 and Table 5.13 seem the same. However, there is a difference in the values of each transformer avg tap position. The similarities appear due to rounding effect of the computer computation.

Table 5.13: Highest tap position maintaining transformers

Transformer	**BELES 400-15 T1**	**DERBA-CEMENT 132-33-15**	**NEGELE BORNA 66-33-15**	**SULULTA-132-33-15 T1**	**DESSIE 66-15 T2**
Avg tap changer position	1.0500	1.0500	1.0500	1.0500	1.0500
Std deviation of Tap changer position ($\times 10^{-4}$)	0.0818	0.1960	0.1504	0.6047	0.4471

CHAPTER 6

CONCLUSION AND RECOMMENDATION

6.1. Conclusion

The devised VSA and RPM schemes in this dissertation work come with capabilities that enable to carry out voltage security assessment and reactive power management tasks. The schemes are realized by designing and improving the components of each scheme.

In this process three major contributions are made. The major contributions of the work are development of new Thevenin impedance determination technique, formulation of new voltage stability indices and development of an improved multi objective particle swarm optimization algorithm for reactive power management. In doing so, current gaps with each component are assessed, improvement mechanisms are proposed, and the improvements are tested using IEEE 14 bus, IEEE 30 bus test systems and applied to the Ethiopian power system.

Around these major findings a number of other capabilities are formulated that enabled full voltage security assessment and reactive power management both for online and offline applications. In developing the schemes, the findings of the dissertation work are put as follows;

1. Voltage security assessment scheme

The voltage security assessment scheme has capabilities of determining high accuracy system Thevenin equivalent, efficient way of determining maximum active power transfer capability, two voltage stability indices suitable for online application, efficient way of determining PV and QV curves, QV sensitivity analysis and reactive power margin determination.

The Thevenin equivalent determination method;

- It is shown to be capable of producing high accuracy Thevenin impedance values, solving the approximation problems of previous approaches.
- It has reduced the requirement of minimum of two measurements by measurement based previous approaches to a single shot measurement requirement. This has

solved problems of large time window requirement, problems with topological change between measurements, and requirement of perturbation between consecutive measurements whose absence in the case of steady state operation creates a Thevenin equivalent unknown times.

- It shows the way to determine Thevenin equivalent voltage which is necessary for the computation of maximum active power transfer.

The ease of determining Thevenin equivalent parameters has brought the following advantages in realizing other capabilities of the VSA scheme.

- Maximum active power transfer capability of load buses is made to be easily calculated. In previous practices, a number of repetitive power flow computations or continuous power flow approach, which itself is an iterative and time-consuming process, were required to compute the maximum active power transfer capability. Our scheme, however, considerably reducing the number of power flow computations, requires only two power flow computations in the case of offline studies, and only one power flow calculation in the case of online application.
- PV and QV curves which are important for the interpretation of voltage instability development are made to be easily drawn. Previously, similar to the computation of maximum active power transfer, large number of power flow computations were employed for the determination of the PV and QV curves. The ease of determining the Thevenin equivalent parameters in this work enabled the computation of these curves in an easy and non-iterative way. PV and QV curve determination in this work requires only two power flow computations in the case of offline studies, and only one power flow calculation in the case of online application.
- An impedance-based stability index, i.e. New Impedance Stability Index (NISI), is developed. The accuracy and speed of Thevenin impedance determination makes the computation of NISI dependable and appealing for online application.
- Another power margin-based index, i.e. PPMI, is devised. This index is capable of indicating the active power loading margin before point of collapse. Previous measurement based Thevenin impedance determination techniques were not capable of calculating the maximum loading margin, for they do not have a mechanism to indicate the Thevenin equivalent voltage. The ease of determining

both Thevenin impedance and Thevenin voltage, in this work makes the realization of this index easy.

- The voltage stability indices developed, so far, are capable of indicating proximity to voltage instability both at rated load and at any load increment. The indices can cope up with varying system loading conditions, which is the actual online application conditions. The indices are compared with previously established indices and with each other, and produced a matching performance for ranking weakest buses. The performance of the indices is also tested for FRPM and showed voltage stability improvement brought by the compensation

These capabilities of the VSA schemes are tested on IEEE 14 bus system, IEEE 30 bus system and the EEP interconnected system. The tests revealed a number of important features regarding to the Thevenin impedances, active power transfer capability and the voltage stability of the systems in response to loading and reactive power compensation. These results are summarized as;

- For the majority load increments the Thevenin impedance shows increment with load increment. Some Thevenin impedances are seen decreasing while system loading is increasing.
- The Thevenin impedance shows higher rate of increment near the point of collapse.
- Load buses close to each other see close values of Thevenin impedance and P_{max}.
- High connectivity areas see low Thevenin impedance. This attributes to the presence of more power routing paths.
- Highest Thevenin impedance seeing buses own lower maximum active power transfer. On the other hand, lower Thevenin impedance seeing buses own higher active power transfer.
- Two conditions determine voltage stability of a given load bus, the network capability and the load on the bus. The network capability is expressed either in terms of maximum active power transfer capability or the Thevenin impedance representation of the system.
- The closer the loading to the power transfer capability the closer the system gets to voltage instability. This is indicated by high NISI and low PPMI values.

2. Reactive power management scheme

In this part, the voltage security ensuring reactive power management scheme is designed to function with two approaches, FRPM and CRPM.

The FRPM uses the stability index values of weak buses as indicator to keep the system far enough from point of collapse. This class is discussed with the response of voltage security assessment indices for reactive power transactions. The tests reveal:

- Reactive power compensation increases the system active power transfer capability.
- PPMI and NISI respond in reverse mode for reactive power compensation. Increasing the reactive power compensation increases PPMI and decreases NISI. This means reactive power compensation increases system voltage stability.
- The analysis of QV curves, for both constant power factor and constant active powers, reveals there is a limit for reactive power loading for which the system can be kept voltage stable.
- As applied to the EEP system, for the majority of buses reactive power compensation is seen reducing Thevenin impedance and increasing the maximum active power transfer.

For the CRPM scheme an algorithm IMOPSO is proposed by this work. The performance of the algorithm is evaluated using inverted generational distance (IGD) on standard test functions ZDT1, ZDT2 and ZDT3. The algorithm is then applied to IEEE 14 bus test system and EEP system. The tests revealed;

- The algorithm is compared with standard MOPSO and NSGA II algorithms and revealed better performance in closing up to the true pareto front with better convergence speed.
- Additionally, IMOPSO produces a more diverse pareto front as measured in terms of CD.
- For voltage security insuring reactive power optimization, objectives, relevant to voltage security only, are defined and system constraints are imposed. The IMOPSO algorithm identified the value of control variables, which give the optimum operation. The implementation of IMOPSO provides considerable alternatives of optimum operating points, which give the operators increased

choice of alternatives. The optimization achieved low voltage deviation and improved voltage stability, improving the voltage security of the test systems. This shows the promising application of IMOPSO for voltage security improvement.

6.2. Recommendation and Future Work

The recommendation of this work, for the EEP, is the schemes to be converted to a user interactive software tool so that it can be used for the national grid operation and control. This work provided a complete scheme from which a software tool can easily get realized.

On the other side, the tests made on the EEP system reveal current voltage security problems emanate from the old aged and high resistance per km owning 66 kV transmission lines. This indicates upgrading these transmission lines is demanding to maintain system voltage security.

On the future expansion of the research aspect, the following directions can be considered as possible extension areas of the research.

- Impact of coupling concept, introduced in this work, can be further extended to study the impact of compensation on the load buses' voltage profile and voltage stability.
- Dynamic voltage security assessment method development is one extension area of the research. Dynamic voltage security assessment is used to assess the system security response during the occurrence of contingencies.
- Improving the speed of optimization is another dimension to be addressed. Optimization techniques inherently adopt a searching approach for the best solutions. This presents a tackle on the speed of the optimization process. Hence, working on improving the speed of the optimization techniques can be taken as another area of research.

REFERENCES

[1] U. S. S. Bureau. " International Database (IDB): Population estimates and projections for 227 countries and areas." https://www.census.gov/data-tools/demo/idb/# (accessed October 1, 2022).

[2] W. bank. "World bank data." https://data.worldbank.org/indicator/EG.ELC.LOSS.ZS?locations=ET (accessed April 10, 2022).

[3] M. K. Heun and P. E. Brockway, "Meeting 2030 primary energy and economic growth goals: Mission impossible?," *Applied Energy,* vol. 251, p. 112697, 2019/10/01/ 2019, doi: https://doi.org/10.1016/j.apenergy.2019.01.255.

[4] I. E. A. (IEA). "Global Energy Review 2021." https://www.iea.org/reports/global-energy-review-2021 (accessed October 3, 2022).

[5] S. Lumbreras and A. Ramos, "The new challenges to transmission expansion planning. Survey of recent practice and literature review," *Electric Power Systems Research,* vol. 134, pp. 19-29, 2016/05/01/ 2016, doi: https://doi.org/10.1016/j.epsr.2015.10.013.

[6] S. Lumbreras, J. D. Gómez, E. F. Alvarez, and S. Huclin, "The Human Factor in Transmission Network Expansion Planning: The Grid That a Sustainable Energy System Needs," *Sustainability,* vol. 14, no. 11, p. 6746, 2022. [Online]. Available: https://www.mdpi.com/2071-1050/14/11/6746.

[7] P. L. Joskow, "Transmission Capacity Expansion Is Needed to Decarbonize the Electricity Sector Efficiently," *Joule,* vol. 4, no. 1, pp. 1-3, 2020/01/15/ 2020, doi: https://doi.org/10.1016/j.joule.2019.10.011.

[8] P. Kundur *et al.*, "Definition and classification of power system stability IEEE/CIGRE joint task force on stability terms and definitions," *IEEE Trans. Power Syst.,* vol. 19, no. 3, pp. 1387-1401, 2004, doi: 10.1109/TPWRS.2004.825981.

[9] G. C. Ejebe and B. F. Wollenberg, "Automatic Contingency Selection," *IEEE Transactions on Power Apparatus and Systems,* vol. PAS-98, no. 1, pp. 97-109, 1979, doi: 10.1109/TPAS.1979.319518.

[10] N. Amjady and M. Esmaili, "Voltage security assessment and vulnerable bus ranking of power systems," *Electric Power Systems Research,* vol. 64, no. 3, pp.

227-237, 2003/03/01/ 2003, doi: https://doi.org/10.1016/S0378-7796(02)00196-7.

[11] A. A. Gharaveisi, M. Rashidinejad, and A. Mousavi, "Voltage security evaluation based on perturbation method," *Int. J. Electr. Power Energy Syst.*, vol. 31, no. 5, pp. 227-235, 2009/06/01/ 2009, doi: https://doi.org/10.1016/j.ijepes.2009.01.007.

[12] M. Glavic *et al.*, "See It Fast to Keep Calm: Real-Time Voltage Control Under Stressed Conditions," *IEEE Power Energy Mag.*, vol. 10, no. 4, pp. 43-55, 2012, doi: 10.1109/MPE.2012.2196332.

[13] P. S. Kundur and O. P. Malik, *Power system stability and control*. McGraw-Hill Education, 2022.

[14] S. Das, A. Verma, and P. Bijwe, "Security constrained AC transmission network expansion planning," *Electric Power Systems Research*, vol. 172, pp. 277-289, 2019.

[15] G. Yesuratnam and D. Thukaram, "Congestion management in open access based on relative electrical distances using voltage stability criteria," *Electric Power Systems Research*, vol. 77, no. 12, pp. 1608-1618, 2007/10/01/ 2007, doi: https://doi.org/10.1016/j.epsr.2006.11.007.

[16] T. K. P. Medicherla, R. Billinton, and M. S. Sachdev, "Generation Rescheduling and Load Shedding to Alleviate Line Overloads-Analysis," *IEEE Transactions on Power Apparatus and Systems*, vol. PAS-98, no. 6, pp. 1876-1884, 1979, doi: 10.1109/TPAS.1979.319366.

[17] R. M. Larik, M. W. Mustafa, and M. N. Aman, "A critical review of the state-of-art schemes for under voltage load shedding," *International Transactions on Electrical Energy Systems*, vol. 29, no. 5, p. e2828, 2019, doi: https://doi.org/10.1002/2050-7038.2828.

[18] D. Feng, B. H. Chowdhury, M. L. Crow, and L. Acar, "Improving voltage stability by reactive power reserve management," *IEEE Trans. Power Syst.*, vol. 20, no. 1, pp. 338-345, 2005, doi: 10.1109/TPWRS.2004.841241.

[19] M. Cortés-Carmona, G. Jiménez-Estévez, and J. Guevara-Cedeño, "Support vector machines for on-line security analysis of power systems," in *2008 IEEE/PES Transmission and Distribution Conference and Exposition: Latin America*, 2008: IEEE, pp. 1-6.

[20] K. Teeparthi and D. M. Vinod Kumar, "Power System Security Assessment and Enhancement: A Bibliographical Survey," *Journal of The Institution of Engineers (India): Series B*, vol. 101, no. 2, pp. 163-176, 2020/04/01 2020, doi: 10.1007/s40031-020-00440-1.

[21] M. Ni, J. D. McCalley, V. Vittal, and T. Tayyib, "Online risk-based security assessment," *IEEE Trans. Power Syst.*, vol. 18, no. 1, pp. 258-265, 2003.

[22] S. R. Khuntia, J. L. Rueda, and M. A. van der Meijden, "Risk-based security assessment of transmission line overloading considering spatio-temporal dependence of load and wind power using vine copula," *IET Renewable Power Generation*, vol. 13, no. 10, pp. 1770-1779, 2019.

[23] B. Shakerighadi, S. Peyghami, E. Ebrahimzadeh, F. Blaabjerg, and C. Leth Back, "A new guideline for security assessment of power systems with a high penetration of wind turbines," *Applied Sciences*, vol. 10, no. 9, p. 3190, 2020.

[24] A. Dissanayaka, U. D. Annakkage, B. Jayasekara, and B. Bagen, "Risk-based dynamic security assessment," *IEEE Trans. Power Syst.*, vol. 26, no. 3, pp. 1302-1308, 2010.

[25] L. Chen and H. Zhang, "Improved voltage deviation security margin index," in *2014 IEEE PES Asia-Pacific Power and Energy Engineering Conference (APPEEC)*, 7-10 Dec. 2014 2014, pp. 1-4, doi: 10.1109/APPEEC.2014.7066063.

[26] N. C. Chang *et al.*, "Developing a Voltage-Stability-Constrained Security Assessment System Part I: Determination of Power System Voltage Security Operation Limits," in *2005 IEEE/PES Transmission & Distribution Conference & Exposition: Asia and Pacific*, 18-18 Aug. 2005 2005, pp. 1-5, doi: 10.1109/TDC.2005.1547128.

[27] T. Yang and Y. Yu, "Static Voltage Security Region-Based Coordinated Voltage Control in Smart Distribution Grids," *IEEE Transactions on Smart Grid*, vol. 9, no. 6, pp. 5494-5502, 2018, doi: 10.1109/TSG.2017.2680436.

[28] T. Jiang, R. Zhang, X. Li, H. Chen, and G. Li, "Integrated energy system security region: Concepts, methods, and implementations," *Applied Energy*, vol. 283, p. 116124, 2021/02/01/ 2021, doi: https://doi.org/10.1016/j.apenergy.2020.116124.

[29] H. Yoshida, K. Kawata, Y. Fukuyama, S. Takayama, and Y. Nakanishi, "A particle swarm optimization for reactive power and voltage control considering voltage security assessment," *IEEE Transactions on Power Systems*, vol. 15, no. 4, pp. 1232-1239, 2000, doi: 10.1109/59.898095.

[30] *IEC standard voltages*, I. E. Commission, 2009.

[31] M. Constantin, M. Eremia, and L. Toma, "Comparative analysis between conventional voltage control using reactors and continuous voltage control using TCR in the Romanian transmission grid," in *2013 IEEE Grenoble Conference*, 16-20 June 2013 2013, pp. 1-6, doi: 10.1109/PTC.2013.6652236.

[32] C. W. Taylor, "Concepts of undervoltage load shedding for voltage stability," *IEEE Transactions on Power Delivery,* vol. 7, no. 2, pp. 480-488, 1992, doi: 10.1109/61.127040.

[33] C. W. Taylor, N. J. Balu, and D. Maratukulam, *Power System Voltage Stability*. McGraw-Hill, 1994.

[34] T. Van Cutsem and C. Vournas, *Voltage stability of electric power systems*. Springer Science & Business Media, 2007.

[35] T. Van Cutsem, J. Kabouris, G. Christoforidis, and C. Vournas, "Application of real-time voltage security assessment to the Hellenic interconnected system," *IEE Proceedings-Generation, Transmission and Distribution,* vol. 152, no. 1, pp. 123-131, 2005.

[36] T. Van Cutsem, "Voltage instability: phenomena, countermeasures, and analysis methods," *Proc. IEEE,* vol. 88, no. 2, pp. 208-227, 2000.

[37] Y. Ma, S. Lv, X. Zhou, and Z. Gao, "Review analysis of voltage stability in power system," in *2017 IEEE International Conference on Mechatronics and Automation (ICMA)*, 6-9 Aug. 2017 2017, pp. 7-12, doi: 10.1109/ICMA.2017.8015779.

[38] M. S. S. Danish, T. Senjyu, S. M. S. Danish, N. R. Sabory, N. K, and P. Mandal, "A Recap of Voltage Stability Indices in the Past Three Decades," *Energies*, vol. 12, no. 8, p. 1544, 2019. [Online]. Available: https://www.mdpi.com/1996-1073/12/8/1544.

[39] B. Gao, G. K. Morison, and P. Kundur, "Voltage stability evaluation using modal analysis," *IEEE Trans. Power Syst.,* vol. 7, no. 4, pp. 1529-1542, 1992, doi: 10.1109/59.207377.

[40] I. Musirin and T. K. A. Rahman, "Novel fast voltage stability index (FVSI) for voltage stability analysis in power transmission system," in *Student Conference on Research and Development*, 17-17 July 2002 2002, pp. 265-268, doi: 10.1109/SCORED.2002.1033108.

[41] K. Sun, F. Hu, and N. Bhatt, "A new approach for real-time voltage stability monitoring using PMUs," in *2014 IEEE Innovative Smart Grid Technologies-Asia (ISGT ASIA)*, 2014: IEEE, pp. 232-237.

[42] C. W. Taylor, "Power system Voltage stability," ed: McGraw-Hil, 1994.

[43] J. D. L. Ree, V. Centeno, J. S. Thorp, and A. G. Phadke, "Synchronized Phasor Measurement Applications in Power Systems," *IEEE Transactions on Smart Grid*, vol. 1, no. 1, pp. 20-27, 2010, doi: 10.1109/TSG.2010.2044815.

[44] S. Corsi and G. N. Taranto, "A real-time voltage instability identification algorithm based on local phasor measurements," *IEEE Trans. Power Syst.*, vol. 23, no. 3, pp. 1271-1279, 2008.

[45] Y. Amirat, Z. Oubrahim, H. Ahmed, M. Benbouzid, and T. Wang, "Phasor estimation for grid power monitoring: Least square vs. linear Kalman filter," *Energies*, vol. 13, no. 10, p. 2456, 2020.

[46] A. G. Phadke, J. S. Thorp, and K. J. Karimi, "State Estimation with Phasor Measurements," *IEEE Trans. Power Syst.*, vol. 1, no. 1, pp. 233-238, 1986, doi: 10.1109/TPWRS.1986.4334878.

[47] M. Randhawa, B. Sapkota, V. Vittal, S. Kolluri, and S. Mandal, "Voltage stability assessment of a large power system," in *2008 IEEE Power and Energy Society General Meeting - Conversion and Delivery of Electrical Energy in the 21st Century*, 20-24 July 2008 2008, pp. 1-7, doi: 10.1109/PES.2008.4596336.

[48] P. Labs. "Voltage security assessment tool (VSAT)." https://powertechlabs.com/vsat/ (accessed June 5, 2021).

[49] H. J. C. P. Pinto, N. Martins, F. X.Vieira, A. Bianco, P. Gomes, and M. G. d. Santos, "MODAL ANALYSIS FOR VOLTAGE STABILITY : Application at Base Case and Point of Collapse," 1999.

[50] T. Weckesser, L. Papangelis, C. D. Vournas, and T. Van Cutsem, "Local identification of voltage instability from load tap changer response," *Sustainable Energy, Grids and Networks*, vol. 9, pp. 95-103, 2017.

[51] U. V. V. Ajjarapu, C. C. Liu, "Real Time Synchrophasor Measurements Based Voltage Stability Monitoring and Control," Power Systems Engineering Research Center, 2017. [Online]. Available: https://pserc.wisc.edu/wp-content/uploads/sites/755/2018/08/S-65_Final_Report.pdf

[52] S. Dasgupta, M. Paramasivam, U. Vaidya, and V. Ajjarapu, "Real-time monitoring of short-term voltage stability using PMU data," *IEEE Trans. Power Syst.*, vol. 28, no. 4, pp. 3702-3711, 2013.

[53] F. Yang, Z. Ling, M. Wei, T. Mi, H. Yang, and R. C. Qiu, "Real-time static voltage stability assessment in large-scale power systems based on spectrum estimation of phasor measurement unit data," *Int. J. Electr. Power Energy Syst.*, vol. 124, p. 106196, 2021/01/01/ 2021, doi: https://doi.org/10.1016/j.ijepes.2020.106196.

[54] P. Akbarzadeh Aghdam and H. Khoshkhoo, "Voltage stability assessment algorithm to predict power system loadability margin," *IET Generation, Transmission & Distribution*, vol. 14, no. 10, pp. 1816-1828, 2020, doi: https://doi.org/10.1049/iet-gtd.2019.0230.

[55] P. Singh, S. K. Parida, B. Chauhan, and N. Choudhary, "Online Voltage Stability Assessment Using Artificial Neural Network considering Voltage stability indices," in *2020 21st National Power Systems Conference (NPSC)*, 17-19 Dec. 2020 2020, pp. 1-5, doi: 10.1109/NPSC49263.2020.9331954.

[56] R. Choudhary and D. V. Kumar, "Real-Time Voltage Stability Assessment using Artificial Neural Network," in *2023 7th International Conference on Computer Applications in Electrical Engineering-Recent Advances (CERA)*, 2023: IEEE, pp. 1-6.

[57] F. Aydin and B. Gümüş, "Study of different ANN algorithms for voltage stability analysis," in *2020 Innovations in Intelligent Systems and Applications Conference (ASYU)*, 2020: IEEE, pp. 1-5.

[58] A. K. Samy and A. Venkadesan, "Evaluation of Voltage Stability Margin in a Power System using an Artificial Neural Network," in *2022 IEEE 10th Power India International Conference (PIICON)*, 2022: IEEE, pp. 1-6.

[59] S. S. Biswas and A. K. Srivastava, "Voltage stability monitoring in power systems," ed: Google Patents, 2018.

[60] S. M. Burchett *et al.*, "An Optimal Thévenin Equivalent Estimation Method and its Application to the Voltage Stability Analysis of a Wind Hub," *IEEE Trans. Power Syst.*, vol. 33, no. 4, pp. 3644-3652, 2018, doi: 10.1109/TPWRS.2017.2776741.

[61] C. K. Alexander, *Fundamentals of electric circuits*. McGraw-Hill, 2013.

[62] O. Wing, *Classical circuit theory*. Springer Science & Business Media, 2008.

[63] J. M. Ramirez, N. Sundriyal, M. R. Arrieta-Paternina, and A. Zamora-Méndez, "12 - Study of harmonics in linear, nonlinear nonsinusoidal electrical circuits by geometric algebra," in *Monitoring and Control of Electrical Power Systems Using Machine Learning Techniques*, E. Barocio Espejo, F. R. Segundo Sevilla, and P. Korba Eds.: Elsevier, 2023, pp. 289-308.

[64] N. Sundriyal, J. M. Ramirez, and E. B. CORROCHANO, "A comparison of geometric algebra and harmonic domain for linear circuit analysis," *Math. Appl*, vol. 12, pp. 115-127, 2023.

[65] J. B. Ward, "Equivalent Circuits for Power-Flow Studies," *Transactions of the American Institute of Electrical Engineers,* vol. 68, no. 1, pp. 373-382, 1949, doi: 10.1109/T-AIEE.1949.5059947.

[66] M. Ramirez-Gonzalez, M. Bossio, F. R. S. Sevilla, and P. Korba, "Evaluation of Static Network Equivalent Models for N-1 Line Contingency Analysis," in *2022 4th Global Power, Energy and Communication Conference (GPECOM)*, 14-17 June 2022 2022, pp. 328-333, doi: 10.1109/GPECOM55404.2022.9815713.

[67] P. Sharma and A. Kumar, "Thevenin's equivalent based P–Q–V voltage stability region visualization and enhancement with FACTS and HVDC," *Int. J. Electr. Power Energy Syst.*, vol. 80, pp. 119-127, 2016/09/01/ 2016, doi: https://doi.org/10.1016/j.ijepes.2016.01.026.

[68] P. Kessel and H. Glavitsch, "Estimating the Voltage Stability of a Power System," *IEEE Transactions on Power Delivery,* vol. 1, no. 3, pp. 346-354, 1986, doi: 10.1109/TPWRD.1986.4308013.

[69] S. M. Burchett *et al.*, "An optimal Thevenin equivalent estimation method and its application to the voltage stability analysis of a wind hub," *IEEE Trans. Power Syst.*, vol. 33, no. 4, pp. 3644-3652, 2017.

[70] I. Smon, G. Verbic, and F. Gubina, "Local voltage-stability index using Tellegen's theorem," *IEEE Trans. Power Syst.,* vol. 21, no. 3, pp. 1267-1275, 2006.

[71] S. Burchett *et al.*, "An Optimal Thevenin Equivalent Estimation Method and its Application to the Voltage Stability Analysis of a Wind Hub," in *2018 IEEE Power & Energy Society General Meeting (PESGM)*, 5-10 Aug. 2018 2018, pp. 1-1, doi: 10.1109/PESGM.2018.8586212.

[72] D. Dinh Thuc and K. Uhlen, "Online voltage stability monitoring based on PMU measurements and system topology," in *2013 3rd International Conference on*

Electric Power and Energy Conversion Systems, 2-4 Oct. 2013 2013, pp. 1-6, doi: 10.1109/EPECS.2013.6713056.

[73] H. Y. Su and T. Y. Liu, "Robust Thevenin Equivalent Parameter Estimation for Voltage Stability Assessment," *IEEE Trans. Power Syst.*, vol. 33, no. 4, pp. 4637-4639, 2018, doi: 10.1109/TPWRS.2018.2821926.

[74] U. Hashmi, R. Choudhary, and J. G. Priolkar, "Online thevenin equivalent parameter estimation using nonlinear and linear recursive least square algorithm," in *2015 IEEE International Conference on Electrical, Computer and Communication Technologies (ICECCT)*, 5-7 March 2015 2015, pp. 1-6, doi: 10.1109/ICECCT.2015.7225946.

[75] B. Alinezhad and H. K. Karegar, "On-Line Thévenin Impedance Estimation Based on PMU Data and Phase Drift Correction," *IEEE Transactions on Smart Grid*, vol. 9, no. 2, pp. 1033-1042, 2018, doi: 10.1109/TSG.2016.2574765.

[76] C. S. Carvalho and G. N. Taranto, "Comparison of Voltage Instability Identification Methods Based on Synchronized Measurements," in *2019 International Conference on Smart Grid Synchronized Measurements and Analytics (SGSMA)*, 21-23 May 2019 2019, pp. 1-7, doi: 10.1109/SGSMA.2019.8784672.

[77] D. T. Duong and K. Uhlen, "Online voltage stability monitoring based on PMU measurements and system topology," in *2013 3rd International Conference on Electric Power and Energy Conversion Systems*, 2013: IEEE, pp. 1-6.

[78] Y. Wang *et al.*, "Voltage Stability Monitoring Based on the Concept of Coupled Single-Port Circuit," *IEEE Trans. Power Syst.*, vol. 26, no. 4, pp. 2154-2163, 2011, doi: 10.1109/TPWRS.2011.2154366.

[79] H. Yuan and F. Li, "A comparative study of measurement-based Thevenin equivalents identification methods," in *2014 North American Power Symposium (NAPS)*, 7-9 Sept. 2014 2014, pp. 1-6, doi: 10.1109/NAPS.2014.6965369.

[80] D. T. Duong, "Online voltage stability monitoring and coordinated secondary voltage control," PhD, Department of Electric Power Engineering, Norwegian University of Science and Technology Trondheim, 2016.

[81] W. Li, Y. Wang, and T. Chen, "Investigation on the Thevenin equivalent parameters for online estimation of maximum power transfer limits," *IET generation, transmission & distribution*, vol. 4, no. 10, pp. 1180-1187, 2010.

[82] J. A. V. Vásquez, A. R. R. Matavalam, and V. Ajjarapu, "Fast calculation of Thévenin equivalents for real-time steady state voltage stability estimation," in *2016 North American Power Symposium (NAPS)*, 2016: IEEE, pp. 1-7.

[83] C. S. Kong, "A general maximum power transfer theorem," *IEEE Transactions on Education*, vol. 38, no. 3, pp. 296-298, 1995, doi: 10.1109/13.406510.

[84] L. Arya and H. Verma, "A method for tracing PV curve for voltage stability analysis with voltage dependent loads," *Electric Machines and Power Systems*, vol. 24, no. 6, pp. 583-596, 1996.

[85] M. Parniani, J. H. Chow, L. Vanfretti, B. Bhargava, and A. Salazar, "Voltage stability analysis of a multiple-infeed load center using phasor measurement data," in *2006 IEEE PES Power Systems Conference and Exposition*, 2006: IEEE, pp. 1299-1305.

[86] M. Nizam, A. Mohamed, and A. Hussain, "Dynamic Voltage Collapse Prediction In Power Systems Using Power Transfer Stability Index," in *2006 IEEE International Power and Energy Conference*, 28-29 Nov. 2006 2006, pp. 246-250, doi: 10.1109/PECON.2006.346655.

[87] V. Komoni, I. Krasniqi, G. Kabashi, and A. Alidemaj, "Increase power transfer capability and controlling line power flow in power system installed the FACTS," 2010.

[88] T. Moger and T. Dhadbanjan, "A novel index for identification of weak nodes for reactive compensation to improve voltage stability," *IET Generation, Transmission & Distribution*, vol. 9, no. 14, pp. 1826-1834, 2015, doi: https://doi.org/10.1049/iet-gtd.2015.0054.

[89] D. O. Dike and S. M. Mahajan, "Voltage stability index-based reactive power compensation scheme," *Int. J. Electr. Power Energy Syst.*, vol. 73, pp. 734-742, 2015/12/01/ 2015, doi: https://doi.org/10.1016/j.ijepes.2015.04.016.

[90] K. Iba, "Reactive power optimization by genetic algorithm," *IEEE Trans. Power Syst.*, vol. 9, no. 2, pp. 685-692, 1994, doi: 10.1109/59.317674.

[91] K. Y. Lee, X. Bai, and Y.-M. Park, "Optimization method for reactive power planning by using a modified simple genetic algorithm," *IEEE Trans. Power Syst.*, vol. 10, pp. 1843-1850, 1995.

[92] S. Pandya and R. Roy, "Particle Swarm Optimization Based Optimal Reactive Power Dispatch," in *2015 IEEE International Conference on Electrical,*

Computer and Communication Technologies (ICECCT), 5-7 March 2015 2015, pp. 1-5, doi: 10.1109/ICECCT.2015.7225981.

[93] S. Mugemanyi, Z. Qu, F. X. Rugema, Y. Dong, C. Bananeza, and L. Wang, "Optimal Reactive Power Dispatch Using Chaotic Bat Algorithm," *IEEE Access*, vol. 8, pp. 65830-65867, 2020.

[94] S. Cheng and M.-Y. Chen, "Multi-objective reactive power optimization strategy for distribution system with penetration of distributed generation," *Int. J. Electr. Power Energy Syst.*, vol. 62, pp. 221-228, 2014/11/01/ 2014, doi: https://doi.org/10.1016/j.ijepes.2014.04.040.

[95] T. Van Cutsem, "Voltage instability: phenomena, countermeasures, and analysis methods," *Proc. IEEE*, vol. 88, pp. 208-227, 2000.

[96] L. Lian, "Reactive power optimization based on adaptive multi-objective optimization artificial immune algorithm," *Ain Shams Engineering Journal*, vol. 13, no. 5, p. 101677, 2022/09/01/ 2022, doi: https://doi.org/10.1016/j.asej.2021.101677.

[97] F. Aydin and B. Gumus, "Determining Optimal SVC Location for Voltage Stability Using Multi-Criteria Decision Making Based Solution: Analytic Hierarchy Process (AHP) Approach," *IEEE Access*, vol. 9, pp. 143166-143180, 2021, doi: 10.1109/ACCESS.2021.3121196.

[98] Y. Amrane and N. E. L. Y. Kouba, "Chapter 1 - A Multiobjective optimal VAR dispatch using FACTS devices considering voltage stability and contingency analysis," in *Predictive Modelling for Energy Management and Power Systems Engineering*, R. Deo, P. Samui, and S. S. Roy Eds.: Elsevier, 2021, pp. 1-26.

[99] J. Mahadevan, R. Rengaraj, and A. Bhuvanesh, "Application of multi-objective hybrid artificial bee colony with differential evolution algorithm for optimal placement of microprocessor based FACTS controllers," *Microprocessors and Microsystems*, p. 104239, 2021/03/02/ 2021, doi: https://doi.org/10.1016/j.micpro.2021.104239.

[100] M. Basu, "Multi-objective optimal reactive power dispatch using multi-objective differential evolution," *Int. J. Electr. Power Energy Syst.*, vol. 82, pp. 213-224, 2016/11/01/ 2016, doi: https://doi.org/10.1016/j.ijepes.2016.03.024.

[101] A. Chebbo, M. Irving, and M. Sterling, "Voltage collapse proximity indicator: behaviour and implications," in *IEE Proceedings C (generation, transmission and distribution)*, 1992, vol. 139, no. 3: IET, pp. 241-252.

[102] M. A. Abido, "Multiobjective Particle Swarm Optimization for Optimal Power Flow Problem," in *Handbook of Swarm Intelligence: Concepts, Principles and Applications*, B. K. Panigrahi, Y. Shi, and M.-H. Lim Eds. Berlin, Heidelberg: Springer Berlin Heidelberg, 2011, pp. 241-268.

[103] D. Devaraj, "Improved genetic algorithm for multi-objective reactive power dispatch problem," *European Transactions on Electrical Power*, vol. 17, no. 6, pp. 569-581, 2007, doi: https://doi.org/10.1002/etep.146.

[104] C. Dai, Y. Wang, and M. Ye, "A new multi-objective particle swarm optimization algorithm based on decomposition," *Information Sciences*, vol. 325, pp. 541-557, 2015/12/20/ 2015, doi: https://doi.org/10.1016/j.ins.2015.07.018.

[105] S. B. Gee, X. Qiu, and K. C. Tan, "A Novel Diversity Maintenance Scheme for Evolutionary Multi-objective Optimization," in *Intelligent Data Engineering and Automated Learning – IDEAL 2013*, Berlin, Heidelberg, H. Yin *et al.*, Eds., 2013// 2013: Springer Berlin Heidelberg, pp. 270-277.

[106] K. Chaitanya, D. V. L. N. Somayajulu, and P. R. Krishna, "Memory-based approaches for eliminating premature convergence in particle swarm optimization," *Applied Intelligence*, vol. 51, no. 7, pp. 4575-4608, 2021/07/01 2021, doi: 10.1007/s10489-020-02045-z.

[107] K. Y. Lee and J. b. Park, "Application of Particle Swarm Optimization to Economic Dispatch Problem: Advantages and Disadvantages," in *2006 IEEE PES Power Systems Conference and Exposition*, 29 Oct.-1 Nov. 2006 2006, pp. 188-192, doi: 10.1109/PSCE.2006.296295.

[108] J. Meza, H. Espitia, C. Montenegro, E. Giménez, and R. González-Crespo, "MOVPSO: Vortex Multi-Objective Particle Swarm Optimization," *Applied Soft Computing*, vol. 52, pp. 1042-1057, 2017/03/01/ 2017, doi: https://doi.org/10.1016/j.asoc.2016.09.026.

[109] A. N. Ünal and G. Kayakutlu, "Multi-objective particle swarm optimization with random immigrants," *Complex & Intelligent Systems*, vol. 6, no. 3, pp. 635-650, 2020/10/01 2020, doi: 10.1007/s40747-020-00159-y.

[110] X. Zheng and H. Liu, "A hybrid vertical mutation and self-adaptation based MOPSO," *Computers & Mathematics with Applications*, vol. 57, no. 11, pp. 2030-2038, 2009/06/01/ 2009, doi: https://doi.org/10.1016/j.camwa.2008.09.023.

[111] G. G. Yen and W. F. Leong, "Dynamic Multiple Swarms in Multiobjective Particle Swarm Optimization," *IEEE Transactions on Systems, Man, and Cybernetics - Part A: Systems and Humans,* vol. 39, no. 4, pp. 890-911, 2009, doi: 10.1109/TSMCA.2009.2013915.

[112] K. Deb and R. B. Agrawal, "Simulated Binary Crossover for Continuous Search Space," *Complex Syst.,* vol. 9, 1995.

[113] K. Deb and H. Beyer, "Self-Adaptive Genetic Algorithms with Simulated Binary Crossover," *Evolutionary Computation,* vol. 9, no. 2, pp. 197-221, 2001, doi: 10.1162/106365601750190406.

[114] J.-B. Park, Y.-W. Jeong, J.-R. Shin, K. Y. Lee, and J.-h. Kim, "A Hybrid Particle Swarm Optimization Employing Crossover Operation for Economic Dispatch Problems with Valve-point Effects," *2007 International Conference on Intelligent Systems Applications to Power Systems,* pp. 1-6, 2007.

[115] H. Wang, Z. Wu, Y. Liu, and S. Zeng, "Particle Swarm Optimization with a Novel Multi-Parent Crossover Operator," *2008 Fourth International Conference on Natural Computation,* vol. 7, pp. 664-668, 2008.

[116] M. A. Tawhid and A. F. Ali, "Simplex particle swarm optimization with arithmetical crossover for solving global optimization problems," *OPSEARCH,* vol. 53, no. 4, pp. 705-740, 2016/12/01 2016, doi: 10.1007/s12597-016-0256-7.

[117] E. Zitzler, K. Deb, and L. Thiele, "Comparison of Multiobjective Evolutionary Algorithms: Empirical Results," *Evol. Comput.,* vol. 8, no. 2, pp. 173–195, 2000, doi: 10.1162/106365600568202.

[118] H. Ishibuchi, H. Masuda, Y. Tanigaki, and Y. Nojima, "Modified Distance Calculation in Generational Distance and Inverted Generational Distance," in *Evolutionary Multi-Criterion Optimization*, Cham, A. Gaspar-Cunha, C. Henggeler Antunes, and C. C. Coello, Eds., 2015// 2015: Springer International Publishing, pp. 110-125.

[119] C. Audet, J. Bigeon, D. Cartier, S. Le Digabel, and L. Salomon, "Performance indicators in multiobjective optimization," *European Journal of Operational Research,* vol. 292, no. 2, pp. 397-422, 2021/07/16/ 2021, doi: https://doi.org/10.1016/j.ejor.2020.11.016.

[120] C. A. C. Coello and N. C. Cortés, "Solving Multiobjective Optimization Problems Using an Artificial Immune System," *Genetic Programming and Evolvable*

Machines, vol. 6, no. 2, pp. 163-190, 2005/06/01 2005, doi: 10.1007/s10710-005-6164-x.

[121] H. S. Salama and I. Vokony, "Voltage stability indices–A comparison and a review," *Comput. Electr. Eng.,* vol. 98, p. 107743, 2022/03/01/ 2022, doi: https://doi.org/10.1016/j.compeleceng.2022.107743.

[122] E. G. C. P. R.B. Prada, J.O.R. dos Santos , A. Bianco, L.A.S. Pilotto "Voltage stability assessment for real-time operation," *IEE Proceedings - Generation, Transmission and Distribution,* vol. Volume 149, no. Issue 2, pp. 175 –181, March 2002, doi: 10.1049/ip-gtd:20020282.

[123] M. Kamel, F. Li, S. Bu, and Q. Wu, "A generalized voltage stability indicator based on the tangential angles of PV and load curves considering voltage dependent load models," *Int. J. Electr. Power Energy Syst.,* vol. 127, p. 106624, 2021/05/01/ 2021, doi: https://doi.org/10.1016/j.ijepes.2020.106624.

[124] S. G. Ghiocel and J. H. Chow, "A Power Flow Method Using a New Bus Type for Computing Steady-State Voltage Stability Margins," *IEEE Trans. Power Syst.,* vol. 29, no. 2, pp. 958-965, 2014, doi: 10.1109/TPWRS.2013.2288157.

[125] V. Ajjarapu and C. Christy, "The continuation power flow: a tool for steady state voltage stability analysis," *IEEE Trans. Power Syst.,* vol. 7, no. 1, pp. 416-423, 1992, doi: 10.1109/59.141737.

[126] A. B. N. Elisabete de Mello Magalhães, Dilson Amancio Alves,, "A Parameterization Technique for the Continuation Power Flow Developed from the Analysis of Power Flow Curves," *Math. Probl. Eng.,* vol. 2012, p. 24 pages, 2012, Art no. 762371, doi: https://doi.org/10.1155/2012/762371.

[127] K. Karthikeyan and P. K. Dhal, "Multi verse optimization (MVO) technique based voltage stability analysis through continuation power flow in IEEE 57 bus," *Energy Procedia,* vol. 117, pp. 583-591, 2017/06/01/ 2017, doi: https://doi.org/10.1016/j.egypro.2017.05.153.

[128] R. Pourbagher, S. Y. Derakhshandeh, and M. E. Hamedani Golshan, "An adaptive multi-step Levenberg-Marquardt continuation power flow method for voltage stability assessment in the Ill-conditioned power systems," *Int. J. Electr. Power Energy Syst.,* vol. 134, p. 107425, 2022/01/01/ 2022, doi: https://doi.org/10.1016/j.ijepes.2021.107425.

[129] C. Liu, A. Bose, M. Han, and X. Chen, "Improved continuation power flow method for AC/DC power system," in *2011 IEEE Electrical Power and Energy*

Conference, 3-5 Oct. 2011 2011, pp. 192-198, doi: 10.1109/EPEC.2011.6070194.

[130] D. K. Molzahn, B. C. Lesieutre, and H. Chen, "Counterexample to a Continuation-Based Algorithm for Finding All Power Flow Solutions," *IEEE Trans. Power Syst.*, vol. 28, no. 1, pp. 564-565, 2013, doi: 10.1109/TPWRS.2012.2202205.

[131] T. Jiang, L. Bai, H. Yuan, H. Jia, F. Li, and H. Cui, "QV interaction evaluation and pilot voltage-reactive power coupling area partitioning in bulk power systems," *IET Science, Measurement & Technology*, vol. 11, no. 3, pp. 270-278, 2017, doi: https://doi.org/10.1049/iet-smt.2016.0232.

[132] C. Vournas, "Power System Voltage Stability," in *Encyclopedia of Systems and Control*, J. Baillieul and T. Samad Eds. London: Springer London, 2020, pp. 1-6.

[133] P. Kundur, N. J. Balu, and M. G. Lauby, *Power System Stability and Control*. McGraw-Hill Education, 1994.

[134] T. Aziz, T. K. Saha, and N. Mithulananthan, "Distributed generators placement for loadability enhancement based on reactive power margin," in *2010 Conference Proceedings IPEC*, 27-29 Oct. 2010 2010, pp. 740-745, doi: 10.1109/IPECON.2010.5697023.

[135] S. Ramesh, S. Kannan, and S. Baskar, "An improved generalized differential evolution algorithm for multi-objective reactive power dispatch," *Engineering Optimization*, vol. 44, no. 4, pp. 391-405, 2012/04/01 2012, doi: 10.1080/0305215X.2011.576761.

[136] G. Naveen Kumar and M. Surya Kalavathi, "Cat Swarm Optimization for optimal placement of multiple UPFC's in voltage stability enhancement under contingency," *Int. J. Electr. Power Energy Syst.*, vol. 57, pp. 97-104, 2014/05/01/ 2014, doi: https://doi.org/10.1016/j.ijepes.2013.11.050.

[137] K. Deb, A. Pratap, S. Agarwal, and T. Meyarivan, "A fast and elitist multiobjective genetic algorithm: NSGA-II," *IEEE Transactions on Evolutionary Computation*, vol. 6, no. 2, pp. 182-197, 2002, doi: 10.1109/4235.996017.

[138] B. Luo, J. Zheng, J. Xie, and J. Wu, "Dynamic Crowding Distance?A New Diversity Maintenance Strategy for MOEAs," in *2008 Fourth International Conference on Natural Computation*, 18-20 Oct. 2008 2008, vol. 1, pp. 580-585, doi: 10.1109/ICNC.2008.532.

[139] N. Riquelme, C. V. Lücken, and B. Baran, "Performance metrics in multi-objective optimization," in *2015 Latin American Computing Conference (CLEI)*, 19-23 Oct. 2015 2015, pp. 1-11, doi: 10.1109/CLEI.2015.7360024.

[140] R. D. Zimmerman, C. E. Murillo-Sánchez, and R. J. Thomas, "MATPOWER: Steady-State Operations, Planning, and Analysis Tools for Power Systems Research and Education," *IEEE Trans. Power Syst.*, vol. 26, no. 1, pp. 12-19, 2011, doi: 10.1109/TPWRS.2010.2051168.

[141] U. o. Waterloo. "14 Bus power flow test case." http://www.ee.washington.edu/research/pstca/pf14/pg_tca14bus.htm (accessed September 10, 2024).

[142] C. Hsiao-Dong, A. J. Flueck, K. S. Shah, and N. Balu, "CPFLOW: a practical tool for tracing power system steady-state stationary behavior due to load and generation variations," *IEEE Trans. Power Syst.*, vol. 10, no. 2, pp. 623-634, 1995, doi: 10.1109/59.387897.

[143] Y.-L. Chen, C.-W. Chang, and C.-C. Liu, "Efficient methods for identifying weak nodes in electrical power networks," *IEE Proceedings-Generation, Transmission and Distribution*, vol. 142, no. 3, pp. 317-322, 1995.

APPENDIX I: MAXIMUM REACTIVE POWER COMPUTATION AT CONSTANT POWER FACTOR

The derivation begins from equation (3.68)

$$Q = \frac{-V^2\cos(\theta-\varphi) \pm V\sqrt{E_{th}^2 - V^2\sin^2(\theta-\varphi)}}{Z_{th}\csc\theta} \quad \text{A.1}$$

At the point of maximum reactive power transfer, the slop of the tangent to the graph gets zero. i.e

$$\frac{dQ}{dV} = 0 \quad \text{A.2}$$

This gives;

$$\frac{dQ}{dV} = \frac{-2V\cos(\theta-\varphi) \pm \dfrac{E_{th}^2 - 2V^2\sin^2(\theta-\varphi)}{\sqrt{E_{th}^2 - V^2\sin^2(\theta-\varphi)}}}{Z_{th}\csc\theta} = 0 \quad \text{A.3}$$

Further computation;

$$\pm\frac{E_{th}^2 - 2V^2\sin^2(\theta-\varphi)}{2V\cos(\theta-\varphi)} = \sqrt{E_{th}^2 - V^2\sin^2(\theta-\varphi)} \quad \text{A.4}$$

$$\frac{E_{th}^4 + 4V^4\sin^4(\theta-\varphi) - 4E_{th}^2V^2\sin^2(\theta-\varphi)}{4V^2\cos^2(\theta-\varphi)} = E_{th}^2 - V^2\sin^2(\theta-\varphi) \quad \text{A.5}$$

$$E_{th}^4 + 4V^4\sin^4(\theta-\varphi) - 4E_{th}^2V^2\sin^2(\theta-\varphi) = 4E_{th}^2V^2\cos^2(\theta-\varphi) - 4V^4\sin^2(\theta-\varphi)\cos^2(\theta-\varphi) \quad \text{A.6}$$

$$E_{th}^4 + 4V^4\sin^4(\theta-\varphi) - 4E_{th}^2V^2\sin^2(\theta-\varphi) = 4E_{th}^2V^2(1-\sin^2(\theta-\varphi)) - 4V^4(\sin^2(\theta-\varphi) - \sin^4(\theta-\varphi)) \quad \text{A.7}$$

$$E_{th}^4 = 4E_{th}^2V^2 - 4V^4\sin^2(\theta-\varphi) \quad \text{A.8}$$

$$4V^4\sin^2(\theta-\varphi) - 4E_{th}^2V^2 + E_{th}^4 = 0 \quad \text{A.9}$$

$$V^2 = \frac{4E_{th}^2 \pm \sqrt{16E_{th}^4 - 16E_{th}^4 \sin^2(\theta - \varphi)}}{8\sin^2(\theta - \varphi)} \quad \text{A.10}$$

$$V^2 = \frac{E_{th}^2(1 \pm \cos(\theta - \varphi))}{2\sin^2(\theta - \varphi)} \quad \text{A.11}$$

The positive sign makes V> Eth which is the impossible condition. Hence, we take the negative option.

$$V^2 = \frac{E_{th}^2(1 - \cos(\theta - \varphi))}{2\sin^2(\theta - \varphi)} \quad \text{A.12}$$

$$V^2 = \frac{E_{th}^2(1 - \cos(\theta - \varphi))}{2\sin^2(\theta - \varphi)} \cdot \frac{1 + \cos(\theta - \varphi)}{1 + \cos(\theta - \varphi)} \quad \text{A.13}$$

$$V^2 = \frac{E_{th}^2}{2(1 + \cos(\theta - \varphi))} \quad \text{A.14}$$

$$V = \frac{E_{th}}{\sqrt{2(1 + \cos(\theta - \varphi))}} \quad \text{A.15}$$

Substituting this value A.15 to A.1.;

$$Q = \frac{-\left(\frac{E_{th}^2}{2(1 + \cos(\theta - \varphi))}\right)\cos(\theta - \varphi) \pm \frac{E_{th}^2(1 + \cos(\theta - \varphi))}{2(1 + \cos(\theta - \varphi))}}{Z_{th}\csc\theta} \quad \text{A.16}$$

$$Q = \frac{-E_{th}^2\cos(\theta - \varphi) \pm E_{th}^2(1 + \cos(\theta - \varphi))}{2Z_{th}\csc\theta\,(1 + \cos(\theta - \varphi))} \quad \text{A.17}$$

Since Q is a load and it should assume a positive value, we eliminate the negative option coming as;

$$Q = \frac{-E_{th}^2\cos(\theta - \varphi) + E_{th}^2(1 + \cos(\theta - \varphi))}{2Z_{th}\csc\theta\,(1 + \cos(\theta - \varphi))} \quad \text{A.18}$$

$$Q = \frac{E_{th}^2\sin\theta}{2Z_{th}(1 + \cos(\theta - \varphi))} \quad \text{A.19}$$

APPENDIX II: DATA EMPLOYED FOR THE TEST SYSTEMS

II. 1. IEEE 14 Bus System

a) Bus data

Bus Number	Bus type (3-slack, 2-PQ bus, 1-PV bus)	Active load (Pd)	Reactive load (Qd)	Compensator		Bus voltage		Vmax	Vmin
				Conductance (Gs)	Susceptance (Bs)	Magnitude (Vm)	Angle (Va)		
1	3	0	0	0	0	1	0	1.06	0.94
2	2	21.7	12.7	0	0	1.045	-4.98	1.06	0.94
3	2	94.2	19	0	0	1.01	-12.72	1.06	0.94
4	1	47.8	-3.9	0	0	1.019	-10.33	1.06	0.94
5	1	7.6	1.6	0	0	1.02	-8.78	1.06	0.94
6	2	11.2	7.5	0	0	1.07	-14.22	1.06	0.94
7	1	0	0	0	0	1.062	-13.37	1.06	0.94
8	2	0	0	0	0	1.09	-13.36	1.06	0.94
9	1	29.5	16.6	0	19	1.056	-14.94	1.06	0.94
10	1	9	5.8	0	0	1.051	-15.1	1.06	0.94
11	1	3.5	1.8	0	0	1.057	-14.79	1.06	0.94
12	1	6.1	1.6	0	0	1.055	-15.07	1.06	0.94
13	1	13.5	5.8	0	0	1.05	-15.16	1.06	0.94
14	1	14.9	5	0	0	1.036	-16.04	1.06	0.94

b) Branch data

From bus	To bus	Resistance (pu)	Reactance (pu)	Susceptance (pu)	Tap ratio
1	2	0.01938	0.05917	0.0528	0
1	5	0.05403	0.22304	0.0492	0
2	3	0.04699	0.19797	0.0438	0
2	4	0.05811	0.17632	0.034	0
2	5	0.05695	0.17388	0.0346	0
3	4	0.06701	0.17103	0.0128	0
4	5	0.01335	0.04211	0	0
4	7	0	0.20912	0	0.978
4	9	0	0.55618	0	0.969
5	6	0	0.25202	0	0.932
6	11	0.09498	0.1989	0	0
6	12	0.12291	0.25581	0	0
6	13	0.06615	0.13027	0	0
7	8	0	0.17615	0	0
7	9	0	0.11001	0	0
9	10	0.03181	0.0845	0	0
9	14	0.12711	0.27038	0	0
10	11	0.08205	0.19207	0	0
12	13	0.22092	0.19988	0	0
13	14	0.17093	0.34802	0	0

c) Generator data

Bus	Active power (Pg)	Reactive power (Qg)	Qmax	Qmin	Vg	Pmax	Pmin
1	232.4	-16.9	10	0	1.06	332.4	0
2	40	42.4	50	-40	1.045	140	0
3	0	23.4	40	0	1.01	100	0
6	0	12.2	24	-6	1.07	100	0
8	0	17.4	24	-6	1.09	100	0

d) Single line diagram of IEEE 14 bus system

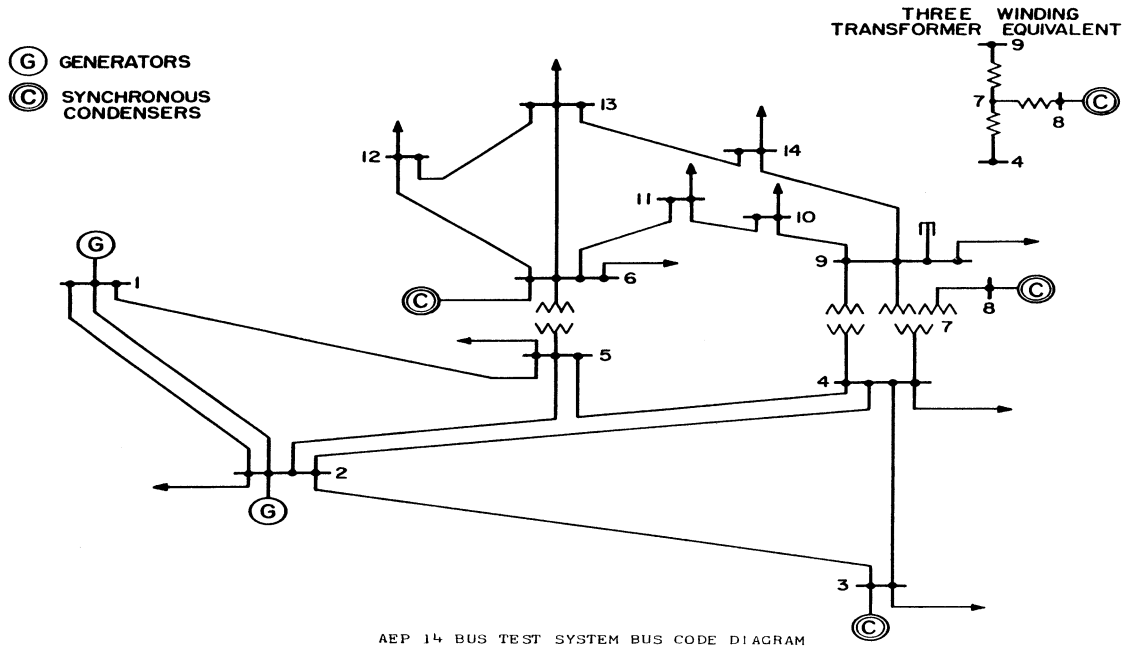

II.2. IEEE 30 Bus System Data

a) Bus data

Bus Number	Bus type (3-slack, 2-PQ bus, 1-PV bus)	Active load (Pd)	Reactive load (Qd)	Compensator		Bus voltage		Vmax	Vmin
				Conductance (Gs)	Susceptance (Bs)	Magnitude (Vm)	Angle (Va)		
1	3	0	0	0	0	1	0	1.05	0.95
2	2	21.7	12.7	0	0	1	0	1.05	0.95
3	1	2.4	1.2	0	0	1	0	1.05	0.95
4	1	7.6	1.6	0	0	1	0	1.05	0.95
5	1	0	0	0	0.19	1	0	1.05	0.95
6	1	0	0	0	0	1	0	1.05	0.95
7	1	22.8	10.9	0	0	1	0	1.05	0.95
8	1	30	30	0	0	1	0	1.05	0.95
9	1	0	0	0	0	1	0	1.05	0.95
10	1	5.8 2	0	0	0	1	0	1.05	0.95
11	1	0	0	0	0	1	0	1.05	0.95
12	1	11.2	7.5	0	0	1	0	1.05	0.95
13	2	0	0	0	0	1	0	1.05	0.95
14	1	6.2	1.6	0	0	1	0	1.05	0.95
15	1	8.2	2.5	0	0	1	0	1.05	0.95
16	1	3.5	1.8	0	0	1	0	1.05	0.95
17	1	9	5.8	0	0	1	0	1.05	0.95
18	1	3.2	0.9	0	0	1	0	1.05	0.95
19	1	9.5	3.4	0	0	1	0	1.05	0.95
20	1	2.2	0.7	0	0	1	0	1.05	0.95
21	1	17.5	11.2	0	0	1	0	1.05	0.95
22	2	0	0	0	0	1	0	1.05	0.95

23	2	3.2	1.6	0	0	1	0	1.05	0.95
24	1	8.7	6.7	0	0.04	1	0	1.05	0.95
25	1	0	0	0	0	1	0	1.05	0.95
26	1	3.5	2.3	0	0	1	0	1.05	0.95
27	2	0	0	0	0	1	0	1.05	0.95
28	1	0	0	0	0	1	0	1.05	0.95
29	1	2.4	0.9	0	0	1	0	1.05	0.95
30	1	10.6	1.9	0	0	1	0	1.05	0.95

b) Generator data

Bus	**Active power (Pg)**	**Reactive power (Qg)**	**Qmax**	**Qmin**	**Vg**	**Pmax**	**Pmin**
1	23.54	0	150	-20	1	80	0
2	60.97	0	60	-20	1	80	0
22	21.59	0	62.5	-15	1	50	0
27	26.91	0	48.7	-15	1	55	0
23	19.2	0	40	-10	1	30	0
13	37	0	44.7	-15	1	40	0

c) Branch data

From bus	To bus	Resistance (pu)	Reactance (pu)	Susceptance (pu)	Tap ratio	Phase shift angle
1	2	0.02	0.06	0.03	0	0
1	3	0.05	0.19	0.02	0	0
2	4	0.06	0.17	0.02	0	0
3	4	0.01	0.04	0	0	0
2	5	0.05	0.2	0.02	0	0
2	6	0.06	0.18	0.02	0	0
4	6	0.01	0.04	0	0	0
5	7	0.05	0.12	0.01	0	0
6	7	0.03	0.08	0.01	0	0
6	8	0.01	0.04	0	0	0
6	9	0	0.21	0	1.0155	0
6	10	0	0.56	0	0.9629	0
9	11	0	0.21	0	0	0
9	10	0	0.11	0	0	0
4	12	0	0.26	0	1.0119	0
12	13	0	0.14	0	0	0
12	14	0.12	0.26	0	0	0
12	15	0.07	0.13	0	0	0
12	16	0.09	0.2	0	0	0
14	15	0.22	0.2	0	0	0
16	17	0.08	0.19	0	0	0
15	18	0.11	0.22	0	0	0
18	19	0.06	0.13	0	0	0
19	20	0.03	0.07	0	0	0
10	20	0.09	0.21	0	0	0
10	17	0.03	0.08	0	0	0
10	21	0.03	0.07	0	0	0
10	22	0.07	0.15	0	0	0
21	22	0.01	0.02	0	0	0
15	23	0.1	0.2	0	0	0
22	24	0.12	0.18	0	0	0
23	24	0.13	0.27	0	0	0
24	25	0.19	0.33	0	0	0
25	26	0.25	0.38	0	0	0
25	27	0.11	0.21	0	0	0
28	27	0	0.4	0	0.9581	0
27	29	0.22	0.42	0	0	0
27	30	0.32	0.6	0	0	0
29	30	0.24	0.45	0	0	0
8	28	0.06	0.2	0.02	0	0
6	28	0.02	0.06	0.01	0	0

d) Single line diagram of IEEE 30 bus system

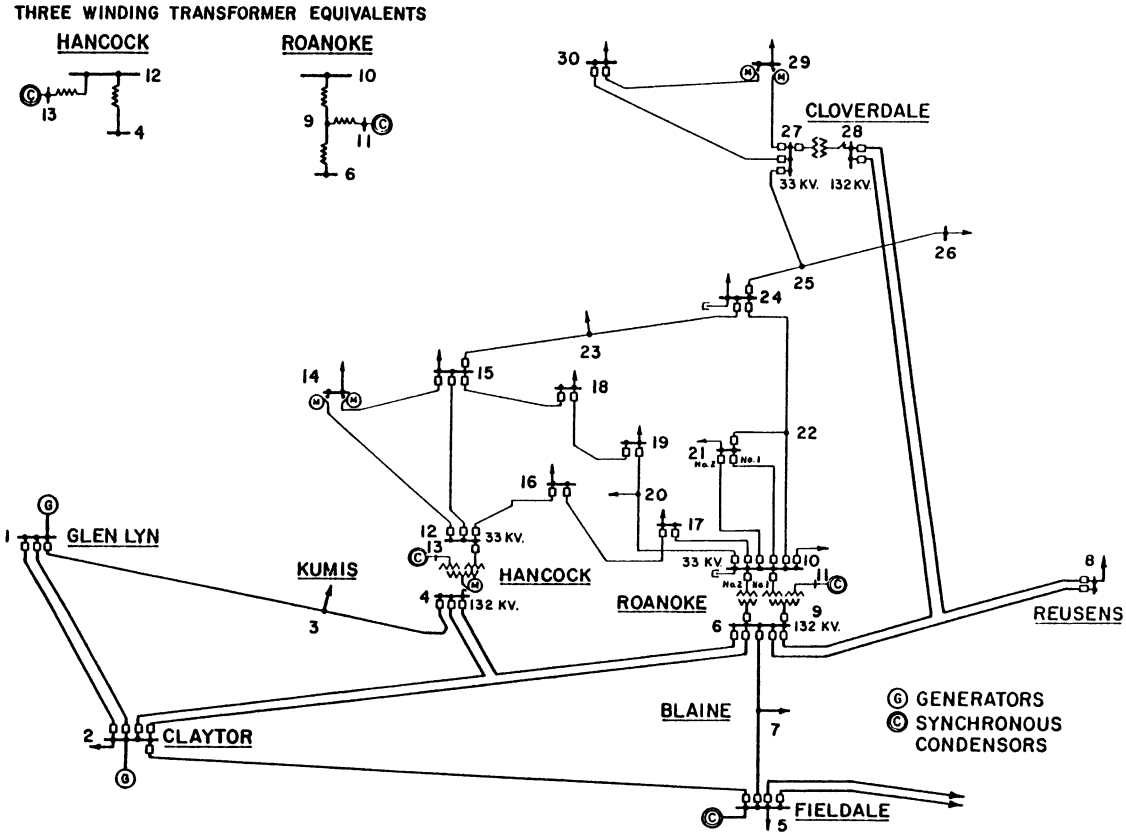

II.3. **EEP** LOAD AND COMPENSATION DATA USED FOR THE ANALYSIS

For the size of the system is large only the load and compensation data, and bus names which are important to understand the results of this work are shown here next. The summary of the remaining components used are shown in section 5.1.

Bus Name	Bus number	Pload (MW)	Qload (Mvar)	Gs	Bs	Area Num	Voltage (pu)	Angle (deg)	Base kV
KEBRIDHER-132	1	0.1897	0.0917	0	-10	3	1	0	132
SUD-GADARF230	2	3193	1531.6863	0	0	11	1	0	230
ADD-EAST1 15	3	25.5833	12.3839	0	0	1	1	0	15
B.WRGENU 15	4	47.8171	23.1607	0	0	1	1	0	15
COTOBIE-15B115	5	10.7505	4.9617	0	0	1	1	0	15
SULULTA-15 15	6	17.3662	8.2696	0	0	1	1	0	15
ADDIS-EAST 215	7	47.63	22.75	0	0	1	1	0	15
COTOBIE-15B215	8	36.3464	6.4141	0	0	1	1	0	15
SULULTA-33 33	9	12.0737	5.7887	0	0	1	1	0	33
BOLE-LEMI MB15	10	3.0821	0.4623	0	0	1	1	0	15
SHEGOLE 15	11	15.1558	6.251	0	0	1	1	0	15
LEGETAFO 15	12	44.4573	21.5138	0	0	1	1	0	15

COTTEBEI 33	13	7.0881	3.4307	0	0	1	1	0	33
AYAT GIS 15	14	0.3535	0.3173	0	0	1	1	0	15
BOLE-LEMI MB33	15	2	3	0	0	1	1	0	33
ADDIS NORTH 15	16	29.6437	14.3248	0	0	1	1	0	15
GEFERSA 15	17	22.5761	11.2467	0	0	1	1	0	15
GEFARSA-3 15	18	9.9158	4.7974	0	0	1	1	0	15
TORHAYLO GIS15	19	7.6328	3.6774	0	0	1	1	0	15
MINILIK GIS 15	20	7.28	3.2551	0	0	1	1	0	15
GEFERSA 15	21	14.5386	7.0309	0	0	1	1	0	15
ADDIS SOUTH 15	22	31.1831	15.2988	0	0	1	1	0	15
AKAKI 1 15	23	3.4446	1.6672	0	0	1	1	0	15
AKAKI-SP 15	24	3.6583	1.7704	0	0	1	1	0	15
KALITI1 15	25	0	0	0	0	1	1	0	15
KALITI2 15	26	14.8505	3.2798	0	0	1	1	0	15
KALTI-NORTH 15	27	31.9207	15.7122	0	0	1	1	0	15
MEKANISA 15	28	28.9424	14.0063	0	0	1	1	0	15
NEFASILK 15	29	46.1324	22.3294	0	0	1	1	0	15
YESU 15	30	28.3526	13.7227	0	0	1	1	0	15
GELAN 15	31	23.1454	11.2098	0	0	1	1	0	15
KALITI GIS 15	32	0.1994	0.0965	0	0	1	1	0	15
EIZ 33	33	32.4858	3.5366	0	0	1	1	0	33
INDODE TS 27.5	34	7.2	3.4848	0	0	1	1	0	27.5
KALITI1 15	35	21.079	7.5066	0	0	1	1	0	15
KALITI2 15	36	9.2929	1.64	0	0	1	1	0	15
GELAN 15	37	13.7903	9.1935	0	0	1	1	0	15
ADDIS-W1 15	38	59.6423	10.4886	0	0	1	1	0	15
GEDJA 15	39	1.4672	0.7101	0	0	1	1	0	15
SEBETA1 15	40	30.4333	14.9097	0	0	1	1	0	15
BLACK-LION 15	41	15	7.26	0	0	1	1	0	27.5
SEBETA1 15	42	34.2033	15.6155	0	0	1	1	0	15
MEKANISA 15	43	8.7704	4.2448	0	0	1	1	0	15
ADDIS CENTER15	44	30.2531	13.8972	0	0	1	1	0	15
BOLE LEMI 33	45	17.4639	8.7319	0	0	1	1	0	33
SINO STEEL P33	46	20.855	9.931	0	0	1	1	0	33
SEBETA-2 36	47	40.0576	7.4427	0	0	1	1	0	36
KILINTO 33	48	18.1275	8.9144	0	0	1	1	0	33
KOYO ABO 15	49	50.7935	20.5124	0	0	1	1	0	15
SEBATA-1 15	50	14.0326	7.0164	0	0	1	1	0	15
D BEREHAN-33	51	1.4543	0.6326	0	0	2	1	0	33
DEBRE BERHAN15	52	4.7086	2.1346	0	0	2	1	0	15
FICHE 15	53	4.9486	2.3952	0	0	2	1	0	15
FITCHE 33	54	1.2847	0.6217	0	0	2	1	0	33
CHANCHO 33	55	17.19	8.03	0	0	2	1	0	33

ADDIS ALEM 15	56	6.4141	2.138	0	0	2	1	0	15
DERBA-33 33	57	2.8449	0.1121	0	0	2	1	0	33
GINCHI 15 15	58	0.9024	0.4383	0	0	2	1	0	15
HORMAT 15	59	14.351	6.4355	0	0	2	1	0	15
MUGER 15	60	12.9351	6.6386	0	0	2	1	0	15
DERBA-6.3	61	19.045	5.1536	0	0	2	1	0	6.6
MUGGER 33	62	7.1789	2.4251	0	0	2	1	0	33
GEBRE-GURCHA33	63	9.1705	4.4385	0	0	2	1	0	33
HABESHA CEM 6.6	64	12.5548	1.2365	0	0	2	1	0	6.6
HORMAT 33	65	0.8624	0.3861	0	0	2	1	0	33
DANGOTE 11.5	66	21.9224	4.0011	0	0	2	1	0	11.5
MUGER 15	67	1.4035	0.6793	0	0	2	1	0	15
AMIBARA 15	68	1.9794	0.9581	0	0	2	1	0	15
AWASH-7KL 15	69	4.0248	1.9481	0	0	2	1	0	15
AMIBARA 33	70	1.3965	0.6758	0	0	2	1	0	33
ADAMI TULU 15	71	6.6379	2.6148	0	0	2	1	0	15
ASSELA 15	72	19.2422	8.5521	0	0	2	1	0	15
AWASH II 15	73	8.5521	4.2761	0	0	2	1	0	15
AWASH-2 15	74	0.539	0.2156	0	0	2	1	0	15
AWASH-3 15	75	3.6259	1.7549	0	0	2	1	0	15
ELALA-GEDA 15	76	10.7213	5.1938	0	0	2	1	0	15
GOBESSA 33	77	3.7451	1.8102	0	0	2	1	0	33
KOKA 15	78	0.539	0.2156	0	0	2	1	0	15
KOKA2 15	79	1.069	0.5345	0	0	2	1	0	15
M.WK-YUG 15	80	0.9452	0.4574	0	0	2	1	0	15
METAHARA 15	81	4.7505	2.3013	0	0	2	1	0	15
MODJO 15	82	5.6714	2.8357	0	0	2	1	0	15
NAZERETH-II 15	83	31.0014	10.6901	0	0	2	1	0	15
NURAERA 15	84	5.4319	1.5224	0	0	2	1	0	15
WONJI PULP 15	85	14.4991	21.4458	0	0	2	1	0	15
NURAERA-33	86	1.8268	0.7612	0	0	2	1	0	33
ADAMI TULU 33	87	5.7986	2.8077	0	0	2	1	0	33
ASSELA 33	88	8.5521	2.138	0	0	2	1	0	33
MOJO II MOB 15	89	9.6986	4.6984	0	0	2	1	0	15
MODJO TS 27.5	90	15	7.26	0	0	2	1	0	27.5
NAZRETH2 MB 15	91	26.0743	12.6199	0	0	2	1	0	15
WON SUG 11	92	0.1749	0.0847	0	0	2	1	0	11
MODJO 15	93	4.6416	1.1645	0	0	2	1	0	15
DEBRE-ZEIT1 15	94	5.4142	2.6168	0	0	2	1	0	15
DEBRE-ZEIT2 15	95	15.8214	7.6541	0	0	2	1	0	15
DUKEM 15	96	1.6501	0.7986	0	0	2	1	0	15

D.ZEIT3 15	97	1.069	0.5345	0	0	2	1	0	15
KNORIA TEXTI11	98	11.287	5.4628	0	0	2	1	0	11
DUKEM 15	99	2.5656	2.4587	0	0	2	1	0	15
DUKEM 15	100	3.5277	2.6725	0	0	2	1	0	15
DEBRE-ZEIT2 15	101	15.2869	7.4831	0	0	2	1	0	15
DEBRE-ZEIT2 15	102	21.1854	10.258	0	0	2	1	0	15
BUTAJIRA 15	103	3.4577	2.034	0	0	2	1	0	15
WOLISO 15	104	9.8312	4.7583	0	0	2	1	0	15
WOLKITE 33	105	7.9837	3.8641	0	0	2	1	0	33
BUTAJIRA33 33	106	4.4273	2.1428	0	0	2	1	0	33
WOLISO-33	107	3.3386	1.6159	0	0	2	1	0	33
WOLKITE 15	108	6.5982	3.1935	0	0	2	1	0	15
HOLETA-33	109	1.4543	0.6326	0	0	2	1	0	33
BUEE 15	110	4.5764	2.034	0	0	2	1	0	15
D.BEHRAN 15	111	1.6282	0.7876	0	0	2	1	0	15
DUKEM 15	112	27.1808	13.5905	0	0	2	1	0	15
HOLETA 15	113	14.9059	6.6844	0	0	2	1	0	33
ELALA GEDA 33	114	14.9059	6.4825	0	0	2	1	0	15
GEORGE SHOE 15	115	12.9651	2.593	0	0	2	1	0	33
GEORGE SHOE 33	116	6.4825	6.4825	0	0	2	1	0	15
TULUFA MOBI 15	117	12.9651	6.4825	0	0	2	1	0	15
GUDERMOBILE 15	118	0.5085	0.2034	0	0	2	1	0	15
AWASH-2 15	119	0.539	0.2156	0	0	2	1	0	15
KOKA 15	120	5.0646	2.6488	0	0	3	1	0	15
ADIGALA 33	121	0.445	0.9111	0	0	3	1	0	33
ALEMAYA 15	122	2.2116	0.5345	0	0	3	1	0	15
ALEMAYA-33	123	1.069	0.5345	0	0	3	1	0	33
ASEBE-33	124	0.9536	0.6357	0	0	3	1	0	33
BABILE 15	125	1.9813	0.9606	0	0	3	1	0	15
BEDESSA 15	126	2.1191	0.4239	0	0	3	1	0	15
CHELENKO 15	127	4.0596	1.9622	0	0	3	1	0	15
DIRE DAW 15	128	22.0381	7.4167	0	0	3	1	0	15
FIK 33	129	0.9905	0.4953	0	0	3	1	0	33
HARAR 15	130	11.5989	5.6061	0	0	3	1	0	15
HARAR3 33	131	0.4344	0.2103	0	0	3	1	0	33
HARAR3 15	132	9.5038	2.3204	0	0	3	1	0	15
HURSO 15	133	0.445	0.2154	0	0	3	1	0	15
BEDESA 33	134	0.6357	0.1058	0	0	3	1	0	33
DEGEHABUR 33	135	4.0572	0.9511	0	0	3	1	0	33
DIRE DAW 33	136	10.8995	8.0565	0	0	3	1	0	33
NATIONAL CEM6	137	22.9644	5.8972	0	0	3	1	0	6

JIJIGA 33	138	1.0596	1.3032	0	0	3	1	0	33
JIJIGA2 15	139	10.8398	5.0008	0	0	3	1	0	15
SIRBA TS 27.5	140	1.0596	0.5127	0	0	3	1	0	33
GODE33	141	0.1971	0.4291	0	0	4	1	0	33
ASSOSA 33	142	4.0261	0.8476	0	0	4	1	0	15
GHIMBI 15	143	1.3773	0.3178	0	0	4	1	0	33
MENDI 33	144	2.7018	0.6199	0	0	4	1	0	15
ASSOSA 15	145	3.8142	0	0	0	4	1	0	33
GHIMBI 33	146	1.96	0.9487	0	0	4	1	0	13.2
FINCHAA 13.2	147	2.8582	1.3834	0	0	4	1	0	15
FINCHA-SUG 115	148	0.6357	0.3077	0	0	4	1	0	15
FINCHA-SUG 215	149	0.1058	0.0513	0	0	4	1	0	33
GHEDO 15	150	3.5213	1.7035	0	0	4	1	0	33
GHEDO 33	151	1.3948	0.6745	0	0	4	1	0	15
FINCHA-SUG 215	152	2.8582	1.3834	0	0	4	1	0	15
GIDA-AYANA 33	153	4.3123	2.087	0	0	4	1	0	33
NEKEMPTE 15	154	7.2605	3.5142	0	0	4	1	0	15
GIDAMI33	155	1.9999	0.9699	0	0	4	1	0	33
DEDESSA 33	156	1.9999	1	0	0	4	1	0	33
NEKEMPTE 33	157	2.6525	1.2875	0	0	4	1	0	33
BAKO 15	158	3.901	1.7553	0	0	4	1	0	15
W SODO-II 15	159	4.238	2.0513	0	0	5	1	0	15
BALEROBE 15	160	6.3572	1.2714	0	0	5	1	0	15
BALEROBE 33	161	1.9071	0.9231	0	0	5	1	0	33
ALABA 15	162	6.781	3.282	0	0	5	1	0	15
ARBA MINCH 15	163	21.635	10.4756	0	0	5	1	0	15
AWASA 15	164	27.0641	11.5989	0	0	5	1	0	15
BOCU LUGUMA 33	165	2.942	1.4264	0	0	5	1	0	33
DILLA 33	166	1.2715	0.6154	0	0	5	1	0	33
H-MARIAM 33	167	5.9434	2.8727	0	0	5	1	0	33
HOSAINA 15	168	6.8429	3.3119	0	0	5	1	0	15
NEGLE-BORENA33	169	0.7999	0.4	0	0	5	1	0	33
SHASHEMENE-115	170	16.4318	7.7326	0	0	5	1	0	15
SAWLA 33	171	2.4369	3.7083	0	0	5	1	0	33
SHAKISO 15	172	5.4213	1.9458	0	0	5	1	0	15
WOLAYTA SODO15	173	6.9335	3.3558	0	0	5	1	0	15
YADOT 33	174	0.2967	0.1436	0	0	5	1	0	33
DILLA-2 15	175	7.4167	3.3905	0	0	5	1	0	15
NEGELE-BORNA15	176	0.85	0.4499	0	0	5	1	0	15
YIRGALEM 15	177	5.7215	1.0596	0	0	5	1	0	15
YIRGALEM 33	178	2.1191	1.0256	0	0	5	1	0	33
RAMO33 33	179	7.6371	3.694	0	0	5	1	0	33
KEY AFER 33	180	1.6316	0.7898	0	0	5	1	0	33

SHAKISO 33	181	2.9043	1.4056	0	0	5	1	0	33
YABELO 33	182	3.7267	2.449	0	0	5	1	0	33
WOLAYTA SODO33	183	1.3563	0.6563	0	0	5	1	0	33
HOSAINA 33	184	1.4834	1.6952	0	0	5	1	0	33
SHASHEMENE 33	185	0.3602	0.1744	0	0	5	1	0	33
YIRGALEM II 15	186	11.7149	5.6719	0	0	5	1	0	15
ARBA MINCH 33	187	2.8607	1.3845	0	0	5	1	0	33
AWASA 33	188	2.3267	1.1262	0	0	5	1	0	33
YADOT 15	189	0.6039	0.2923	0	0	5	1	0	15
AWASA MOBILE33	190	3.2812	1.5861	0	0	5	1	0	33
AWASA MOBILE15	191	8.4762	4.1024	0	0	5	1	0	15
SHASHEMENE-115	192	4.579	1.0648	0	0	5	1	0	15
HOSAINA 15	193	9.6808	4.6856	0	0	5	1	0	15
ALEM-KETEMA 33	194	1.5939	0.7715	0	0	6	1	0	33
AKISTA 33	195	10.4893	0.6251	0	0	6	1	0	33
COMBOL-1 15	196	5.2195	2.4164	0	0	6	1	0	15
DESSIE 15	197	10.3424	4.9972	0	0	6	1	0	15
LALIBELA 15	198	5.0938	2.4647	0	0	6	1	0	15
SEKOTA 15	199	5.3839	2.6098	0	0	6	1	0	15
SHEWA-ROBIT 15	200	3.6129	0.1058	0	0	6	1	0	15
WOLDIA 15	201	4.2495	2.0568	0	0	6	1	0	15
KEMISS33	202	2.5266	0.9615	0	0	6	1	0	33
KEMISS15 15	203	2.9725	0.4573	0	0	6	1	0	15
WOLDIA 33	204	1.8745	0.9072	0	0	6	1	0	33
SHEWA-ROBIT 33	205	3.8871	1.8749	0	0	6	1	0	33
WOLDIYA MOB 15	206	3.1572	1.528	0	0	6	1	0	15
WOLDIYA MOB 33	207	6.3144	3.0562	0	0	6	1	0	33
DESSIE 15	208	5.3451	3.207	0	0	6	1	0	15
DESSIE 15	209	6.9486	1.069	0	0	6	1	0	15
GASHENA 33	210	4.3445	0.2287	0	0	6	1	0	33
DITCHETO 33	211	4.2761	6.4141	0	0	6	1	0	33
SEMERA 33	212	5.9227	2.8666	0	0	6	1	0	33
COMBOL-1 15	213	5.2195	2.4164	0	0	6	1	0	15
BAHIR DAR1 15	214	6.766	2.9667	0	0	7	1	0	15
BAHIR DAR2-115	215	15.88	7.6929	0	0	7	1	0	15
BITCHENA 15	216	0.9514	0.4062	0	0	7	1	0	15
DABAT 15	217	3.1216	1.5109	0	0	7	1	0	15
DEBRE MARKOS15	218	10.0836	4.8804	0	0	7	1	0	15
FINOTE-SELAM15	219	8.6992	2.8997	0	0	7	1	0	15
GONDAR2 33	220	1.5806	0.7651	0	0	7	1	0	33
GONDER1 15	221	5.6061	2.1265	0	0	7	1	0	15
METEMA 33	222	2.0167	0.9761	0	0	7	1	0	33
MOTA 33	223	2.5617	1.2399	0	0	7	1	0	33
NEFAS MEWCHA33	224	4.7419	0.5127	0	0	7	1	0	33

PAWIE 15	225	0.9666	0.4833	0	0	7	1	0	15
WORETA 33	226	1.1991	0.5804	0	0	7	1	0	33
BAHIR DAR-2 15	227	29.9944	14.4958	0	0	7	1	0	15
GONDAR2 15	228	13.5025	6.5352	0	0	7	1	0	15
PAWIE 33	229	1.1599	0.5799	0	0	7	1	0	33
WORETA 15	230	3.2951	1.5949	0	0	7	1	0	15
DANGLA 33	231	2.638	1.2768	0	0	7	1	0	33
DANGLA 15	232	5.39	2.156	0	0	7	1	0	15
B.DAR2 33	233	0.5661	0.4246	0	0	7	1	0	33
BITCHENA 33	234	8.9891	3.8515	0	0	7	1	0	33
DEBREMARKOS 33	235	0.4579	0.2216	0	0	7	1	0	33
DABAT 33	236	9.2742	4.4887	0	0	7	1	0	33
D/TABOR MOBI15	237	9.7365	4.8683	0	0	7	1	0	15
DEMBI DO 15	238	2.6065	1.2615	0	0	8	1	0	15
GAMBELA1 15	239	3.7083	1.7289	0	0	8	1	0	15
GAMBELA2 33	240	0.8476	0.4103	0	0	8	1	0	33
METU 33	241	0.7204	0.3487	0	0	8	1	0	33
METU 15	242	6.569	3.1794	0	0	8	1	0	15
DEMBI DO 33	243	1.2715	0.6154	0	0	8	1	0	33
ABA 15	244	1.8012	0.8718	0	0	8	1	0	15
AGARO 15	245	2.154	1.0769	0	0	8	1	0	15
B.BEDELE 15	246	3.9097	1.8923	0	0	8	1	0	15
BONGA 15	247	2.2482	1.0881	0	0	8	1	0	15
GILGEL GIBE 15	248	2.1191	1.0256	0	0	8	1	0	15
G.GIBE NEW 33	249	4.9295	1.4499	0	0	8	1	0	33
JIMMA 15	250	1.4858	0.7191	0	0	8	1	0	15
MIZAN 33	251	1.0172	0.4923	0	0	8	1	0	33
TEPI 15	252	2.8289	0.9504	0	0	8	1	0	15
JIMMA OLD 15	253	14.0916	6.8203	0	0	8	1	0	15
AGARO 33	254	0.4344	0.2103	0	0	8	1	0	33
B.BEDELE 33	255	2.1191	1.0256	0	0	8	1	0	33
JIMMA OLD 33	256	4.238	2.0513	0	0	8	1	0	33
MIZAN 15	257	4.6782	2.2231	0	0	8	1	0	15
ADIGRAT 15	258	6.5636	3.1753	0	0	9	1	0	15
ADWA 15	259	13.3596	6.4668	0	0	9	1	0	15
ALAMATA1 15	260	8.7093	4.2153	0	0	9	1	0	15
HUMERA 33	261	8.4222	4.0763	0	0	9	1	0	33
MAYCHEW 15	262	4.7466	2.2974	0	0	9	1	0	15
MEKELE 15	263	36.4213	17.628	0	0	9	1	0	15
MESOBO 6.3	264	24.9693	12.089	0	0	9	1	0	6.3
TEKEZE-33 33	265	2.0513	0.9928	0	0	9	1	0	33
TEKEZE-DS 6.6	266	0.3358	0.2119	0	0	9	1	0	6.6

WUKRO 15	267	6.5266	3.1589	0	0	9	1	0	15
SHIRE 33	268	7.2106	3.4894	0	0	9	1	0	33
SHIRE-33-2 15	269	15.4652	7.4426	0	0	9	1	`0	15
MEHONI 15	270	4.2275	1.6635	0	0	9	1	0	15
HUMERA 15	271	2.4189	1.1707	0	0	9	1	0	15
ADWA 33	272	0.5022	0.2431	0	0	9	1	0	33
WUKRO 33	273	0.9905	0.4953	0	0	9	1	0	33
MEKELLE 33	274	1.6952	0.8205	0	0	9	1	0	33
ALAMATA 33	275	0.9905	0.4953	0	0	9	1	0	33
ABIADI MB 33	276	5.7164	2.7667	0	0	9	1	0	33
MEKELE MB 15	277	9.4717	4.5842	0	0	9	1	0	15
ADWA 15	278	11.5989	5.7994	0	0	9	1	0	15
ADIGRAT 15	279	6.4571	3.127	0	0	9	1	0	15
WELKAYT 33	280	11.5989	5.7994	0	0	9	1	0	33
AXUM 15	281	10.2511	4.1004	0	0	9	1	0	15
GRAN RENAIS 20	282	11.5472	4.2301	0	0	4	1	0	20
GRAN RENAIS 20	283	4.8329	6.766	0	0	4	1	0	20